Neural mechanisms underlying violation of expectations in the attentive brain

Priyanka Ghosh

Thesis submitted to

National Brain Research Centre

for the award of

Doctor of Philosophy in Neuroscience

National Brain Research Centre

(Deemed University)

Manesar, Haryana-122052, India

CERTIFICATE

This is to certify that the thesis entitled "**Neural mechanisms underlying violation of expectations in the attentive brain**" is the result of work carried out by **Priyanka Ghosh** in the Division of Cognitive and Computational Neuroscience at National Brain Research Centre, Manesar, Haryana, India, towards requirements for Ph.D. degree.

The work presented herein is original and has not been submitted previously for the award of any degree or diploma to National Brain Research Centre (Deemed University) or to any other University. The work is as per the guidelines given by National Brain Research Centre (Deemed University) and is a record of the candidate's own efforts.

Dr. Arpan Banerjee   (Director, NBRC)

Additional Professor/ Scientist V

NBRC, Manesar

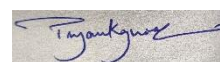(Supervisor)

DECLARATION BY CANDIDATE

I, **Priyanka Ghosh**, hereby declare that the work presented in the form of this thesis was carried out by me under the guidance of **Dr. Arpan Banerjee**, Additional Professor/Scientist V, National Brain Research Centre (Deemed University), Manesar, Haryana, India.

I declare that no part of the thesis contains any plagiarized material. Any previously published or other material sourced from anywhere else has been appropriately attributed to the source.

I also declare that no part of the thesis has been previously submitted for the award of any degree or diploma to National Brain Research Centre (Deemed University) or to any other university.

Place: Manesar   Priyanka Ghosh

Date: 08.08.2022

Dedicated to all the lives we lost during Covid, the ones who survived and all

the healthcare providers who made it possible

Acknowledgement

My Ph.D. in NBRC has taught me some of the most important life lessons. It has not only enhanced my scientific acumen as a researcher but has also transformed me as a human being. I am immensely grateful to all the people who were a part of this enriching journey in every small and big way possible and I wish to express my gratitude towards them here.

First and foremost, I would like to express my heartfelt gratitude to my mentor Dr. Arpan Banerjee, for giving me the intellectual freedom to pursue the research questions of my interest and for believing in me throughout the journey. Coming from a different academic background, I was overwhelmed by the neuroimaging tools and computational analyses but it was for his guidance, support and encouragement that my learning curve always kept growing. He has always been very patient with me and most importantly, has taught me to have a positive and rational outlook towards research and life in general.

I would also like to extend my gratitude to my co-supervisor, Dr. Dipanjan Roy, for his immense literature knowledge on scientific advancements around the world that kept me updated and inspired throughout. His excitement for my work during the doctoral committee meetings and critical comments during my presentations have always helped me look at things from a different perspective. I would also like to thank the other doctoral committee members – Prof. Soumya Iyengar and Prof. Ellora Sen for evaluating my work over the years.

Gourav, Amit and Utsav for their wonderful company, great food and amazing trips. NBRC did not have dull moments with you guys around. I thank my roommate Atrayee for bearing me for 5 long years and successfully bidding goodbye without a single fight over the years. My friends outside NBRC- Kunal, Pratibha and Mehta deserve a special mention who were always just a phone call away.

This journey wouldn't have been possible without the support of my family who gave me the best education, the independence to pursue an academic career and the strength to reach the finish line.

<div style="text-align: right;">

I wish you all love, light, peace and happiness.

Priyanka Ghosh

August 2022

</div>

Table of Contents

List of Figures

List of tables

List of Abbreviations

AMI   Alpha Modulation Index

BOLD   Blood Oxygen Level Dependent

BEM   Boundary Element Method

CSD   Cross-Spectral Density

DAN   Dorsal Attention Network

eLORETA   Exact low-resolution brain electromagnetic tomography

EEG   Electroencephalography

ERP   Event Related Potential

fMRI   Functional Magnetic Resonance Imaging

GGC   Granger-Geweke Causality

IFG   Inferior Frontal Gyrus

MMN   Mismatch Negativity

MPRAGE   Magnetization-Prepared Rapid Acquisition Gradient Echo

MFG   Middle Frontal Gyrus

MVGC   Multi-Variate Granger Causality

NT   Neutral Trials

ST   Salient Trials

WT   Without saliency Trials

PCA   Principal Component Analysis

RT   Reaction Time

TPJ   Temporo-Parietal Junction

TRGC   Time-Reversed Granger Causality

VAN   Ventral Attention Network

Chapter 1

Introduction

"Everyone knows what attention is. It is taking possession of the mind, in clear and vivid form, of one out of what seems several simultaneously possible objects or trains of thought. Focalization, concentration of consciousness are of its essence. It implies a withdrawal from some things in order to deal effectively with others."

— *William James*

The famous account on attention by William James from his 1890 book "The Principles of Psychology", has been challenged to be misleading at times. Attention is certainly far from a clear or unified concept and moreover, according to a recent study by Hommel et al. (2019), no one knows what attention is. In its most generic form, attention can be described as merely an overall level of alertness or the ability to engage with the surroundings. In neuroscience, the term "attention" refers to the neurological and psychological mechanisms that enable the identification and prioritization of important events amidst competing distractions. Rather than a state, it's a cognitive function that involves orienting, focussing and selecting relevant stimuli from a surfeit of sensory information. Due to limited computational resources in the brain, our attentional systems let us focus on specific information while tuning out irrelevant details, and may also affect our perception of the stimuli surrounding us. Nearly every aspect

of our life depends on attention, making it one of the most significant areas of research in neuroscience.

1.1. Historical background of attention
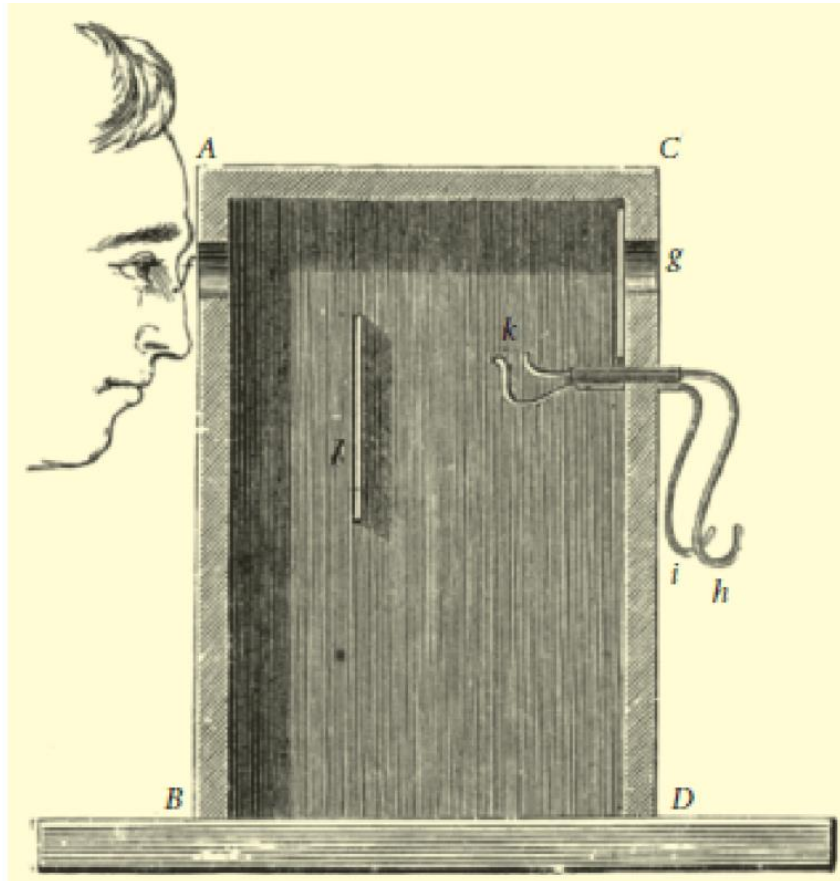
Figure 1.1. Helmholtz devised a device to study the range of perception without moving the eyes. A drawing was attached to the back of a hollow box painted black from inside (at location g). The observer kept his gaze fixed on a tiny hole that was always visible in the drawing. A spark was triggered by establishing electrical contact between the two wires (i and h) which illuminated the artwork. The light from the spark was reflected onto the artwork by a white piece of cardboard (l) which also protected the viewer's eye. The sparks were generated via a huge Ruhmkorff induction coil linked to the terminals of a Leyden jar. The primary coil's contact was created or broken manually. Adapted from Helmholtz (1866).

Some of the earliest known empirical studies on selective attention were carried out by Herman von Helmholtz (Helmholtz, 1867). He created a device resembling a tachistoscope that could briefly flash a display of letters (**Figure 1.1**). He used it to address the limitations of our perceptual capacity, pointing out that it was impossible to see all the letters at once in a single glimpse. He then demonstrated how we may direct our attention to particular spatial locations while still keeping our eyes fixed on a single spot. By covertly directing attention to each individual part of the array, one at a time, he was able to reassemble the full array over several iterations.

William James (1890) provided insightful and coherent accounts on the variations, effects and mechanisms of attention by reviewing early fundamental experiments and using introspective methods that are still rich and relevant. According to James (1890), at any given moment, the span of consciousness is limited to a single object or thought, attended to automatically or voluntarily, based on its relevance. Orienting attention through anticipatory preparation using ideational centers, focused on the stimulus to which attention is paid, causes adjustments in our sense organs that improve how well and how quickly stimuli are perceived, conceived, distinguished or remembered.

In the mid-twentieth century, Moruzzi and Magoun (1949) used cats to study arousal in the midbrain reticular system. In their study, attention was associated with a state in which the high-voltage slow waves were replaced with low-voltage fast activity when the animal was aroused from sleep or less extreme states of relaxation or drowsiness through stimulations. Sutton et al. (1965), discovered a strong positive deflection in voltage at around 300 ms in response to surprising or unexpected events that might capture one's attention. In the late 1970s, scientists Mountcastle (1978) and Wurtz et al. (1980), examined the mechanisms of orienting to visual objects using microelectrodes in alert animals and their findings suggested

that the superior colliculus and parietal lobe were crucial for a shift of visual attention. After the identification of "attention-related cells" in the posterior parietal lobe of awake monkeys, the concept that patients with lesions of the right parietal lobe could show severe neglect of the space opposite the lesion received widespread acceptance. Using scalp electrodes, Van Voorhis and Hillyard (1977) investigated the time differences in neural activity between attended and unattended visual sites and discovered that the early visual event-related potentials (ERPs) showed attention-specific changes beginning at about 100 ms after sensory input. Their results demonstrated that scalp recordings might be an accurate reflection of the underlying temporal structure of brain activity. The findings were hence a significant advancement for mental chronometry - the study of the time course of information processing in the human brain. In 1980, Michael Posner (Posner, 1980) developed a basic paradigm to trace the time course of attention shifts where the participant needed to press a response key to the target. Prior to the target, a cue was presented which, on 80% of the trials indicated where the target would occur (valid cue) and, on the remaining 20% indicated the position opposite the target (invalid cue). The cue could either be an arrow at the centre (endogenous cue) or it could appear at the target's position (exogenous cue). Reaction times to valid trials were faster than when the person was invalidly cued. In the 1990s, positron emission tomography (PET) was used as a neuroimaging tool to explore brain activity during attention (Corbetta et al., 1993; Posner and Raichle, 1998, 1994). The conclusion from neuroimaging research that cognitive processes engage a variety of different anatomical locations led to increased emphasis on tracking the temporal dynamics of these areas during tasks involving attention. It was challenging to track attention shifts using hemodynamic imaging because the changes can be very rapid. To address this problem, algorithms were created (Lins et al., 1993) to link the scalp distribution recorded from high-density electrical

or magnetic sensors on or near the skull to brain regions active during hemodynamic imaging

(Dale et al., 2000).

1.2. Neural correlates of attentional capture

Studies on attentional capture over the past years (Theeuwes, 1996; Yantis, 1996) have

demonstrated that a salient singleton distractor, even though irrelevant to the current task,

no matter what captures attention. For instance (see **Figure 1.2**), in a visual search task for

a unique shape target (circle) where participants are required to make a speeded response to

the orientation (horizontal or vertical) of the line segment inside the target shape, the

presence of distractor singletons (red diamonds) result in poor performance in the task

(increased RTs) (De Fockert et al., 2004).
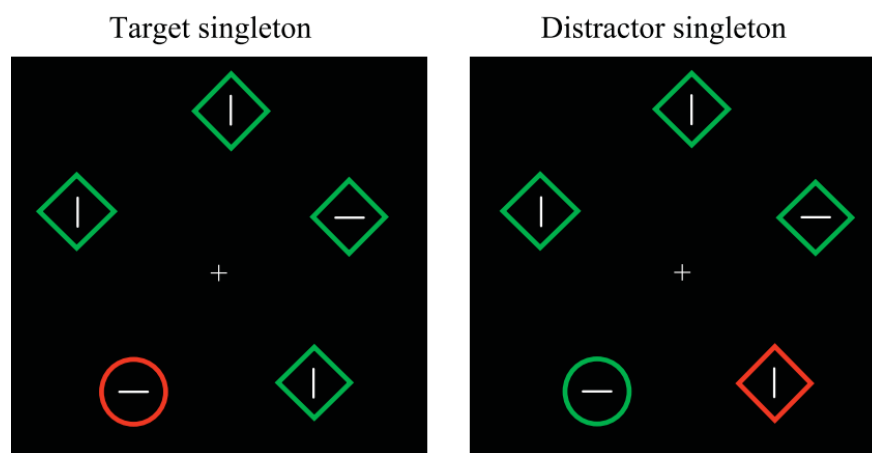
Figure 1.2. A color singleton task. The participants need to identify the target singleton which is orientation of the line (vertical or horizontal) inside the circle in each array. Distractor singletons (right panel) lead to attentional capture, causing increased reaction times/error rates in identifying the target singleton. Adapted from De Fockert et al. (2004).

The presence of unanticipated (task-irrelevant) stimuli in these tasks cause attentional capture primarily because of violation of expectations (discussed in the next section) during the target identification process. Stimulus-driven/automatic/reflexive shifts of attention due to unexpected salient stimuli are fundamentally classified as "exogenous attention" as opposed to "endogenous attention" which is a voluntary, goal-driven and effortful form of attention. This popular distinction based on the presence or absence of voluntary control is rather intuitive: while searching for a friend in a crowd, we voluntarily change our focus from one face to the next until the external sensory input matches our internal representation of the friend's physical appearance. In contrast, in a throng of people all wearing dark clothing, we will instantly spot a person dressed in bright red, who will automatically capture our attention. Such sensory-driven mechanisms carry inherent bottom-up biases which help prioritize events that stand out either due to their local contrast or physical conspicuity (e.g., bigger, brighter, or faster) (Yantis and Jonides, 1984). Such biases in the competing perceptual mechanisms have helped us gain an advantage during the evolution of our perceptual systems. Understanding how these mechanisms are reflected in the oscillations of the brain has garnered a lot of interest in recent years (Herrmann et al., 2004; Kahana, 2006; Raghavachari et al., 2001). Neural oscillations represent rhythmic fluctuations in the excitability of individual neurons, local neuronal populations, or large ensembles of neurons in different parts of the brain. Some prominent electroencephalography (EEG) research in the past advocated that alpha-band oscillations can be actively invoked across multiple sensory systems when the cortical regions are involved in processing irrelevant or distracting information (Foxe and Snyder, 2011; Jensen and Mazaheri, 2010a; Klimesch, 2012a). Jensen et al. (2012), suggested that posterior alpha oscillations (8–13 Hz) provide a mechanism for prioritizing and ordering unattended visual input according to its relevance. Pascucci et al., (2018) provided novel insights into how alpha activity from the parietal cortex orchestrates

selective attention by disrupting the coupling between alpha and gamma frequencies in the visual regions. Magnetoencephalographic (MEG) brain imaging has reported differences in the strength of the theta (4–8 Hz) and alpha (8–12 Hz) cortical oscillations in the temporoparietal junction, the ventral frontal cortex, and the insula (all three being the neural generators of the ventral attention network, discussed in detail in section 1.4) between the congruent and incongruent trials of an Eriksen flanker task (Hoffman et al., 2021; McDermott et al., 2019, 2017; Webb et al., 2016).

1.3. Violation of expectations and reorientation
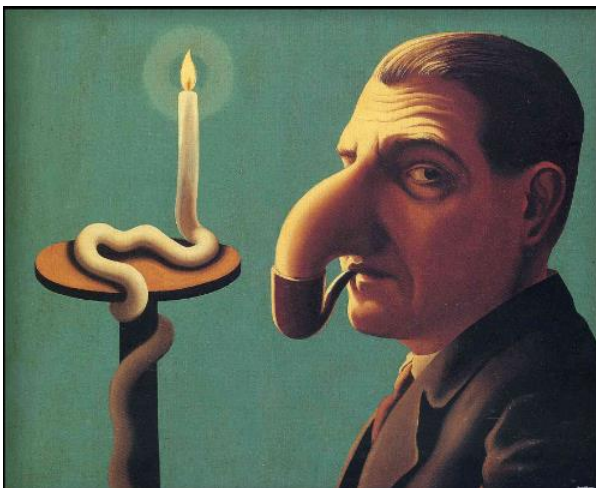
Figure 1.3. "The Philosopher's Lamp (La Lampe philosophique)" is one of the popular paintings by the 20th century surrealist Rene Magritte which is an ironic symbol of knowledge (the candle coil) through philosophical contemplation (a nose/head that smokes itself).

This painting by the famous Belgian artist when viewed without its philosophical context appears 'odd' because the man's nose in the picture is distended like an elephant's trunk and flops down into the bowl of the pipe he is smoking. In general, the human nose neither has a trunk-like shape nor is it so disproportionately bigger than the rest of the facial features. The man's nose in the painting (along with the coiled candle) thus leads to the violation of a set pattern of existing representations of the human nose in our brain.

Violation of expectations arise from any mismatch between the expected and presented sensory inputs, causing prediction errors and, subsequently leading to an update of the underlying model representations (Bubic et al., 2009). The first study that emphasized the importance of isolating the neural correlates of the violation of expectancy consisted of targets presented at unexpected spatial or temporal locations is a PET investigation by Nobre et al. (1999). Through the reanalysis of data from a previous study (Coull and Nobre, 1998), these authors compared brain activations recorded during phases of a Posner-like task in which the percentage of valid trials was either 100% or had a valid–to–invalid ratio of 60:40%. The invalid trials selectively activated the inferior-orbitofrontal cortex bilaterally, the inferior parietal areas bilaterally with a larger engagement of the right hemisphere and the right lateral premotor cortex. The authors concluded that the inferior orbitofrontal cortex is activated in response to trials that fail to match the expected cue and target, while the parietal and premotor areas are predominately involved in more intricate spatial-attentional processes as a result of the shift in attentional focus. Such spatial representations underlying breaches in expectations are temporally characterized by some specific event-related potentials (ERPs) in the brain. In distraction paradigms associated with the processing of (irrelevant) auditory stimuli (like in auditory-auditory and auditory-visual paradigms), a typical sequence of ERP components is observable in the deviants compared to the standards, reflecting different stages of sensory processing and attentional modulation related to behavioral distraction (Berti, 2012, 2008; Berti et al., 2004; Escera et al., 2001; Escera and Corral, 2007; Hölig and Berti, 2010; Horváth et al., 2008; Schröger and Wolff, 1998). Task irrelevant violation of expectations elicits the mismatch negativity (MMN), P3a, and reorienting negativity (RON), with the MMN indexing the pre-attentive sensory processing (Näätänen, 1990), the P3a indexing reorientation towards the new information (Friedman et al., 2001), and the RON indexing the subsequent voluntary switch of attention

back to the task-relevant information (Berti, 2008; Schröger and Wolff, 1998). Collectively, these steps of involuntary and voluntary switching of attention triggered by change detection interfere with the processing of the task-relevant information, resulting in prolonged reaction times and/or increased error rates (Escera et al., 1998; Schröger, 1996). Nevertheless, this mechanistic concept of a 3-step processing chain underpinning violation followed by distraction appears to be overly basic to tap the functional diversity of adaptable flexibility to continuous changes in the sensory environment.

In the real world, salient changes around us automatically grab our attention and trigger the process of reorientation, even when attention is focused elsewhere. However, there has to be the right balance between orienting to the current important task while remaining receptive to novel stimuli that may be behaviorally relevant, necessitating a change in focus. If the scales tip too heavily in favor of the current task, behavior becomes rigid and maladaptive. On the other hand, effective task performance is impossible if the balance tilts too far towards being receptive to unattended stimuli. For example, a driver driving down a busy road is likely to fixate on the road ahead (**Figure 1.4**), while covertly attending to the incoming traffic on the left. However, if he suddenly spots an animal on the right which is about to jump in front of the car, it is necessary to apply the brakes on time.

Figure 1.4. A driver typically focusses his/her gaze ahead on the road, covertly attending to the incoming traffic on the left. The sudden appearance of a dog about to jump on the road from the right needs to be reacted to, on time. In real-life situations, the ability to detect unattended stimuli is highly important. However, the processing has to be fairly limited and constrained to only the most salient visual objects. Adapted from Jensen et al. (2012).

Therefore, the reorientation of attention is primarily dependent on the ability of the underlying neural mechanisms to prioritize the processing of stimuli based on their saliency (see Posner et al., 1984, for a detailed account of "engagement" and "disengagement" of spatial attention). In the next section, we elaborate on how the neural responses to such

salient stimuli are controlled by the underlying neural networks based on the dissociation between automatic, stimulus-driven, processes from the ones that are affected by task goals.

1.4. The Ventral Attention Network

Through a series of experiments by Corbetta and Shulman (Corbetta et al., 2000; Corbetta and Shulman, 2002), the most influential subdivision of attention came into existence where attention was controlled by two functionally distinct circuits in the brain - the dorsal attention network (DAN) and the ventral attention network (VAN) (**Figure 1.5**). Voluntary and endogenous shifts of spatial attention were mediated by the dorsal frontoparietal network, whereas, unexpected, reflexive, exogenous shifts of spatial attention were mediated by the ventral network comprising of the inferior frontal gyrus and the temporal parietal junction (including the supramarginal gyrus and superior temporal gyrus). This classification was based on the functional connectivity patterns of blood oxygen level-dependent (BOLD) responses.
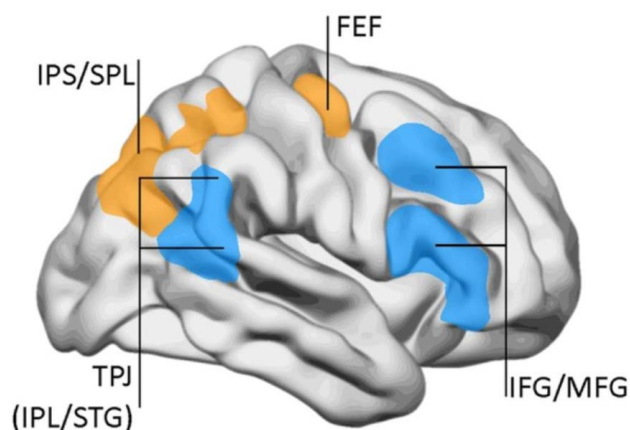
Figure 1.5. *Blue:* The ventral attention network (VAN) with its nodes at IFG, inferior frontal gyrus; MFG, middle frontal gyrus; TPJ, temporo-parietal junction; STG, superior temporal gyrus; IPL, inferior parietal lobe. *Orange:* The dorsal attentional network (DAN) with its nodes at FEF, frontal eye fields; IPS, inferior parietal sulcus; SPL, superior parietal lobe. Adapted from Corbetta and Shulman (2002).

Corbetta and colleagues proposed a theory in which, during the reorientation of attention, outputs from the ventral attention network act as "circuit-breaker" signals interrupting ongoing goal-directed attention in the dorsal system and shifting attention toward the novel object of interest (Corbetta and Shulman, 2002). Their theory was supported by the distinct patterns of activations in event-related fMRI tasks where the ventral parietal and frontal regions responded more strongly to targets that had been invalidly cued, appearing at unexpected locations (as also reported previously by Kastner et al., 1999).

In recent years, however, such a strict dichotomy in the networks has been questioned. DAN and VAN may possibly interact with each other at a more physiological level and may have common areas of activations as reported by some investigations in the visual (Serences and Yantis, 2007) and auditory (Salmi et al., 2009) domain. Macaluso and Doricchi, (2013) proposed that the VAN performs moment-to-moment match/mismatch operations by comparing current expectations with the actual sensory input. Furthermore, the strict correspondence of the ventral network to exogenous orienting may be challenged. The appearance of an invalidly cued target may cause attention to shift reflexively toward its location and disengage from its previous site, but it may also activate numerous other processes like propagating a mismatch signal in response to the violation of expectation to further direct action and update knowledge of the stimulus contingencies, in addition to the motivational and emotional factors related to the violation (Nobre et al. 1999).

The ventral attention network is reported to be a right-lateralized network that is modulated by the detection of unattended or infrequent events, independent of their sensory modality or target location. Numerous neuroimaging investigations have established the network's specialization for reorientation of attention and have highlighted how sensory salience, stimulus expectancy and target response are related to this network (Fox et al., 2006; Kim,

2014; Wen et al., 2012). The VAN, however, does not provide a dedicated mechanism for exogenous orienting in a temporally structured context (Kincade et al., 2005) as naturalistic situations that evoke reorienting often involve salient stimuli that occur 'rarely' and 'unexpectedly' (e.g., reorienting to a loud sound). In such scenarios, stimuli of high sensory salience may be automatically given behavioral importance thus, activating the ventral attention network. Although paradigms involving exogenous shifts of attention from one location to another have provided a convenient model for studying reorientation, the ventral attention network needs to be studied elaborately with a wider range of stimuli, such as stimulus-driven shifts of attention to novel features at the same location, as in oddball tasks (see Corbetta & Shulman, 2002).

1.5. Clinical significance

Spatial neglect is a common consequence of stroke where the patients fail to attend and respond to stimuli on the side contralateral to the affected area. Neglect is more frequent after damage to right than to the left hemisphere and is anatomically localized around the regions of the VAN resulting in problems with change detection and reorienting in patients. Carter et al. (2012), proposed that stroke may impair behavioral functions by disrupting communication in the brain networks relatively specific to certain behavioral domains. Therefore, examining stroke through the lens of connectivity within VAN may improve our ability to correlate behavioral deficits to structural/functional indices of dysfunction. Studies on schizophrenia have highlighted the faulty suppression of the VAN (White et al., 2013; Wynn et al., 2015) causing an inability to detect targets from non-targets (Jimenez et al., 2016). The aberrated salience processing has been proposed to be linked to a hyperdopaminergic system in the brain (Kapur, 2003; Van Os, 2009). Future research can

help assess the potential connection between an altered VAN and dopaminergic system in schizophrenia. Diminished homogeneity in the VAN has been observed in the pathogenesis of right temporal lobe epilepsy (Li et al., 2021). A lower resting state functional connectivity in the VAN is significantly correlated with higher levels of attention deficit hyperactivity disorder (ADHD) symptoms causing persistent inattention and attentional impairment (McCarthy et al., 2013). Taken together, a better understanding of the functioning and communication within the VAN will open a window to treat many prevalent neurological conditions. Similarly, identification of the associated brain oscillations or the underlying oscillopathies linked to VAN can represent important markers for early disease identification, progress monitoring, and pharmacological design (Nimmrich et al., 2015) towards deficits in the attentional mechanisms.

1.6. Scope of the thesis

To flexibly adapt to the novel circumstances in a dynamic environment, the detection of unanticipated changes in the sensory environment is a crucial prerequisite. Survival throughout the animal kingdom is dependent on the ability to change the current course of action and respond swiftly to potentially beneficial or threatening unexpected stimuli. This is achieved through diversion in the ongoing behavior by the automatic processing of salient sensory input that may be irrelevant to the ongoing task, allowing an assessment of the environmental changes around us. As described in the earlier sections, this mechanism involves the reorientation of attention, primarily controlled by the Ventral Attention Network (VAN) in the brain. The structural and functional connectivity of this network across various sensory modalities has undergone extensive research over the past two decades. However, to get a complete understanding of the dynamics of this network, it is

important to identify the brain waves through which the core regions of the network communicate with each other. The huge body of fMRI research on VAN could not quantify these metrics because of the sluggishness of the hemodynamic BOLD response. Due to a lack of the necessary temporal resolution needed to accurately capture the transient process of reorientation, the underlying neural oscillations and the causal architecture within this network remain elusive. Therefore, to address these knowledge gaps in the extant literature, we used non-invasive scalp electroencephalography (EEG) on healthy human volunteers to identify saliency-specific behavioral and oscillatory changes across the visual and auditory modalities and to estimate the directed information flow between the core regions (obtained using source localization techniques) of the ventral attention network. We also explicated the cortical sources of the various ERPs elicited during violation of expectations to highlight the modality-(in)dependent modulations across multisensory modalities. In the following chapters, we will focus on the specific objectives of the thesis which are:

1. To study the brain oscillations and connectivity dynamics of the underlying networks associated with processing unexpected salient objects in the *visual modality* across two different temporal scales.

2. To study the brain oscillations and connectivity dynamics of the underlying networks associated with processing unexpected salient sounds across three different spectro-temporal scales in the *auditory modality*.

3. To study the temporal markers of violation of expectations and their spatial representation across the brain using *unisensory audio*, *unisensory visual* and *audio-visual modalities*.

Chapter 2

Spectral markers of context independent processing of salient visual distractors via the ventral attention network

The material presented in this chapter has been previously published in Ghosh, P., Roy, D., & Banerjee, A., 2021. Organization of directed functional connectivity among nodes of ventral attention network reveals the common network mechanisms underlying saliency processing across distinct spatial and spatio-temporal scales. NeuroImage, 231, 117869.

2.1. Introduction

The ability to reorient our attention towards unexpected salient changes around us while performing routine tasks (e.g., spotting a speeding car while crossing the street) is critical for our survival. Where in one hand, goal-directed 'top-down attention' is required to orient attention towards a target to achieve a pre-decided goal in a task, response to a 'pop-out' or salient stimulus involves the rapid capture of attention by shifting the attentional focus from an ongoing goal-directed task through what is known as 'bottom-up attention' guided by the Ventral Attention Network (VAN) (Corbetta et al., 2008; Corbetta and Shulman, 2002). This process of attentional reorientation is essential but transient at the same time as attention needs to be oriented back to the task at hand. Since the brain is limited by attentional resources, synchronization or desynchronization of alpha oscillations (8–12 Hz) is one way

how the brain gates attentional selection at the neural level (Klimesch et al., 2007). One view is that synchronized alpha-band oscillations inhibit and desynchronized alpha-band activity excites sensory cortical areas (or at least reflects these processes) (Foxe and Snyder, 2011; Jensen and Mazaheri, 2010). A vast body of existing literature has linked alpha oscillations to distractor suppression (Foxe et al., 1998; Worden et al., 2000; Foxe et al., 2005; Snyder and Foxe, 2010; Banerjee et al., 2011), however, the role of drivers mediating information flow in the alpha frequency band remains poorly understood. Extant literature implicates the VAN comprising of the anterior insula, the right temporo-parietal junction (rTPJ) and the lateral prefrontal cortical areas (lPFC) including inferior frontal/middle frontal gyri (IFG/MFG) to be responsible for processing salient stimuli or oddballs (Allan et al., 2020; Vossel et al., 2014; Han and Marois, 2014; Corbetta et al., 2008). Abnormal VAN function is associated with many clinical conditions like depression (Liu et al., 2019) and spatial neglect (Corbetta et al., 2005), making the study of this network an important field of research. Even though the VAN has been studied in much structural and functional detail, the existing studies offer very limited insight into the directed functional connectivity within this network. Till date, only a few fMRI studies have tried to investigate the causal architecture underlying the VAN using dynamic causal modeling (DCM) (Liu et al., 2019; DiQuattro et al., 2014; Vossel et al., 2012). The sampling rate (repetition time or TR) for fMRI is, however, very low (in the order of seconds), which is much slower than the temporal resolution (in the order of milliseconds) required to capture the neural responses of such instantaneous attentional shifts. Hence, the study of network dynamics underlying the process of reorientation of attention may be limited by the sluggishness of the BOLD hemodynamic responses. To circumvent this problem, we used high-density EEG in this study with simultaneous behavioral recordings from healthy human participants. Accurate source reconstruction techniques that involved co-registration of EEG with individual

subjects' brain MR images were employed to locate the brain networks underlying alpha modulation, followed by characterization of the causal architecture of the constituent regions using Granger-Geweke causality (GGC) analysis– a well-established tool that measures the directed information flow among random variables in time and frequency domain (Dhamala et al., 2008; Pagnotta et al., 2018b, 2018a; Anzolin et al., 2019). Data obtained from EEG recordings of continuous neural activity are well suited to GGC by virtue of having a high temporal resolution. Moreover, mechanisms underlying the VAN are crucial to furthering our understanding of how salient distractors are processed by the brain across slow and fast time-scales as attention is just not limited by resources but also by time (Nobre and Coull, 2012).

Task-related brain activity is often sensitive to the temporal scale (fast or slow) at which a stimulus is presented (Papo, 2013). Previous studies have reported that the minimum dwell time for attention at a fixed location is about 200 ms (Cavanagh et al., 2014). On the other hand, when the focus of attention is changing along with time, a given location on the moving target's path can be selected for extremely brief time periods approximating to 50 ms (Cavanagh et al., 2014). Hence, the study of the neurobiology of attention requires a detailed understanding of the resource-wise allocation of attention both in space and time, depending on the task at hand. For instance, how the brain processes information to execute a visual search over a static image is entirely different from the sensory and cognitive processing deployed in executing a task involving tracking a dynamic stimulus (Kulikowski and Tolhurst, 1973; Battelli et al., 2007, 2001; Stigliani et al., 2017). Unlike a static stimulus, attention to a dynamic stimulus has limits extending over space and time, because when the speed of the stimulus increases, tracking ability decreases (Cavanagh and Alvarez, 2005). Similarly, the spatial properties of a moving distractor would change faster (e.g., on a

millisecond time scale) and slower (e.g., on a second or minute time scale) for a static distractor. There is also evidence that shows different cortical regions are sensitive to different time scales of stimulus processing (Monsa et al., 2020). Thus, a broader question that arises here is whether the process of reorientation of attention towards inclement bottom-up signals across tasks driven by different or common brain circuits?

We hypothesize that the underlying networks responsible for bottom-up attention and the oscillatory dynamics involved in the processing of salient distractors are time-scale invariant and do not depend on the nature of the task. To test this hypothesis in the visual modality first, we designed two attention tasks involving static (stationary) and dynamic (moving) stimulus processing, where the participants were presented with a salient distractor in the same visual space as the target during an ongoing goal-directed task. Such an experimental design was chosen to keep the visual stimulation close to what one would experience in a real-life situation. Previous EEG/MEG studies on bottom-up attention are severely limited by their presentation method where the salient distractors were either part of the visual display right from the onset of a trial along with the target (Kiss et al., 2012; Carretié et al., 2017) or there were separate trials (involving valid/invalid cues) for endogenous and exogenous attention (Dugué et al., 2018; Feng et al., 2017; Peelen et al., 2004) that were evaluated independently of each other which we believe is an unwarranted measure to study the process of reorientation. The present study aims to determine a direct relationship between neural networks underlying the alpha power enhancement and salient distractors across two completely different task conditions, on a comparative scale where in one, the stimulus (both target and distractor) evolves rapidly through time and in the other, it does not.

2.2. Methods

2.2.1. Participants

22 healthy human volunteers (11 females and 11 males) aged between 21-29 (mean = 26.9, SD = ±2.15) years were recruited for the study. All participants had University degrees or higher; were right-handed (indexed by laterality score according to the Edinburgh handedness questionnaire); reported normal or corrected-to-normal vision; and declared no history of neurological or psychiatric disorders. The participants were requested to avoid the intake of any stimulant or medication (e.g., coffee, sedatives, etc.) before coming for the experiment.

2.2.2. Ethics statement

The study was carried out following the ethical guidelines and prior approval of the Institutional Human Ethics Committee (IHEC) of the National Brain Research Centre, India. Written informed consent was obtained from all participants before the commencement of the experiment and they were remunerated for the time of their participation.

2.2.3. Rest block

Before starting with the experimental task, five minutes of eyes open resting-state EEG data were collected from the participants. During this period, a blank black screen was presented on the monitor. The participants were asked to relax or think at free will while viewing the monitor screen placed before them. They were requested to make minimal head, body and eye movements.

2.2.4. Stimulation blocks

All the participants performed two visual attention-based tasks which incorporated two stimulus conditions: static and dynamic **(Figure 2.1)**. The entire experiment was divided into 16 blocks (8 blocks of each stimulus condition). Each block was presented in random order during the experiment but was never repeated. Both the visual tasks had three categories of trials: 'Without Saliency Trials' **(WT)**, 'Saliency Trials' **(ST)** and 'Neutral Trials' (**NT**). The presentation order of the three categories was randomized in each block. The participants were not aware of the categorization in trials and were instructed only about the static and dynamic tasks' respective goals before the experiment.
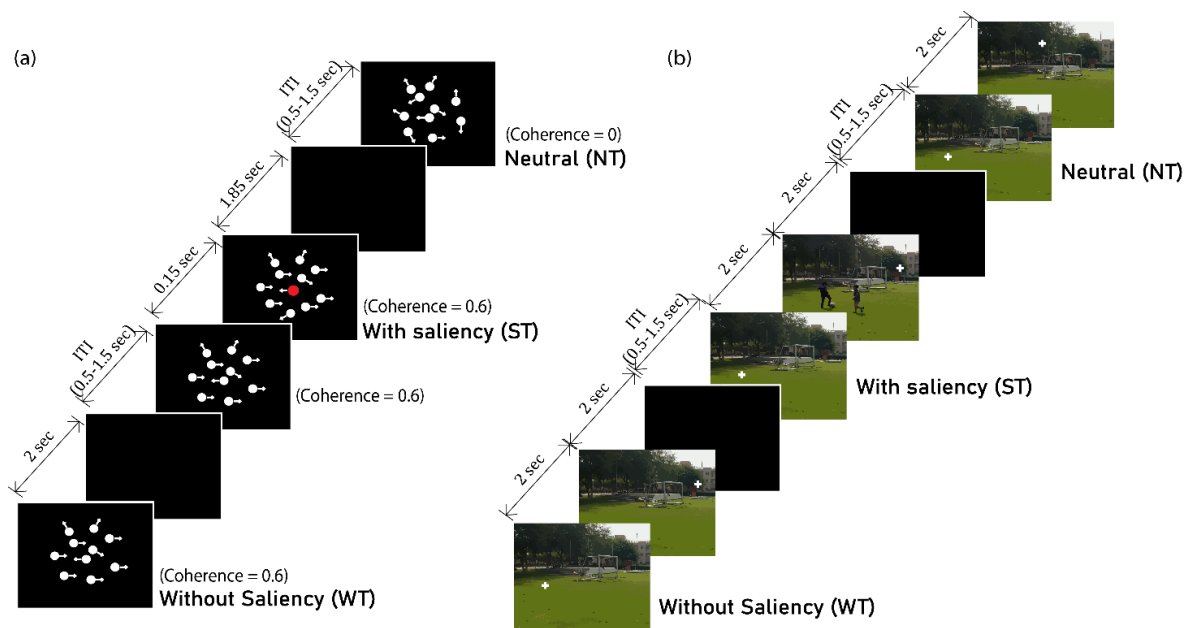
Figure 2.1. Visual Paradigm. An example of the task design is shown which comprises of videos in the (a) Dynamic stimulus condition and static images in the (b) Static stimulus condition. The figures illustrate the three different categories of trials: neutral trials (NT), without saliency trials (WT) and saliency trials (ST) along with their presentation durations within a block.

Dynamic stimulus: The dynamic stimulus viewing task was a four-alternative forced-choice (4-AFC) task. The stimuli were designed using Psychtoolbox-3 in MATLAB R2016b and were exported as videos with a frame rate of 60 Hz. The participants were presented with these videos which consisted of white-colored equal-sized randomly moving dots where a proportion of dots moved in a particular direction according to a certain coherence assigned to them. The coherence of the dots was kept at 0.6 for all the trials, which means that out of 100 dots, 60 dots moved in one specific direction and the other 40 moved in random directions, uniformly distributed over 0-360 degrees. The speed of motion of all the dots was kept constant across all trials. The participants were instructed to identify the net direction of the moving dots which could either be left/right/up/down and respond using the respective arrow keys on the keyboard. Each video was presented for 2000 ms. The goal in the task was the same for WT, NT and ST, with the only difference in ST being the emergence of a salient dot at a timestamp of 150 ms from the onset of the trial, moving randomly within the same aperture as the other dots. The 150 ms latency was decided to create an interference in the decision-making process (Teichert et al., 2016) of the participant while doing the goal-directed task. In the case of NT, the dots moved with zero coherence, i.e., all the dots (white-colored equal-sized) moved in random directions. The experimental schematic is illustrated in **Figure 2.1(a).**

Static stimulus: The static stimulus consisted of a two-alternative forced-choice (2-AFC) task. The participants were presented with two similar pictures on the screen, successively. Each picture pair made up one trial and was randomly selected from a pool of twenty such picture pairs. Thirty picture pairs were presented in one block. The pictures were naturalistic images (from both indoor and outdoor settings; no faces included), captured using a 16 MP camera keeping the settings the same for all images. Using Adobe Photoshop CC 2015.5, a

white-colored '+' shape (size 1/800th of the image) was added to all the images at random positions. Multiple copies of a single image with a '+' shape at different positions were created such that there was no image and '+' position memory association. Each picture was presented for 2000 ms. This was a visual search task where the participants had to search for the white-colored '+' shape in both the pictures and report its change in position in the second picture with respect to the first picture. For convenience, the participants were advised to imagine a vertical line bisecting the screen into left and right halves. They were instructed to press the upward arrow key if the '+' sign moved to the same half of the screen in the second picture, i.e, the '+' sign did not cross the imaginary line to move to the other half; and to press the downward arrow key if the '+' sign changed its position and moved to the other half of the screen i.e, from the left half to the right half or vice versa. The goal in the task remained the same for WT, NT and ST. However, the only difference in stimulus in the NT was that the '+' sign was presented on the imaginary midline itself (instead of left or right half) in either of the two pictures whereas in the ST a salient ('pop-out') object was introduced in the second picture at any random position. Examples of each of these categories are presented in **Figure 2.1(b).**

The NT in both the tasks served as a control to the participants' attention. They were introduced to check if the participants were attentive throughout the experiment and were just not making random responses. The NT were designed to give an impression of the most difficult trials to the participants which, if attended to, were expected to produce the longest reaction times. Technically, these trials did not have any correct response as such but the participants were unaware of it. The distribution of trials within a block for both the static and dynamic visual tasks is given in **Table 2.1.**

Inter-stimulus intervals (ISI) between successive trials were randomly drawn from a uniform distribution with values ranging between 500 ms and 1500 ms (mean = 1000ms) in which a blank black screen was presented to avoid any saliency-related effects due to central fixation. Stimulus presentation and behavioral response collection were done using Neurobehavioral Systems (NBS) Presentation software. Participants viewed the stimuli on a 21'' LED screen (1280 X 1024 pixels) with a 60 Hz refresh rate placed on a 74-cm-high desktop. The center of the screen was placed within 10–20° of the participant's line of sight, at a 60–70 cm distance. The stimuli were presented on a black background over which the static stimulus covered an area of 20 X 20 cm on the screen whereas the diameter of the aperture in the dynamic stimulus was 20 cm.

Table 2.1. Trial distribution across tasks.

Trial Information	Dynamic stimulus	Static stimulus
Total no. of blocks	8	8
No. of trials per block	70	30
Neutral trials (NT)	20	10
Without saliency trials (WT)	20	10
Saliency trials (ST)	30[*]	10

*To reduce the drop in the pop-out effect of salient distractors due to habituation after multiple trial presentations, 3 kinds of salient distractors were used, varying in either color or size or both from the other moving dots. 10 trials each of an equisized red, a larger red and a larger white dot were presented in a block as a salient distractor along with the rest of the moving dots in ST.

2.2.5. EEG Data Acquisition

Behavioral and EEG data were acquired in the EEG recording room where ambient noise, lights and other interferences were strictly controlled during the experiment to the same levels for all recording sessions. A Neuroscan EEG recording and acquisition system (Scan 4.3.3 & Presentation), which included an elastic cap (EasyCap) with 64 Ag/AgCl sintered electrodes and amplifier (SynAmps2), was used. The 64-channel EEG signals were recorded according to the International 10–20 system of electrode placement. The reference electrode was present on the z line between Cz and CPz (closer to Cz), grounded to AFz and the impedances of all channels were monitored to be below 10 kΩ. The data were acquired at a sampling rate of 1000 Hz. A Polhemus Fastrak system was used to record the 3D location of electrodes using a set of fiducial points (Cz, nasion, inion, left and right pre-auricular points) while the EEG cap was placed on the participant's head.

2.2.6. Behavioral Data Acquisition

All the responses were made on a computer keyboard using left/right/up/down arrow keys and were recorded through the NBS Presentation software by receiving triggers at keyboard presses. At the beginning of the experiment, the participants were briefed on the tasks and asked to watch the stimulus carefully before making any response. They were instructed to be as quick and accurate as possible and respond to an ongoing trial before it's offset. A blank screen followed by the subsequent trial appeared automatically after the offset of the ongoing trial, regardless of whether the participants had responded or not. They were also asked to respond to all the trials. If more than one response was made for a trial, only the first response was considered for further analysis. A rest period was allowed after every

block, with the participant deciding the length of the rest period to maintain minimum fatigue.

2.2.7. EEG Data Preprocessing

For both the static and the dynamic tasks, pre-processing steps and analysis pipelines were identical. All the pre-processing steps were done with the EEGLAB toolbox (Delorme and Makeig, 2004) and custom-written scripts in MATLAB (www.mathworks.com).

Raw EEG data from all the participants were imported using EEGLAB toolbox following which they were first filtered using a band-pass filter of 0.1-80 Hz followed by a notch filter between 45-55 Hz to eliminate line noise at 50 Hz. Post filtering, the data were visually inspected and the trials with any abnormal or noisy segments (jitters with very large amplitudes) were removed. Data of two participants were discarded at this step due to very noisy recordings. Next, the filtered data were average re-referenced by computing the average of the signal at all electrodes and subtracting it from the EEG signal of each electrode. This was done to avoid any common reference problem that may have detrimental effects on functional connectivity measures (Pagnotta et al., 2018b). Epochs of 1000 ms post salient stimulus onset were extracted using trigger information and were sorted from WT, ST and NT categories. Trial-by-trial detrending of each epoch category was performed to remove linear trends from the signal. To further remove eye-blink, ocular, muscular and electrocardiograph artifacts, a threshold of $\pm75\mu V$ was set and trials with a magnitude beyond this threshold at any time point were rejected from all the channels. Overall, about 70% of the trials for each task condition from each subject were preserved after artifact rejection.

2.2.8. Behavioral Analysis

The reaction times and accuracies of all the trials were calculated. Since attention is a key component in our experiment and any form of distraction (internal/external) could shift attention away from the task, blocks with response accuracies less than 70% (less than 6% of all blocks) were excluded from further analysis. Reaction times faster than 100 ms (mostly anticipations) were also excluded from the analysis. To decrease the number of false positives and minimize the chances of including responses made without the involvement of attention, all incorrect trials including the trials with no response were also excluded. For the NT, any response was considered as correct. Data from one participant were discarded due to very poor performance, specifically in the dynamic task trials. To rule out the possibility of incorrect responses being made because of a specific directional bias in any participant, we computed the percentage of incorrect responses for each direction and found that it was nearly the same for all directions in each individual.

From the remaining 19 participants, the reaction times of the correct trials were sorted for all the participants for both static and dynamic tasks. The reaction time was the duration from the onset of the salient distractor (matched equally for WT and NT) till the participant hit the response button. To ensure an equal contribution of trials from each participant, the number of trials from the participant with the minimum number of remaining trials after artifact rejection was chosen for further analysis. Those many trials were randomly sampled and extracted from all three categories for each participant. Since 35 was the minimum number, we had a total of 665 (19*35) trials from each category in both static and dynamic tasks.

2.2.9. Spectral Analysis

To understand the neural correlates of the behavior and hence, the processing of saliency by the brain, we looked at the constituent frequencies between 0.1-80 Hz in the individual trial categories of both tasks. The analysis scheme was designed in a way that could tease out the effect of the salient distractor while doing the goal-directed task and therefore, a time window of 1000 ms from the onset of saliency was considered (timestamps were matched accordingly for WT and NT) which was first normalized for all trials. The power spectral density for each trial was then computed using a multi-taper spectral analysis method provided by the Chronux toolbox (Bokil et al., 2010). This method involves the utilization of discrete prolate spheroidal sequences (DPSS) (Slepian and Pollak, 1961) known as tapers which are multiplied to the time series. The product is then Fourier-transformed and the resulting transforms are averaged to provide smooth spectral density function estimates. Using the toolbox script mtspectrumc.m, we applied 5 Slepian tapers to each time window (1000 ms) and a time-bandwidth product equal to 3 was used. The sampling frequency was kept at 1000 Hz and frequencies were estimated between 0.1-80 Hz.

Before analyzing the spectral modulations in the power spectra during saliency processing, it is important to ensure that the oscillations are free of 1/f noise. To remove the aperiodic component from the power spectra (mostly concentrated at the lower frequencies), we first modeled the $1/f$ trend of the log-transformed power spectrum using a least-squares method (Neto et al., 2015). The $1/f$ trend was then subtracted from the original power spectrum (Nikulin and Brismar, 2006; Haegens et al., 2014) and further statistical analyses were performed on the 1/f trend removed power spectrum.

2.2.10. Source Reconstruction using individual T1 MRI images

To localize the sources of the alpha band activity, we applied a current density technique: exact low-resolution brain electromagnetic tomography (eLORETA) implemented by the MATLAB-based Fieldtrip toolbox. eLORETA (Pascual-Marqui, 2007a) is a linear inverse solution method that can reconstruct cortical electrical activity with exact localization and zero error in the presence of measurement and structured biological noise (Pascual-Marqui, 2007b; Dattola et al., 2020). eLORETA provides a weighted minimum norm inverse solution where the weights are unique, endowing inverse solutions with very low localization error and fewer false positives compared to other methods for both point and distributed sources in the brain (Halder et al., 2019).

We first created the forward models of individual participants using their respective T1-weighted structural MRI images (MPRAGE) collected from a Philips Achieva 3.0T MRI scanner using the following acquisition parameters: TR = 8.4 ms, FOV = 250 X 230 X 170, flip angle = 8 degrees, and fiducials marked at nasion, left and right pre-auricular points with Vitamin E capsules. The origin (0,0,0) of all the T1 images was set to the anterior commissure using SPM 8 before generating individual head models. Using the Boundary Element Method (BEM), the brain was segmented into a mesh/grid based on the geometrical and tissue properties of the brain. The Polhemus data with the electrode locations of individual subjects were then fitted over these individual head models co-registered to the MRI fiducial points to create the leadfield matrix corresponding to each participant. For a frequency-domain source analysis, the cross-spectral density (CSD) matrix, which contains the cross-spectral densities for all sensor combinations, was computed for individual participants from the Fourier transformed data for the alpha frequency band (8-9 Hz).

Using the CSD matrix and the lead field matrix, a spatial filter was calculated for each grid point. A spatial filter reduces the correlations among the scalp-recorded channels induced by the source mixing in EEG signals due to volume conduction (Van de Steen et al., 2019). By applying this spatial filter to both the trial conditions (WT and ST) individually, the power estimate for each grid point was obtained. For calculating the source power, a common filter approach was used to ensure that the differences in the source powers across the two trial conditions were actually because of differences in the brain activity and not because of differences in the filter output (which might arise due to variations in the signal-to-noise ratio and subsequently varying CSD matrices) in the two trial conditions (WT and ST). Using this common inverse filter, the net source power was computed for each participant and the individual grids were interpolated with their respective T1 weighted images followed by normalization over a common Colin 27 brain template. The statistical threshold was set to the 95th percentile and the source powers of grid points to cross this threshold were considered as significant sources of activation.

2.2.11. Source Time-series Reconstruction

For both the trial conditions (WT and ST), we reconstructed the time series for each participant at the source level by multiplying the spatial filter generated using the statistically significant grid points of the static and the dynamic tasks with the pre-processed EEG time-series data of the respective task conditions. Common electrode placements were used for all participants which were computed by taking the average of their Polhemus 3D locations. The projection of the filter onto the EEG time-series data for each condition yielded 3 source dipole time-series with their orientations along the x, y and z directions. Since the interpretation of results becomes difficult while dealing with three dipole orientations, the

time series were projected along the strongest dipole direction. This was done by determining the largest (temporal) eigenvector corresponding to the first singular value. Further, using k-means clustering, the grid points were classified into nodes based on the centroid of the clusters. Sources corresponding to the dynamic task were classified into 9 nodes whereas, for the static task, they were classified into 5 nodes. Time series corresponding to each node were reconstructed for 1000 ms post onset of saliency (matched for WT and ST). The reconstructed time series from each participant was treated as a trial, making a total of 19 trials from 19 participants. Next, to understand how the processing of salient distractors is supported by the underlying networks, we investigated the statistical dependencies among the time series by computing the directional interactions between the nodes in the presence and absence of salient distractors.

2.2.12. Directed Functional Connectivity Analysis

Granger Causality (GC) was used to evaluate the directionality of information flow among cortical sources from the reconstructed source time series. The GC between two simultaneously acquired time series can be understood in this way: if the state variable represented from channel i by a time series at present time x_t could be improved further by including the past information of another time series of another channel j ($y_{t-1},\dots,y_{t-p}$) in addition to its own past ($x_{t-1},\dots,x_{t-p}$) where p is a finite period in past of relevance, we can say that y_t has a causal influence on x_t (Granger, 1969). The traditional pairwise bivariate GC implementation cannot distinguish a direct interaction between two signals from the influence of a common driver (e. g. z_t) acting on both the signals in a system where more than two time series are present (Geweke, 1982). In this case, conditional GC provides a more reliable framework of GC estimation as it is based on multi-variate autoregressive

modeling (MVAR) that accounts for any indirect causations (Chen et al., 2006; Wen et al., 2013). Yet in this approach, GC is inferred "parametrically", where separate model fitting (computation of p) processes are conducted for each combination of nodes. Such an approach may introduce unwanted variability and uncertainty because of model parameter (e.g. model order: the parameter which determines how many past time samples are taken into account for predicting activities at present time) inconsistency for each combination of nodes (Seth et al., 2015). This problem has been solved recently by an MVGC (multi-variate Granger causality) approach where an MVAR model is fitted to the time-series data only once and all subsequent calculations are based on the estimated model parameters (for more information, please refer to the MVGC toolbox (Barnett et al., 2018a, 2018b; Barnett and Seth, 2014). The estimation of the correct model order however, still remains a major concern. Therefore, to bypass this step of parametric data modeling, we employed a non-parametric method of GC computation in the spectral domain (Chen et al., 2006; Dhamala et al., 2008) as our study mainly focuses on modulations in the alpha oscillations. This method, known as Granger–Geweke causality (GGC), has an advantage over the classical MVAR approach by having fewer apriori assumptions (Pagnotta et al., 2018b, 2018a; Faes et al., 2019) and is well suited to characterize time-varying causal influences between neural systems with good temporal resolution.

In the non-parametric GGC approach, we first obtained the auto and cross spectra from the multi-variate time series using the multi-taper method of Fourier transformation. The spectral matrix was then factorized to yield the transfer function and the noise covariance matrix (Wilson, 1978).

The directed information flow from channel j to channel i conditional to the remaining w channels was calculated as:

$$GGC_{j \to i|w}(f) = ln\left(\frac{\Omega_{ii}}{Q_{ii}(f)\Sigma_{ii}\,Q_{ii}^*(f)}\right) \tag{1}$$

where, Σ and Ω are the noise covariance matrices of the full system (with all channels) and

of the subsystem in which channel j is excluded, respectively; while, Q_{ii} is obtained from:

$$
\begin{aligned}
Q(f) &= \begin{bmatrix} Q_{ii}(f) & Q_{ij}(f) & Q_{iw}(f) \\ Q_{ji}(f) & Q_{jj}(f) & Q_{jw}(f) \\ Q_{wi}(f) & Q_{wj}(f) & Q_{ww}(f) \end{bmatrix} \\[2mm]
&= \begin{bmatrix} G_{ii}(f) & 0 & G_{iw}(f) \\ 0 & 1 & 0 \\ G_{wi}(f) & 0 & G_{ww}(f) \end{bmatrix}^{-1} \begin{bmatrix} H_{ii}(f) & H_{ij}(f) & H_{iw}(f) \\ H_{ji}(f) & H_{jj}(f) & H_{jw}(f) \\ H_{wi}(f) & H_{wj}(f) & H_{ww}(f) \end{bmatrix}
\end{aligned} \tag{2}
$$

where, H and G are the transfer function matrices of the full system and of the subsystem in

which channel j is excluded, respectively. These two spectral transfer matrices are obtained

using Geweke's normalization method, which consists of multiplying transfer functions and

covariance matrices by transformation matrices to make the noise terms independent (Ding

et al., 2006; Wen et al., 2013).

One of the underlying assumptions of the above mentioned GGC algorithm is that the time

series being tested are stationary (Cohen and Van Gaal, 2013). Though any neural time-

series data obtained empirically is never fully stationary in nature, the non-stationarities can

be reduced by removing the evoked potentials from EEG data. For this purpose, we filtered

our reconstructed time-series data between 5-45 Hz to remove the slower frequencies below

5 Hz and avoid contamination of signals due to any residual line noise (50 Hz), which was

followed by a z-transformation trial-by-trial. Data from Subject#14 still showed some large

amplitude jitters in the time series because of which it was not considered for further

analysis. We also verified the stationarity of the remaining signals using an augmented

Dickey-Fuller test (Said and Dickey, 1984). Here, the signal is fitted with an autoregressive

or "AR" model of the following form

$$y_t = y_{t-1} + \beta_1 \Delta y_{t-1} + \beta_2 \Delta y_{t-2} + \cdots + \beta_p \Delta y_{t-p} + \varepsilon_t \tag{3}$$

against the alternative model

$$y_t = \phi y_{t-1} + \beta_1 \Delta y_{t-1} + \beta_2 \Delta y_{t-2} + \cdots + \beta_p \Delta y_{t-p} + \varepsilon_t \tag{4}$$

where,

1. Δ is the differencing operator, such that $\Delta y_t = y_t - y_{t-1}$.

2. ε_t is a mean zero innovation process and p is the model order of lagged difference terms. We kept $p = 1$ and fitted the value of ϕ .

Subsequently, the statistical test with null hypothesis of a unit root $H_0 : \phi = 1$; was undertaken against an alternative hypothesis of $\phi < 1$.

All the time-series data in both static and dynamic task conditions showed rejection of the unit root null in favor of the alternative model indicating that the signals were stationary.

2.2.13. Statistical Analysis

From the output of the GGC algorithm, the mean of the causal scores was calculated across all trials. Each cell in the matrix obtained (9 X 9 for dynamic stimulus and 5 X 5 for static stimulus) indicated the causal score between a set of two nodes at 8-9 Hz. The statistical significance of these scores was validated using a permutation test. For each task condition, a null distribution was generated empirically by random permutations of the reconstructed time series across all nodes, run over 1000 iterations. Subsequently, the spectral Granger causality estimates were obtained for the 1000 permutations. The mean and the standard deviation of the spectral GC values between 8-9 Hz were computed to generate a confidence interval at 95% and the values higher than the right (positive) tail of the confidence interval were considered to be statistically significant.

We further cross-validated the significance of the statistical scores using time-reversed Granger Causality (TRGC) which is an adaptation of the MVGC that uses time-reversed data as surrogates for statistical testing (Haufe et al., 2013, 2012). It has been shown that the application of this method for testing Granger Causality leads to correct estimates of directional information flow as it reduces the effects of intermixing of source signals due to volume conduction in EEG (Vinck et al., 2015; Winkler et al., 2016; Anzolin et al., 2019). The idea behind TRGC is: if the temporal order of a time series is the deciding factor to tell a driver from an effector, the directed information flow should be reduced (if not reversed), if the temporal order is reversed. This method rejects false causal interpretations from signals that are correlated but non-interacting leading to much lesser detection of false positives. Here, the net causal influence from channel j to channel i is inferred only if $\Delta GGC_{j \to i}^{(net)}$ is a positive value (since negative GC values hold no physical meaning).

$$\Delta GGC_{j \to i}^{(net)} = GGC_{j \to i}^{(net)} - \widetilde{GGC}_{j \to i}^{(net)} = (GGC_{j \to i} - GGC_{i \to j}) - (\widetilde{GGC}_{j \to i} - \widetilde{GGC}_{i \to j}) \quad (5)$$

where the tilde denotes GGC estimates computed on time-reversed data. This test however, only works for unidirectional causations because if a bidirectional causality exists, time-reversal would still show a valid causation.

After all the directional causations were inferred with TRGC as well as the permutation test, we used the statistically significant GC scores to create brain networks that were visualized using BrainNet Viewer (Xia et al., 2013).

2.3. Results

2.3.1. Behavioral performance

The reaction time distribution of all the trials from each trial condition for both the dynamic and static tasks have been shown in **Figure 2.2(a) and 2.2(b)** respectively. Clearly, the distribution follows a similar pattern in both the tasks: the reaction times of NT > ST > WT. The box plots in **Figure 2.2(c)** represent the summary statistics of reaction times in milliseconds, with 25th, 50th (median) and 75th percentiles reported for the dynamic task during WT (523, 622, 773), ST (541, 655, 812), and NT (838, 1096, 1388); and in **Figure 2.2(d)** for the static task during WT (770, 944, 1137), ST (833, 1033, 1276) and NT (912, 1126, 1397). Since the distributions of RTs were visually asymmetric, we employed the non-parametric Wilcoxon rank-sum test to compute the statistical significance of differences between the medians of reaction times of any two categories within a given task condition. The test rejected the null hypothesis that data from two distributions have equal medians at 5% significance level for all category-wise comparisons within a task condition. We also checked the effect size of the difference in medians of any two categories within a task by determining the Cohen's d values. For dynamic task, the reaction time of NT was greater than WT ($p<0.001$, z-value=22.55, d=1.121), the reaction time of NT was greater than ST ($p<0.001$, z-value=21.85, d=1.084) and the reaction time of ST was greater than WT ($p=0.05$, z-value=1.93, d=0.097). For static task, the reaction time of NT was greater than WT ($p<0.001$, z-value=10.72, d=1.261), the reaction time of NT was greater than ST ($p<0.001$, z-value=5.24, d=0.671) and the reaction time of ST was greater than WT ($p<0.001$, z-value=5.51, d=0.707).

(a)

(b)

(c)

(d)
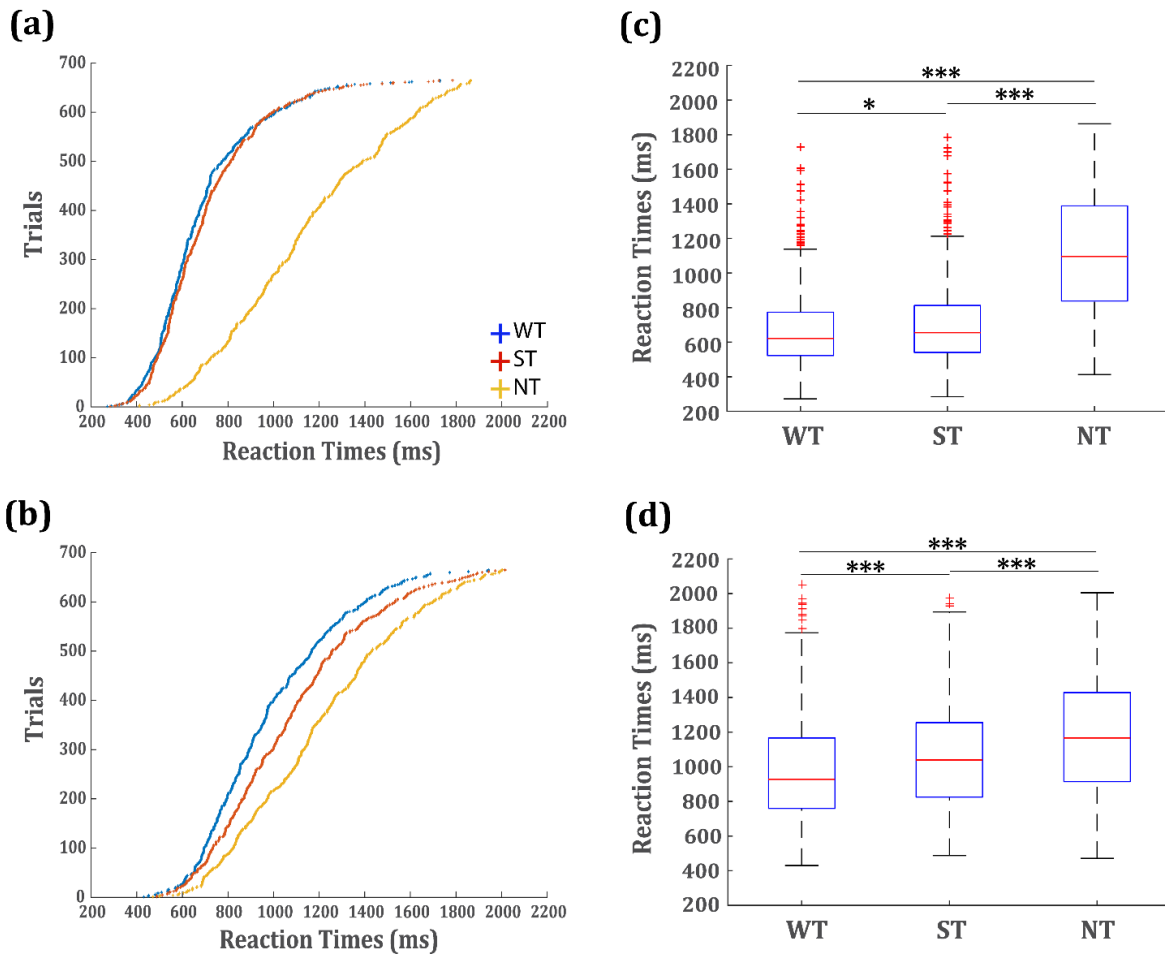
Figure 2.2. Behavior. Scatter plots showing the distribution of reaction times (RTs) sorted across trials in ascending order, during the (a) Dynamic task and the (b) Static task for the three trial categories: neutral trials (NT), without saliency trials (WT) and saliency trials (ST). Each data point corresponds to the RT of one trial. The medians of the trial categories within the (c) Dynamic task and the (d) Static task conditions are statistically compared in the box-and-whisker plots using a rank-sum test. On each box, the central red line indicates the median, and the bottom and the top edges of the box indicate the 25th and 75th percentiles, respectively. The whiskers extend to the most extreme data points not considered as outliers, and the outliers are plotted individually using the '+' symbol. Significant differences were tested at 5% significance and indicated using * (p≤0.05), ** (p≤0.01) and *** (p≤0.001). Note: This common convention for marking significance has been used for all the plots reported in this study.

The highest reaction times in NT in both the tasks are possibly due to the highest difficulty level in these trials as compared to ST and WT as there were no obvious correct responses in this category. Also, reaction times of ST were significantly higher than reaction times of WT in both the task conditions reflecting the processing costs involved in reorienting attention to the salient distractors. Hence, it is important to characterize whether the neural dynamics corresponding to a salient stimulus are due to an attentional shift alone or attention combined with task difficulty.

2.3.2. Neural dynamics in the spectral domain

To characterize the underlying oscillatory signatures in saliency processing, the power spectra were calculated for WT, ST and NT of all the participants, trial-by-trial, which were subsequently averaged and collapsed across all the 64 sensors to obtain the global power spectra for each trial category. Although WT, ST and NT had almost overlapping power spectra between 1-80 Hz in their respective task conditions, notable differences were seen in power spectral densities (PSDs) of the alpha band (7-12 Hz). The ST showed an enhanced alpha power, interestingly in both dynamic (**Figure 2.3(a)**) and static (**Figure 2.3(b)**) task conditions. Statistical significance was computed for the enhanced alpha power from the 1/f trend removed data using the Wilcoxon rank-sum test at a significance level of 5% and the effect sizes were calculated using Cohen's d measure. In the dynamic task, alpha power of ST was significantly higher than that of WT (p=0.041, z-val=2.044, d=0.114) and NT (p=0.049, z-val=1.961, d=0.155) between 8-9 Hz but there was no significant difference in the alpha powers of WT and NT (p=0.954, z val=0.057, d=0.043) (**Figure 2.3(c)**). In the static task, alpha power of ST was significantly higher than that of WT (p=0.0007, z-val=3.382, d=0.138) and NT (p=0.012, z-val=2.490, d=0.164) between 8-9 Hz but again

there was no significant difference in the alpha powers of WT and NT (p=0.369, z val=0.897, d=0.029) (**Figure 2.3(d)**).
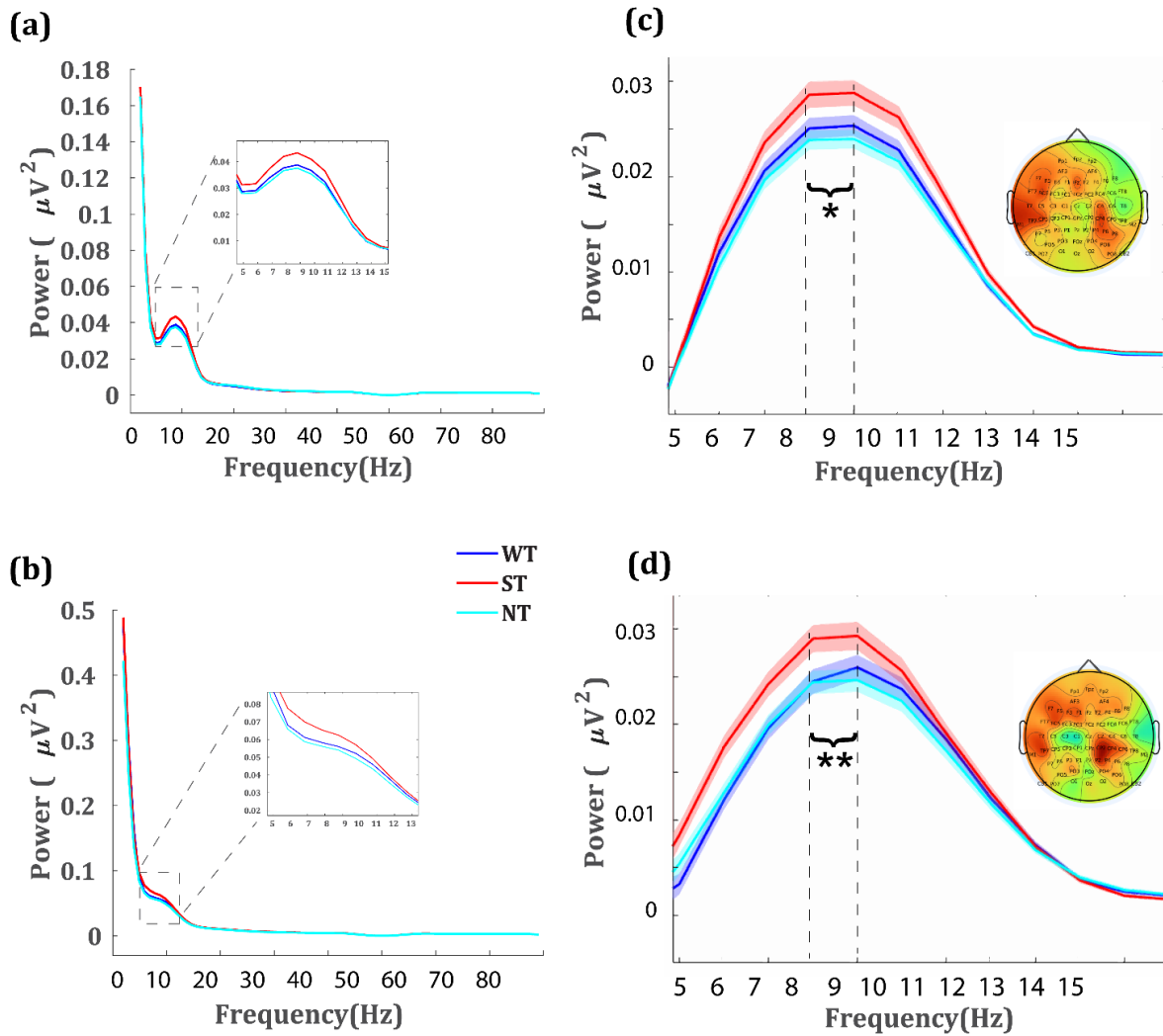
Figure 2.3. Power spectral density. The mean global power spectra plots for the (a) Dynamic task condition and the (b) Static task condition are shown, representing the normalized power spectra of neutral trials (NT), without saliency trials (WT) and saliency trials (ST). The insets are the zoomed-in portions at frequencies (~ 6 to 14 Hz) where these three trial categories show differences in magnitudes of their powers. Also, the aperiodic 1/f trend removed power spectra with the standard

error of mean (SEM) as shaded region is shown for (c) Dynamic task and (d) Static task, where, the powers of ST>WT and ST>NT between 8-9 Hz in both the tasks as tested at 5% significance level. No significant differences were seen in the powers of WT and NT in both tasks. The corresponding topoplots represent the enhancement of alpha power (8-9 Hz) in ST wrt WT, computed using the alpha modulation index (AMI).

No significant enhancement of alpha power in the case of NT (even though they had the highest reaction times) compared to WT thus rules out the possibility of alpha power increase stemming from task complexity/difficulty level. This suggests that the underlying cause for the alpha power enhancement in the ST was distractor suppression (to improve task performance) which is consistent with the role of alpha oscillations as reported in a vast body of literature (Fries et al., 2001; Fu et al., 2001; Jensen and Mazaheri, 2010; Klimesch, 2012; Zumer et al., 2014; Liu et al., 2014; Feng et al., 2017). The net increase in the alpha power in ST as compared to WT was calculated using the alpha modulation index (AMI) (Sokoliuk et al., 2019) between 8-9 Hz.

$$AMI = \frac{Sensor\ power\ of\ ST - Sensor\ power\ of\ WT}{0.5 * (Sensor\ power\ of\ ST + Sensor\ power\ of\ WT)} \qquad (6)$$

The sensor-wise distribution of the AMI has been shown in the topoplots for dynamic (**Figure 2.3(c)**) and static (**Figure 2.3(d)**) tasks. Sensors Fz, F5, F7, FC5, FT7, T7, CP5, TP7, CP4, CP6, P4, P6, P8 and PO6 showed the maximum increase in alpha power (8-9 Hz) in the dynamic task. Similarly, sensors F1, F3, F5, F7, FC5, T7, TP7, CP2, CP4, CP6, P2, P4 and P6 showed an alpha power (8-9 Hz) increase in the static task. Overall, in both the tasks, enhanced alpha power concentrated around the temporo-parietal sensors on both the hemispheres; centro-parietal and parietal sensors on the right; and the frontal, fronto-central sensors on the left.

2.3.3. Underlying cortical sources of neural activity

The underlying sources responsible for the enhanced alpha power in ST with respect to WT were calculated using AMI between 8-9 Hz after computing the individual sources for ST and WT using eLORETA (as described in section 2.10). The relative difference in source powers of ST and WT conditions produced the residual source powers. We argue that the dynamic or static task-specific information was thus negated and the residuals reflect the effect of the salient stimuli only. The source powers of all participants were grand-averaged and tested for statistical significance. The grid points that survived 95th percentile threshold were considered as significant sources of enhanced alpha power in response to salient distractors. For plotting, the source coordinates in the 3D voxel space were projected to a surface plot as represented in **Figure 2.4** using customized MATLAB codes. Spurious activations towards the center of the brain arising from noise were removed by masking the grid points deep inside the brain with an ellipsoid of optimum radii centered at the anterior commissure. All the underlying sources of alpha enhancement with their respective coordinates have been listed in **Table 2.2**.

a) Dynamic stimulus condition

x	y	z	Brodmann area	Region
-37.423	-36.441	16.042	Left-BA-40	Left anterior Temporo-parietal junction (Supramarginal gyrus)
37.865	-60.175	24.873	Right-BA-39	Right posterior Temporo-parietal junction (Angular gyrus)
34.247	-31.582	18.582	Right-BA-40	Right anterior Temporo-parietal junction (Supramarginal gyrus)
-33.438	8.240	13.889	Left-BA-44	Left lateral pre-frontal cortex (Inferior/middle frontal gyrus)
39.084	16.886	4.927	Right-BA-44	Right lateral pre-frontal cortex (Inferior/middle frontal gyrus)
33.937	-92.210	4.712	Right-BA-18	Right Visual Area (Visual Association area)
-41.900	-86.704	8.421	Left-BA-19	Left Visual Area
-37.258	-14.939	5.351	Left-BA-13	Left Insula
37.606	-11.191	13.270	Right-BA-13	Right Insula

b) Static stimulus condition

x	y	z	Brodmann area	Region
33.371	-29.377	20.384	Right-BA-40	Right anterior Temporo-parietal junction (Supramarginal gyrus)
32.592	20.498	9.936	Right-BA-45	Right lateral pre-frontal cortex (Inferior/middle frontal gyrus)
33.801	-79.569	3.153	Right-BA-18	Right Visual Area (Visual Association area)
-31.293	-21.868	12.106	Left-BA-13	Left Insula
37.371	-9.490	11.243	Right-BA-13	Right Insula

Table 2.2. Areas involved in processing saliency. Coordinates of centroids of the reconstructed sources (clustered through k-means) involved in saliency processing along with their corresponding brain areas.

The underlying sources of alpha enhancement in the dynamic task were the left and the right anterior temporo-parietal junction (supramarginal gyrus), the right posterior temporo-parietal junction (angular gyrus), the left and the right insula, the left and the right lateral prefrontal cortex and, the left and the right visual areas. The sources corresponding to alpha power enhancement in the static task were the right anterior temporo-parietal junction (supramarginal gyrus), the left and the right insula, the right lateral prefrontal cortex and the right visual area.

The observed alpha power enhancement during dynamic stimulus processing corresponds to two sub-regions of the right TPJ: the anterior and the posterior right TPJ. To further confirm whether the two clusters obtained were not from a single big activation region due to a limitation of the clustering algorithm, we calculated the Euclidean distance between the right anterior and right posterior TPJ based on their coordinates, which was equal to 28.80 mm, which suggested that the two sub-regions were considerably far apart to be considered as two distinct ROIs.
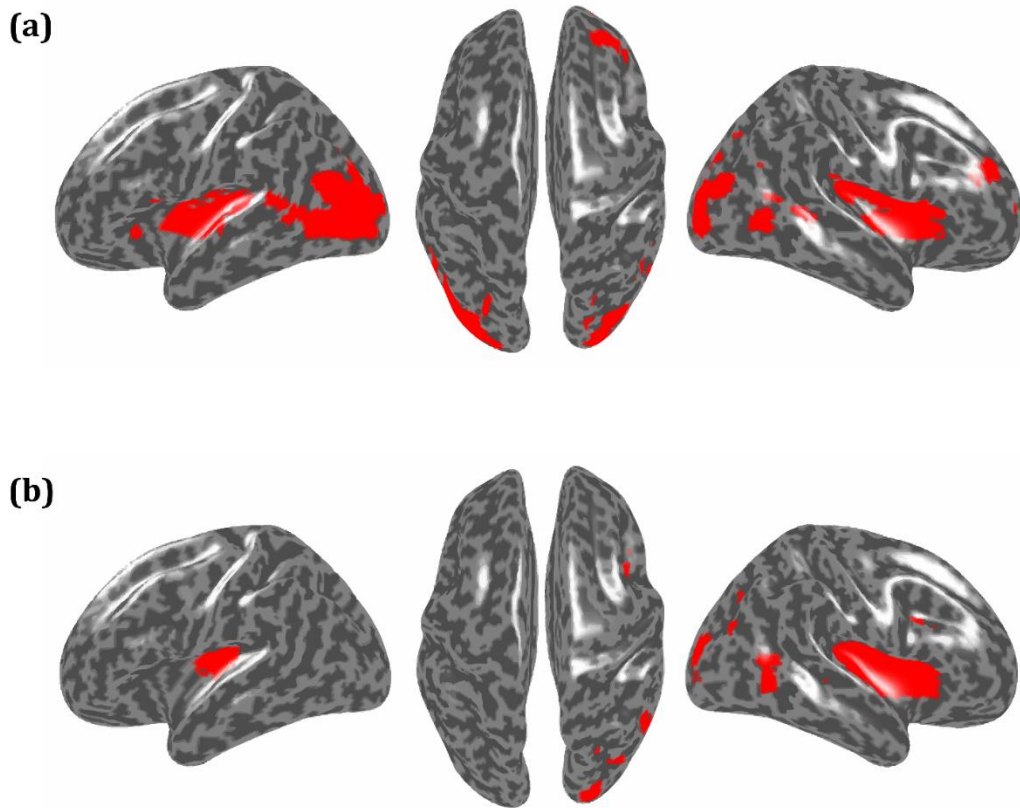
Figure 2.4. Sources of alpha power. The figure represents the cortical sources involved in processing saliency at the alpha frequency band (8-9 Hz) when the power of ST is contrasted with the power of WT using alpha modulation index (AMI). The sources identified were the left and the right anterior temporo-parietal junction, the right posterior temporo-parietal junction, the left and the right insula, the left and the right lateral prefrontal cortex (inferior/middle frontal gyrus), the left and the right visual areas for (a) Dynamic Stimulus; and the right anterior temporo-parietal junction, the left and the right insula, the right lateral prefrontal cortex (inferior/middle frontal gyrus) and the right visual area for (b) Static Stimulus. All regions were approximated to the nearest Brodmann areas of the human brain.

2.3.4. Directed functional connectivity among underlying sources

Source time series computed from the 9 sources of dynamic stimulus and the 5 sources of static stimulus processing conditions were subjected to spectral Granger-Geweke causality (GGC) analysis to investigate the directional interactions between the sources involved in processing the salient distractors in the alpha frequency range of 8-9 Hz. Please refer to the **Appendix** for the GGC indices. We present the significant unidirectional flows between areas with → and bi-directional flow as ←→.

Directed information flows in the presence of salient distractor (ST) revealed by GGC can be classified into a) *intra-hemispheric:* Right Insula → Right posterior TPJ, Right Insula ←→Right anterior TPJ, Right Insula ←→ Right lateral PFC, Right Insula ←→ Right visual, Right visual area ←→ Right lateral PFC, Right lateral PFC ←→ Right anterior TPJ, Right visual area ←→ Right posterior TPJ, Right visual area ←→ Right anterior TPJ, Right visual area ←→ Right lateral PFC, Right anterior TPJ ←→ Right posterior TPJ, Left Insula → Left lateral PFC, Left Insula ←→ Left visual area, Left visual area ←→ Left anterior TPJ, Left visual area ←→ Left lateral PFC, Left anterior TPJ → Left lateral PFC and b) *inter-hemispheric:* Right Insula ←→ Left anterior TPJ, Right Insula ←→ Left lateral PFC, Right Insula ←→ Left Insula, Left Insula ←→ Right anterior TPJ, Left Insula ←→ Right lateral PFC, Left Insula ←→ Right visual area, Left visual area → Right Insula, Left visual area ←→ Right posterior TPJ, Left visual area ←→ Right lateral PFC, Right visual area → Left visual area, Right visual area ←→ Left anterior TPJ, Right visual area ←→ Left lateral PFC, Right lateral PFC ←→ Left lateral PFC, Left lateral PFC ←→ Right anterior TPJ, Right anterior TPJ ←→ Left anterior TPJ, Left anterior TPJ ←→ Right posterior TPJ for dynamic viewing (**Figure 2.5(a)**). For static viewing conditions (**Figure 2.5(c)**), the a) *intra-hemispheric* directional flows were: Right anterior TPJ ←→ Right Insula, Right anterior

TPJ ←→ Right lateral PFC, Right Insula → Right visual area, Right insula ←→ Right lateral PFC and, Right visual area ←→ Right lateral PFC, while the b) *inter-hemispheric* ones were: Right insula ←→ Left insula, Right visual area ←→ Left insula, and Right lateral PFC → Left Insula.

In the absence of salient distractors (WT) for dynamic viewing conditions, directed information flows were as follows, a) *intra-hemispheric*: Right Insula ←→ Right posterior TPJ, Right Insula ←→ Right visual area, Right visual area ←→ Right lateral PFC, Right visual area ←→ Right posterior TPJ, Right visual area ←→ Right anterior TPJ, Right anterior TPJ → Right posterior TPJ, Left Insula → Left anterior TPJ, Left Insula ←→ Left lateral PFC, Left Insula → Left visual area, Left anterior TPJ → Left visual area, Left lateral PFC → Left visual area, Left lateral PFC → Left anterior TPJ and; b) *inter-hemispheric:* Right Insula ←→ Left anterior TPJ, Left Insula ←→ Right posterior TPJ, Left Insula ←→ Right visual area, Left visual area → Right visual area, Right visual area ←→ Left lateral PFC, Right lateral PFC → Left anterior TPJ, Left lateral PFC ←→ Right posterior TPJ, Left lateral PFC ←→ Right anterior TPJ, Right anterior TPJ → Left anterior TPJ, Right posterior TPJ ←→ Left anterior TPJ, Right posterior TPJ → Left visual area, Right anterior TPJ → Left visual area, Right lateral PFC → Left visual area, Left anterior TPJ → Right visual area, Right anterior TPJ → Left insula, Left lateral PFC → Right Insula (**Figure 2.5(b)**). For static viewing, the following directed information flows were observed for WT, a) *intra-hemispheric:* Right visual area → Right insula, Right anterior TPJ → Right lateral PFC, Right lateral PFC ←→ Right visual area and; b) *inter-hemispheric:* Right visual area → Left insula, Left insula ←→ Right anterior TPJ and Left insula → Right Insula (**Figure 2.5(d)**).

Here, the information flow between Right Insula → Right lateral PFC and Right anterior TPJ → Right visual area (both for static stimulus, WT) were not taken into account because

they passed the permutation test but yielded negative TRGC values. The causality scores in dynamic stimulus condition for Right posterior TPJ → Right lateral PFC and Left lateral PFC → Right lateral PFC in WT; and for Right posterior TPJ → Left lateral PFC and Right posterior TPJ → Left Insula in ST were significant in the permutation test but showed negative TRGC values and hence, were overall considered as non-significant. All other causations were statistically significant and are illustrated in **Figure 2.5**.
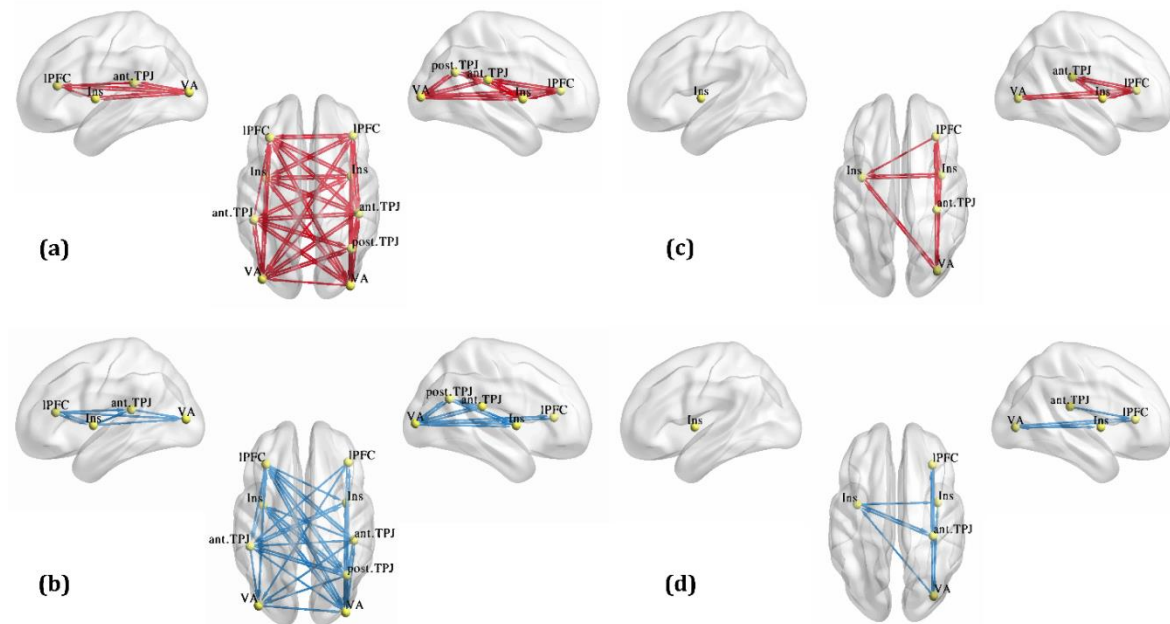
Figure 2.5. Directed interactions between the nodes of the Ventral Attention Network. The figure represents all significant causal interactions in the spectral domain (8-9 Hz) for node pairs based on their Granger causality scores for 'with saliency' (ST) as well as 'without saliency' (WT) trials in the dynamic (a, b) and the static (c, d) task conditions, respectively. The arrows point from the driver node towards the effector node. Red arrows indicate causations in trials with saliency (ST) whereas the blue arrows indicate causations in trials without saliency (WT).

2.4. Discussion

We investigated the importance of context specificity while processing saliency and the extent to which it reflects in the alpha modulation and its underlying neural networks. Three major empirical findings are underscored by our study. *First,* the spectral power corresponding to trials with saliency for two completely different task conditions, static and dynamic, show similar patterns of enhancement in terms of frequency (alpha band, 8-9 Hz) and magnitude. Spectral power modulations were not seen in any other frequency bands between 0.1 to 80 Hz. This suggests a task-independent role of alpha oscillations whose characteristic properties do not change with the task condition (e.g., static/ dynamic) *per se* while processing salient distractors. We verified that the rise in alpha power is only tagged to "saliency" and not to the complexity/difficulty level of a task condition, as the neutral trials (NT) which were the most difficult trials (seen through their significantly high reaction times than other categories of trials) did not show an increase in their alpha powers as compared to powers of Without saliency trials (WT) in both the tasks. *Second,* the underlying sources of the alpha oscillations obtained through EEG source localization were the lateral pre-frontal cortex (lPFC) (including IFG and MFG), the temporo-parietal junction (TPJ), the insula and the visual areas comprising Broadman area 18 (visual association area) and 19 (Please refer to **Table 2.2** for details). All these regions (except the visual area) together form the Ventral Attention Network, as reported in numerous previous studies (Allan et al., 2020; Vossel et al., 2014; Han and Marois, 2014; Corbetta et al., 2008), also known to be the main underlying network in the process of reorientation. The sources showed significant activations in both static and dynamic tasks on contrasting ST versus WT, further reiterating our earlier inference that the neural patterns of alpha enhancement vis-à-vis saliency and the underlying VAN are completely agnostic to task conditions in the visual modality. *Third,*

the directed information flow between the key regions of the VAN also reflected a common pattern of interaction across static and dynamic task conditions: Right anterior TPJ ←→ Right insula ←→ Right lateral PFC ←→ Right anterior TPJ, also indicating the presence of a more right-lateralized network, operational only in the presence of salient distractors. This pattern of interactions was missing in the trials without saliency and was consistent across both static and dynamic tasks. This common pattern of interactions also highlights the mode of directional information flows among the individual node-pairs, showing a bidirectional interaction rather than following a unidirectional bottom-up approach (**Figure 2.6**).

(a) **(b)**
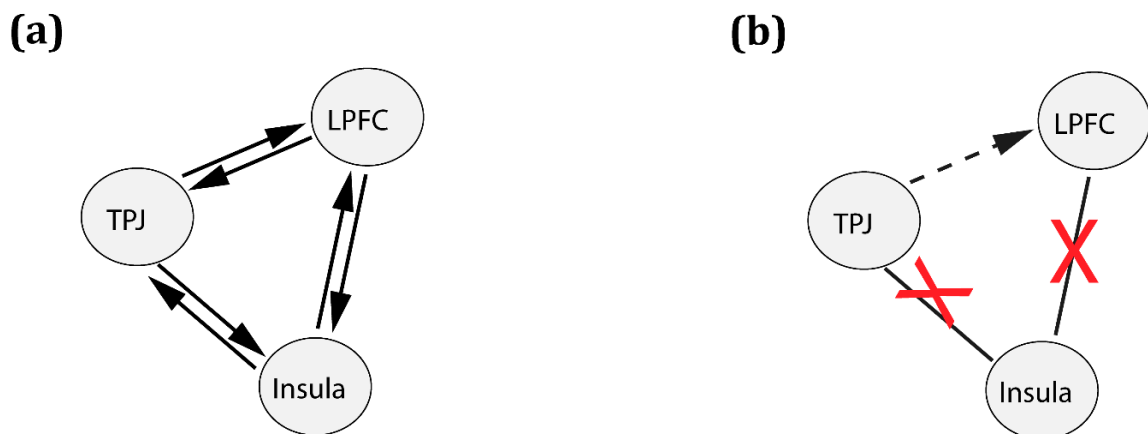
Figure 2.6. Organization of directed functional connectivity among the nodes of the Ventral Attention Network. The schematic outlines the common causal patterns from static and dynamic stimulus conditions between the right hemispheric nodes in the (a) presence (ST) and (b) absence (WT) of a salient distractor while performing a goal-directed task. The solid arrows indicate significant causations in both static and dynamic stimulus conditions while the dashed arrow indicates significant causation (95% confidence interval) only in static stimulus condition.

Neural oscillations and behavioral correlates of saliency processing

Behavioral results of the present study indicated that the salient distractor in the ST caused an increased latency in reaction time (Noonan et al., 2016) as compared to WT in both the task conditions (**Figure 2.2(c), 2.2(d)**). This can be attributed to 1) the 'pop-out' property of the salient distractor because of which there was an attentional reorientation and 2) the re-engagement of attention back to the goal-driven task. These two sub-processes are absent in WT, and hence they have a comparatively shorter reaction time.

Power spectral density results showed significantly enhanced alpha power (8-9 Hz) for salient trials (ST) compared to WT (**Figure 2.3**). Whether this enhanced alpha response arises from increased neuronal processing or is a functional mechanism for filtering distracting visual stimuli may be disentangled using directed functional connectivity analysis as discussed in the later sub-sections. Consistent with our PSD results, several studies using attentional (spatial) cueing paradigms have previously reported an increased amplitude in alpha band power for the to-be-ignored as compared with the to-be-attended location (Capilla et al., 2014; Capotosto et al., 2009; Feng et al., 2017; Frey et al., 2014; Ikkai et al., 2016; Kelly et al., 2006; Rihs et al., 2007; Schneider et al., 2019; Thut et al., 2006; Voytek et al., 2017; Worden et al., 2000). We not only replicated these findings but also extended the results for a task with spatio-temporal complexity (dynamic stimulus) as well. Our results that salient distractors cause an alpha power increase are, however, not in agreement with a previous MEG study (McDermott et al., 2017), where they observed an alpha power decrease in the incongruent condition as compared to the congruent condition during the performance in an Eriksen flanker task. Interestingly, these alpha modulations were observed between a frequency range of 9-12 Hz, which opens up future avenues for research to test how the low (8-9 Hz) and high (9-12 Hz) alpha frequencies of the brain respond differentially

to saliency. Although such deviation in results could also be due to differences in EEG and MEG sensitivity to cortical responses.

Underlying cortical sources of saliency processing across task conditions

A comparison between the two topoplots (**Figure 2.3(c), 2.3(d)**) indicated the presence of a possible overlap of regions comprising the right centro-parietal and parietal; the left fronto-central and frontal; and the temporo-parietal regions of the cortex in both the tasks while processing saliency related information (ST contrasted to WT) and guided us to further delve into the source space. Source reconstruction results revealed the presence of common sources across both the task conditions indicating a task-independent (static/dynamic) processing of salient distractors. One might argue here that the relative increase of alpha power calculated using alpha modulation index (AMI) might have negated all task-specific information, leaving behind stimulus properties attributable only to the salient distractors. In this context, we would like to emphasize the point that our dynamic and static task conditions consisted of salient distractors which too were dynamic and static, respectively, which supports our claim for the involvement of common neural correlates in saliency processing across different stimulus conditions.

We observed more bilateral sources in the case of dynamic stimulus condition which comprised both right and left anterior TPJ, insula, lateral pre-frontal cortices and visual areas. Sources for processing saliency in static stimulus condition were however, more right lateralized where, all the aforementioned regions were present only in the right hemisphere (except for the insula which showed a bilateral activation). As per extant literature, all these regions constitute the Ventral Attention Network (Vossel et al., 2014; Corbetta and Shulman,

2002; Downar et al., 2000) which has mostly been reported as "right-lateralized" (Schuwerk et al., 2017; Eddy, 2016; Krall et al., 2015; Han and Marois, 2014). It is this right-lateralized VAN that has particularly been implicated in spatial reorienting and in computing the behavioral relevance of salient signals (Krall et al., 2015; Carter and Huettel, 2013; Decety and Lamm, 2007). This right-hemispheric asymmetry is also seen in patients with hemi-neglect where there is a predominance of right rather than left TPJ lesions (Downar et al., 2001). The presence of a bilateral insula in both the task conditions corroborates with previous studies where the insula has been reckoned as the key hub of a bilateral "salience network", another relevant network involved in the detection of novel salient stimuli and task switching (Jakobs et al., 2012; Menon and Uddin, 2010; Seeley et al., 2007). However, the insula has also been considered as a part of the VAN in several studies (Farrant and Uddin, 2015; Han and Marois, 2014) because the anterior insula overlaps with the Ventral Frontal Cortex (VFC) which is an important node of the VAN (Corbetta and Shulman, 2002).

Since the VAN is believed to facilitate the detection of salient/distracting stimuli, it is not surprising that the regions of this network would show stronger responses during ST compared to WT. Although studies suggest that the VAN does not work in isolation but concomitantly with the Dorsal Attention Network (DAN) to process salient stimuli (Vossel et al., 2014), our source localization results for the modulated alpha (8-9 Hz) did not show activation in regions of the DAN. One possible reason for the conspicuous absence of DAN may be related to the fact that the frequency domain of interest in this study was at the low alpha range. Another possible reason could be when ST was contrasted with WT, the source powers of the regions of the DAN got negated if present somewhat equivalently in both, ST and WT. Therefore, we chose to consider only VAN nodes for the directed functional connectivity analysis.

Directed functional connectivity between the regions of VAN

In this study, the identification of a common set of brain areas underlying alpha enhancement across two types of stimuli warrants an understanding of the directed functional connectivity among candidate nodes of the VAN in various task contexts. Higher number of causal connections in the dynamic task (**Figure 2.5(a), 2.5(b)**) may be attributed to the spatio-temporal demands of the task where the distractor changed its position in space at every instant of time and needed to be actively ignored via attentional mechanisms for the entire stimulus display. Overall, the sensory areas comprising the left and the right visual areas direct brain regions commonly attributed to higher order processing, more strongly in ST than in WT (detailed GGC values are presented in the *Appendix*) suggesting the involvement of enhanced bottom-up attention to process salient events during ST. In the dynamic task, we observed that the lateral PFC, the insula and the anterior TPJ have a higher causal strength of inter-hemispheric connections in ST as compared to WT. Such bilateral interactions between the node-pairs indicate a coordinated activity of both the hemispheres of the brain required to process salient distractors in a spatio-temporally complex environment. Functional connectivity patterns in earlier studies showed that it is the anterior TPJ that is mainly connected with the inferior frontal gyrus (part of the lPFC) and the anterior insula as part of the VAN (Gillebert et al., 2013). Our directed functional connectivity analysis further extends these results with consistency where we see significant causal interactions of the insula and lateral PFC with the right anterior TPJ (supramarginal gyrus) but not with the right posterior TPJ (angular gyrus), particularly in the trials with saliency (ST).

Two previous fMRI studies have investigated the effective connectivity and causal interactions between DAN and VAN using DCM (Vossel et al., 2012) and Granger Causality (Wen et al., 2012b), respectively. In the DCM study, directed influences within the VAN

were observed from the right TPJ to the right lateral PFC (right IFG in particular) during the reorientation of attention to invalid cues in a grating orientation discrimination task. Both these studies however did not consider the effect of Insula in the VAN and focussed mostly on the connectivity modulations between rTPJ and rIFG/rMFG in the presence and absence of saliency. In our study, using a GC approach we also considered the interactions of insula with rTPJ and rlPFC, as we obtained all the 3 regions from source reconstruction in both static and dynamic task conditions. Also, since insula plays an important role in task switching (Pedrazzini and Ptak, 2019) and interference suppression demanding moment-to-moment adjustments (Wilk et al., 2012), we believe that it is important to incorporate the region to clearly identify the directed functional connectivity underlying saliency processing. We observed that the **Right anterior TPJ ←→ Right insula ←→ Right lateral PFC ←→ Right anterior TPJ** across both the tasks but only in ST (**Figure 2.6(a)).** This organization of directed information flow was completely absent in the absence of saliency (WT) (**Figure 2.6(b)**) which in accordance to previous literature suggests that the VAN remains suppressed while performing a goal-directed task. This suppression however, might not be because of the suppression of the VAN nodes as such, but because of the suppression in directional interactions between the nodes. Our results demonstrate that the operational mechanism of flexibly switching from a goal-directed task to saliency processing may lie in reconfiguration of network interactions for the reorientation of attention. Our results particularly characterize how information flows between the TPJ, the insula and the IFG in the right hemisphere are crucial for processing saliency across tasks. The directional interactions within the nodes of the DAN have been well investigated previously (Bressler et al., 2008) but as per our knowledge, this is the first EEG study to report the directional interactions among the nodes of the VAN and to capture the neural oscillations associated with the activity of this network. As a cautionary note, the spatial accuracy of these nodes

based on EEG source localization comes with several limitations, nonetheless, underpinning the transient changes in neural dynamics during reorientation of attention requires temporal precision which is difficult to achieve through other neuroimaging techniques like fMRI. Some recent evidence has shown that the detection of very focal activations for cortical sources may be possible using the source reconstruction algorithm eLORETA (Halder et al., 2019a). Furthermore, we have co-registered the EEG of individual participants with their respective brain MR images instead of directly warping the individual brain recordings to a standard template, to get a more accurate spatial estimate.

Finally, a prospective avenue for future research will be to study the interaction of the VAN with other intrinsic networks of the brain such as the default mode network (DMN), saliency network (SN), dorsal attention network (DAN) and central executive network (CEN) which is currently outside the scope of this study. Another interesting direction to investigate will be to explore the thalamic contribution to the reorientation of attention as some resting state studies have recently hypothesized a major role of the thalamus in saliency processing (Das et al., 2020). Some previous studies have shown that abnormality in alpha oscillations correlates with attentional disorders (Lenartowicz et al., 2018; Mazaheri et al., 2014). Atypical alpha asymmetry during covert attention has been observed in attention deficit hyperactivity disorder (ADHD) compared with neurotypical populations (Hale et al., 2009). Extending our study to other modalities like auditory and multisensory can establish communication in alpha frequencies via the VAN nodes as a marker of saliency processing which is agnostic to task conditions. Such a marker can prove to be of significant diagnostic use in clinical studies.

Chapter 3

Spectral markers of context-independent processing of salient auditory distractors

3.1. Introduction

Sudden salient sounds in the environment always grab our attention reflexively even if it requires switching from a goal-driven task where attention is already engaged. While trying to process such sudden sounds (e.g., phone-ring during a lecture), we almost invariably look around for the source of the sound while trying to visualize it. This is however, not the case for visual salient distractors as we would not really be bothered by how a visual object would sound (pop-up ads while reading an article on the laptop) even if its appearance is sudden. Why does the auditory modality become dependent on the visual modality when processing such sounds? Yet, it is actually the auditory system that is more capable of detecting events that can happen from any direction in the 3D space. The core brain regions (the right TPJ, the right insula, the MFG/IFG) carrying out the attentional switch towards such distractor sounds together form a right-lateralized attentional network, known as the Ventral Attentional Network (VAN) (Corbetta et al., 2008; Downar et al., 2000). This network is involved in the reorientation of attention to such salient stimuli in both the visual and the auditory modalities (Fritz et al., 2007) but its presence in the auditory modality is reported to be bilateral (KIEHL et al., 2001; Mayer et al., 2006). Most of the existing studies have used fMRI BOLD signals to identify VAN activations during processing of salient stimuli

because of which they have been unable to capture the neural oscillations through which the regions of this network communicate with each other. Since abnormal VAN functioning is associated with several clinical conditions like ADHD and spatial neglect *(as discussed in Chapter 1)*, identifying the aberrant oscillations in this network can serve as early diagnostic tools to these pathologies. To achieve this goal, one must first identify the various oscillations underlying VAN processing and classify them across different stimulus contexts and modalities. Recent EEG study from our group (Ghosh et al., 2021) found that the regions of the VAN underlie modulations in the alpha frequency band (8-9Hz) during the process of reorientation to 'visual' salient distractors while performing stationary and moving visual attention tasks (thus reflecting context-independent processing within the visual modality). Based on these findings, we hypothesize that the neural mechanisms associated with processing salient auditory distractors too are not contingent upon the context (e.g., speech or non-speech) of the ongoing goal-driven auditory task and are executed by modulations in the alpha frequency band.

To test out our hypothesis, we designed three novel auditory tasks constituting three different auditory contexts including – a) pure tones (constant frequency over time), b) FM sweeps (increasing/decreasing frequency over time) and c) speech syllables (non-linear frequency modulations over time). These three contexts were carefully selected based on previous studies showing tasks involving categorization across non-speech sounds (pure tones, tonal contours, etc.) depended upon basic audio property extraction from the stimulus and hence, involved the low-level auditory areas of the brain only unlike speech sounds where, natural speech representations mostly existed in the auditory areas and categorizations thus involved higher order processing (Luo et al., 2005; Rogers et al., 2014). Palva et al., (2002) reported that different responses were evoked by speech and non-speech sounds in the gamma-frequency band but not in the low-frequency (0.1–20 Hz) bands at around 40–60ms from the

onset of the stimulus. The mismatch negativity (MMN), an electrophysiological response to an unexpected novel stimulus, was different for speech and non-speech stimuli (Aulanko et al., 1993; Phillips et al., 2000; Shtyrov et al., 2000; Vihla et al., 2000). Gootjes et al., (1999) on the other hand found significantly stronger N100m responses to vowels than to non-speech tones or piano notes over the left but not the right hemisphere. Eulitz et al., (1995) and Tiitinen et al., (1999) found a slightly later N100m for speech sounds than for tones, in both hemispheres. The peak latency of N100m was delayed for complex sounds as compared to basic sounds and, further, for speech sounds (Parviainen et al., 2005). In order to understand how auditory distractor sounds are processed while attending to the different auditory contexts/conditions, we looked at the spectral changes at the neural level due to the occurrence of naturalistic salient sounds while attending to tasks with steady-state, dynamic and speech audio stimuli. We used 60 such distractor sounds which were introduced at 200 ms post attentional engagement to the auditory contexts in an EEG study on healthy humans.

3.2. Methods

3.2.1. Participants

28 healthy human volunteers (median=26 years; min=22 years; max=36 years; 16 females) participated in this study with written informed consent. All participants were right-handed and reported no history of neurological or audiological problems. The study was conducted according to the ethical guidelines and prior approval of the Institutional Human Ethics Committee of the National Brain Research Centre, India. All participants had University degrees or higher and were remunerated for their participation. To avoid any attentional bias in the data, they were discouraged from consuming any stimulant/medication (e.g., tea/coffee/sedatives) before reporting for the experiment.

3.2.2. Experiment

The participants listened to auditory stimuli presented via sound tubes while performing a duration discrimination task (**Figure 3.1**). The task required participants to identify the longer/shorter audio (prompted before the presentation of a block) from a pair of identical sounds differing only in their durations of presentation. There were 6 blocks in total with 90 trials in each block. The target in 50% of the blocks was to identify the longer audio (and shorter audio in the other 50%). The responses were made using keyboard keys - key 1 was pressed if the response was the first audio and key 2 was pressed in case the response was the second audio. Each trial was made up of an audio pair (sound1 + delay + sound2) which lasted for a total duration of 1200 ms. There was a brief period of silence (delay) between sound 1 and sound 2 and its length was decided by the individual lengths of sound 1 and sound 2 such that the total length of a trial was fixed at 1200 ms. The audio pair durations used were: 300-500ms, 350-500ms and 350-550ms (and also, 500-300ms, 500-350ms and 550-350ms), standardized after pilot experiments on participants to set easily identifiable perceptual differences between sound 1 and sound 2. An inter-trial interval jittered between 1800-2200ms was used to minimize the temporal expectancy of the next upcoming trial.

3.2.3. Stimuli

All the participants performed 3 auditory attention-based tasks which consisted of 3 conditions of auditory stimuli, classified based on their changing frequency characteristics across the temporal scale : *Condition I* – Steady-state frequency, *Condition II* – Linearly rising/falling frequency and *Condition III* – Non-linear frequency modulation. The Condition I stimuli consisted of pure tones of frequencies 400 Hz, 600 Hz, 800 Hz, 1000 Hz and 1200 Hz; the Condition II stimuli consisted of up and down FM sweeps (1000-2000Hz,

600-1400Hz, 200-800Hz, 2000-1000Hz, 1250-500Hz); and the Condition III stimuli consisted of speech syllables (/ba/, /ta/, /tha/, /ka/, /ha/) in both male and female voices. All the stimuli were matched for loudness and were ramped up/down by 0.5ms at the beginning/end to prevent click illusion. The frequency patterns of Condition II stimuli were chosen such that they were equi-spaced on a log frequency (Mel) scale. All Condition III stimuli were generated using text-to-speech converting software Notevibe (https://notevibes.com/). Sound1 and sound2 of each trial were joined using the audio editing software Audacity (www.audacityteam.org). Each auditory task (or stimulus Condition) had three categories of trials called 'Without Saliency Trials' *(WT),* 'Saliency Trials' *(ST)* and 'Neutral Trials' *(NT)*, 30 each in every block (**Table 3.1**). Within a block, their presentation order was randomized. The paradigm design in WT was exactly as described above in the experiment section. In ST, additionally, a salient distractor sound was introduced at a latency of 200 ms from the onset of Sound1 which was played till the end of the trial such that post salience duration was 1000ms long (**Figure 3.1**). The salient distractor sounds ranged from phone bell ring to dog bark sounds which were obtained from a repository of naturalistic sounds called Soundbible (http://soundbible.com/). We used 60 such distractor sounds as listed in **Table 3.2**. To maintain uniformity, we ensured that ST across all the 3 stimuli conditions consisted of the same distractor sounds and since each stimulus condition corresponded to 2 blocks (and each block had 30 ST), none of these sounds were presented more than 3 times to preserve their saliency effect. In NT, sound 1 and sound 2 were equal in length but the participants were unaware of it and hence gave the perception of the most difficult trials. These trials were introduced to keep a check on the participant's attention such that if the participant was indeed attending to a task block, it would reflect in the reaction times across the 3 categories of trials.
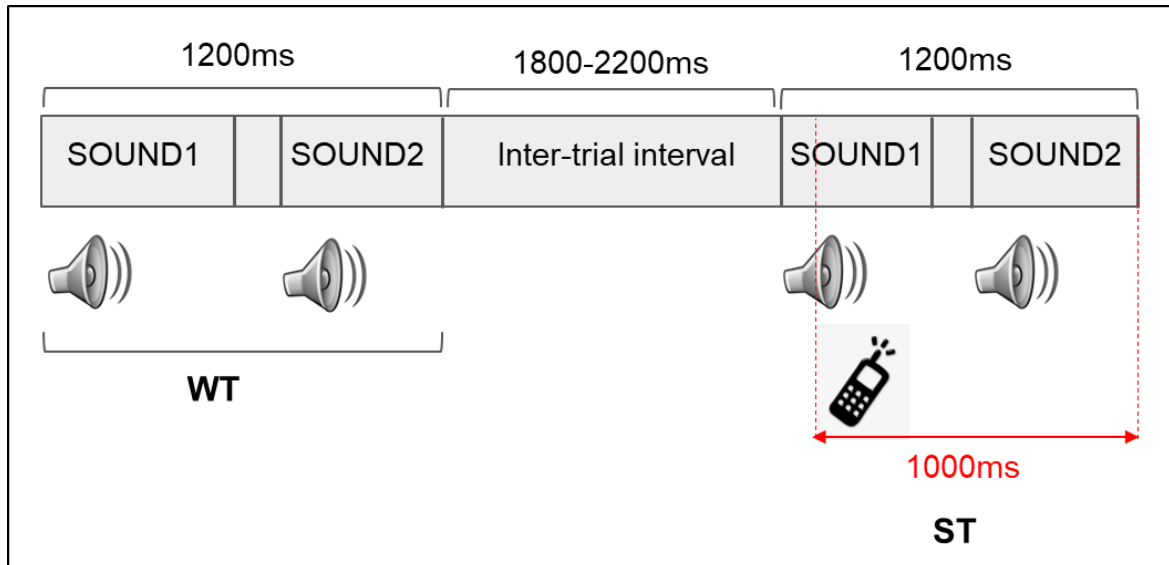
Figure 3.1. Auditory paradigm. An example of the auditory duration discrimination task is shown which comprises two identical sounds, sound1 and sound2, differing in their individual durations. The task was to identify the longer/shorter sound as prompted at the beginning of each block. Each block could comprise either of the three types of sound stimuli between pure tones (steady-state), FM sweeps (increasing/decreasing frequencies) or speech syllable sounds (in male/female voice). Within a block, there were 3 categories of trials - Without Saliency (WT), With Saliency (ST) and Neutral Trials (NT), presented in random order. In ST, a salient sound was additionally introduced at 200 ms from the onset of sound1, presented till the offset of sound2.

Table 3.1. Trial distribution across conditions.

Trial Information	Condition I	Condition II	Condition III
Total no. of blocks	2	2	2
No. of trials per block	90	90	90
Neutral trials (NT)	30	30	30
Without saliency trials (WT)	30	30	30
Saliency trials (ST)	30	30	30

Table 3.2. List of salient sounds used in the experiment.

SALIENT SOUNDS				
Phone ring	Big bell	SMS notification	Fire alarm	Utensils falling
Truck siren	Whistle	Crowd clapping	Thunder	Sheep bloating
Dog Bark	Drum roll	Saw sound	Rooster call	Night crickets
Cat meow	Evil laugh	Car racing	Cycle horn	Sniffing
Child cheering	Steam engine	Bomb drop	Airplane taking off	Brooming
Woman screaming	Dog growling	Angry growl	Baby crying	Milk pouring
Welding	Fireworks	Guitar playing	Devotional chanting	Tyrannosaurus
Brook	Flock of seagulls	Birds chirping	Clash of swords	Coughing
Eagle screeching	Bats screeching	Lion roaring	Helicopter	Nose blow
Spanish no. counting	Funny human sound	Child speaking gibberish	Car engine starting	Tongue rolling
Coins dropping	Gibbon monkeys	Bottles rattling	Toilet flush	Generator start
Gunshot	Cartoon	Party crowd	Motorbike	Wind chimes

3.2.4. EEG data acquisition

The participants were seated in a dark soundproof room during the experiment and were asked to focus on a central '+' fixation displayed on the computer screen placed right in front of them to minimize eye movements. EEG data were collected from 63 active electrode channels using Brain Vision EEG recording system and acquisition software with the reference electrode at FCz and ground anterior to AFz. The channel impedances were constantly monitored and maintained below 10 kΩ. Data were acquired at a sampling rate of 1000 Hz and a 50 Hz line noise filter was applied online in the Brain Vision software. All the responses were marked by receiving triggers at key presses on a computer keyboard recorded through the NBS Presentation software. The participants were briefed about the task before the commencement of the experiment and a short demo of the paradigm was presented to them for a better understanding of the task. They were instructed to listen to the stimuli carefully during the experiment and to respond as fast and as accurately as possible to all the trials. If a trial had more than one response, only the first response was considered for further analysis. The blocks were randomized across participants and a rest period was allowed after every block. After the EEG session, the 3D location of electrodes were recorded using a Polhemus Fastrak system with a set of fiducial points (Cz, nasion, inion, left and right pre-auricular points) while the EEG cap was placed on the participant's head.

3.2.5. EEG data preprocessing

The EEG data were pre-processed using the EEGLAB toolbox (Delorme and Makeig, 2004) and custom-written scripts in MATLAB (www.mathworks.com). The raw data were first imported and bandpass filtered between 1-90 Hz using zero-phase Hamming-windowed sinc FIR filter. The filtered data corresponding to time stamps before and after a block

presentation period were removed. The data were visually inspected at this stage and one participant's data was discarded because there were more than 5 noisy channel recordings. One channel (T8) in another participant was noisy and was hence interpolated to neighboring channels. Independent component analysis (ICA) was then applied block-wise to each participant's data and the ICs corresponding to eyeblinks and eye movements were visually identified and removed. Next, the data were average re-referenced, epoched and sorted according to the trial categories, i.e., WT, ST and NT, based on their trigger information. Each epoch was 1400 ms long, with 200 ms of pre- and 1200 ms of post-stimulus activity. Each trial (epoch) was baseline corrected and any linear trends were removed from them. To ensure that our neural data were free from any muscular or electrocardiograph artifacts, we further set a threshold of $\pm75\mu V$ such that trials with an amplitude more than this threshold were rejected from all the channels.

3.2.6. Data analysis

The reaction time and accuracy of each trial was recorded across all conditions using NBS Presentation software. The reaction time was defined as the duration from the onset of a trial till the participant hit the response key. To have a better estimate of the participant's engagement with the task, the blocks with accuracy <70% were rejected for further analysis. Such blocks represented around 7% of the total blocks. Reaction times (RTs) less than 100ms, responses made after the commencement of the subsequent trial and the trials without any responses were not considered for analysis. All trials from the 27 participants were sorted based on the above criteria and their reaction times and % accuracies were computed and compared across WT, ST and NT for conditions I, II and III. The pre-processed EEG data was Fourier transformed using the mt_spectrumc (multi-taper method)

function of Chronux toolbox. As the behavioral performance was above 70% correct, we included both the correct and incorrect trials to have a good signal-to-noise ratio. For all these trials, we used 1000 ms data segments post-saliency to have an even comparison across WT, ST and NT. Therefore, for WT and NT, data were extracted 200 ms onwards post-stimulus onset which was exactly when saliency was introduced in ST. The sampling frequency was set to 1000 Hz, time-bandwidth product to 3, Slepian tapers to 5 with padding set to zero (default). Using these parameters, we obtained the power spectrum between 1-90 Hz. Next, we removed the 1/f aperiodic component from the power spectrum as it can severely bias the observable changes in power, especially at the lower frequencies. To do this, we modeled the 1/f trend of the log-transformed power spectrum using a least-squares method and then subtracted it from the original power spectrum (Neto et al., 2015; Haegens et al., 2014).

3.2.7. Statistics

The statistical analyses on reaction times and power spectra were performed using non-parametric Wilcoxon signed rank test at 5% significance level to compare any significant differences across WT, ST and NT in conditions I, II and III.

3.3. Results

3.3.1. Behavioral performance

The overall accuracy (% correct responses) of participants in WT for task conditions I, II and III were 93.64, 90.6 and 88.4, respectively that dropped in the presence of salient distractors (ST) to 89.4, 84.5 and 72.9, respectively **(Figure 3.2).** Since the neutral trials

(NT) were not designed to have any correct responses, they were not a part of the accuracy comparisons. The trial-wise medians of RTs (in milliseconds) in WT, ST and NT, respectively for Condition I were 1649.4, 1694.6 and 1905.9; for condition II were 1663.7, 1745.2 and 1891.3; and for condition III were 1708.1, 1802.9 and 1938. In all three conditions, the RTs of NT were significantly higher than that of ST ($p<0.0001$) and WT ($p<0.0001$), whereas the RTs of ST were significantly higher than that of WT ($p<0.0001$), exhibiting a common trend where RTs of NT>ST>WT **(Figure 3.3).**
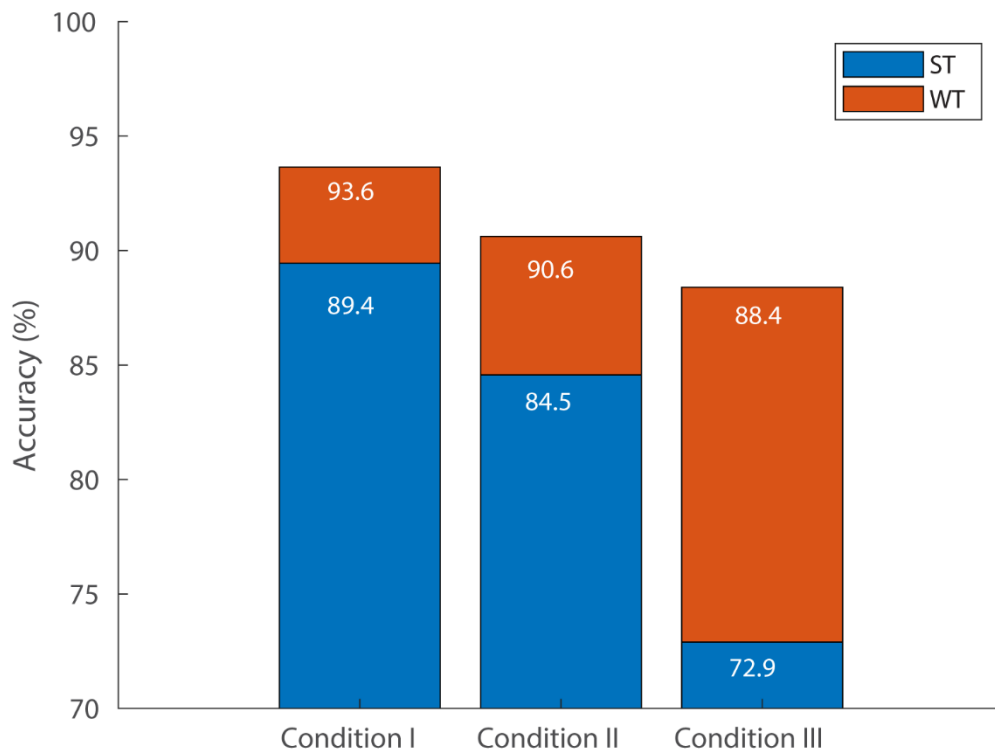
Figure 3.2. Accuracy across tasks. The stacked barplots represent the average percent accuracies of all participants in trials Without Saliency (WT) and With Saliency (ST) across conditions I, II and III.

(a) Condition I

(b) Condition II
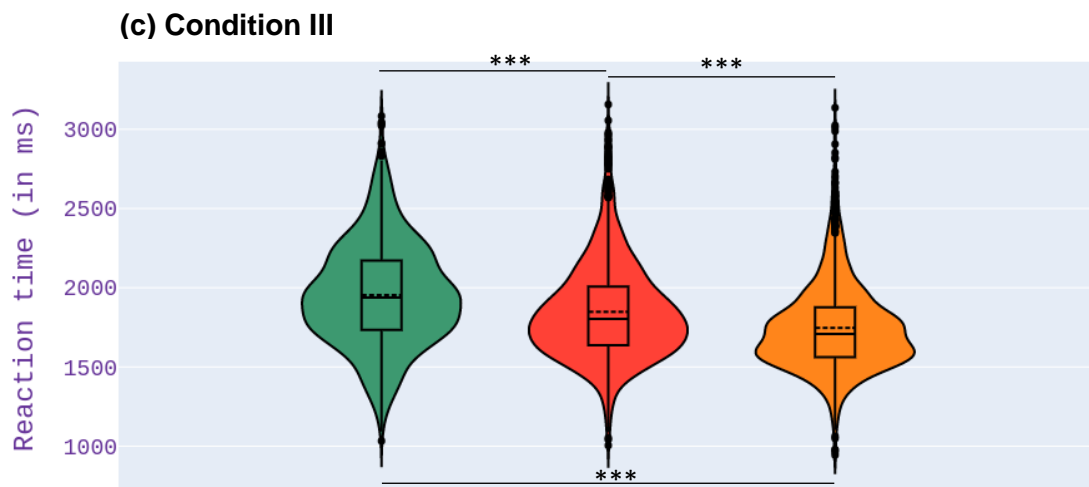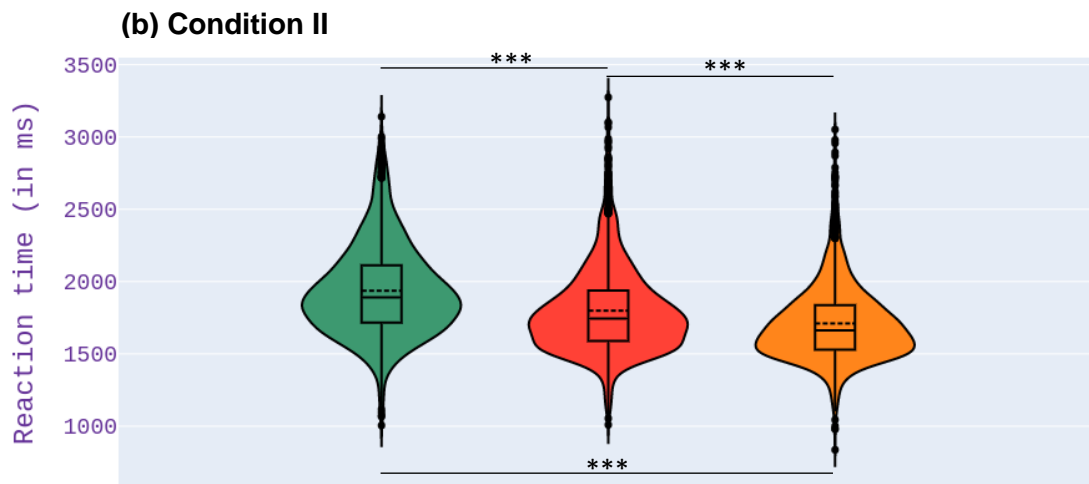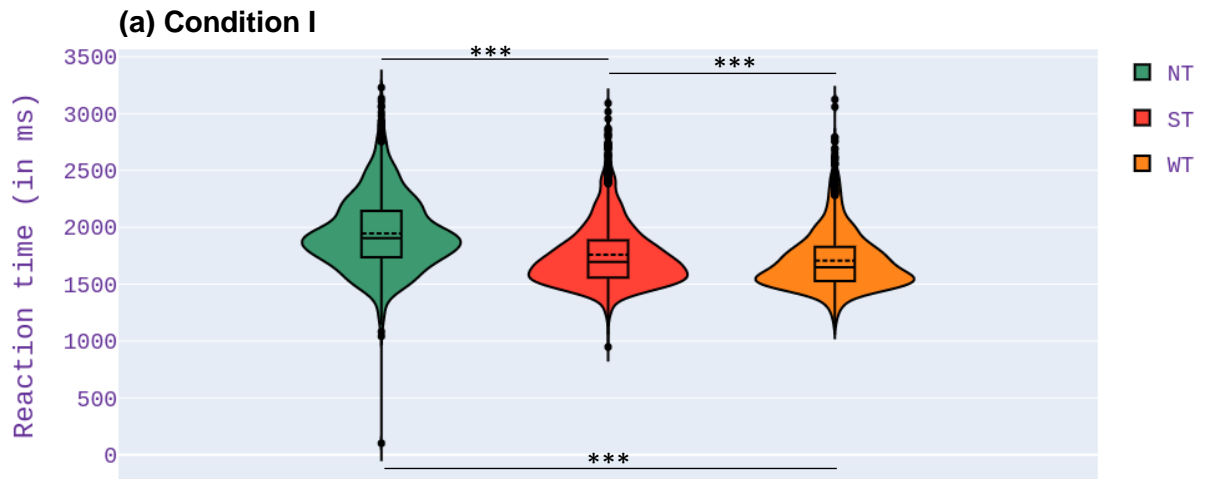
(c) Condition III

Figure 3.3. Reaction times (RTs) across tasks. The violin plots represent the distribution of reaction times of all trials in Without Saliency (WT), With Saliency (ST) and Neutral Trial (NT) categories for (a) Condition I, (b) Condition II and, (c) Condition III. The solid line at the center represents the median of the distribution and the dotted line represents the mean. The *** represents a significant ($p<0.0001$) difference between any two categories of trials.

3.3.2. Modulations in the power spectra

The power spectrum obtained for each trial was averaged and collapsed across all the 63 sensors to obtain the grand-average power spectra of WT, ST and NT for conditions I, II and III (**Figure 3.4**). Between 1-90 Hz, significant differences were seen in the power spectra of WT and ST at the alpha frequency (8-10 Hz) and the late beta frequency (25-29 Hz) bands for all three stimulus conditions. In condition I, the alpha power of ST was significantly lower than that of WT ($p=0.035$) but no such differences were seen in the power of NT. In condition II, the alpha power of ST was significantly lower than that of both WT ($p=0.032$) and NT ($p=0.002$) but there were no significant differences in the alpha power of WT and NT. In condition III, the alpha power of ST was significantly lower than that of WT ($p=0.003$) and again, no significant differences were seen in the power of NT. Interestingly, we also observed significantly reduced late beta power in ST as compared to WT in Condition I ($p=0.0001$), Condition II ($p=0.028$) and Condition III ($p<0.0001$) but no such differences were observed between the late beta powers of WT and NT. We observed significantly lower beta power of ST as compared to NT in Condition I ($p<0.0001$) and III ($p=0.005$).

(a) Condition I
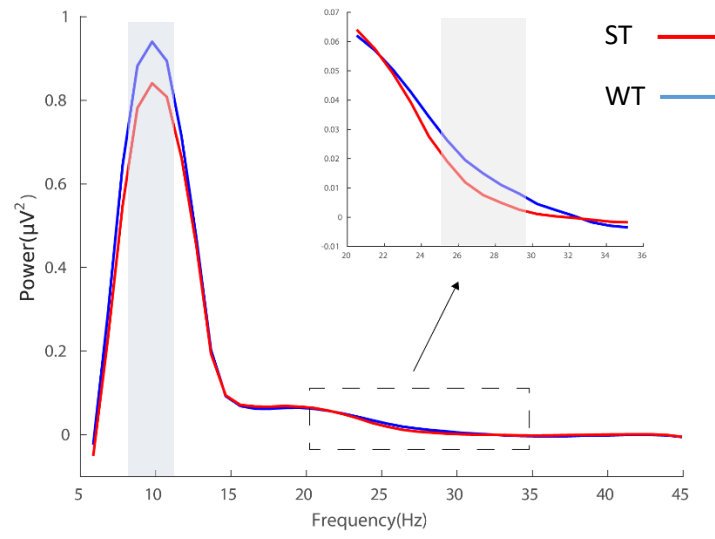
(b) Condition II
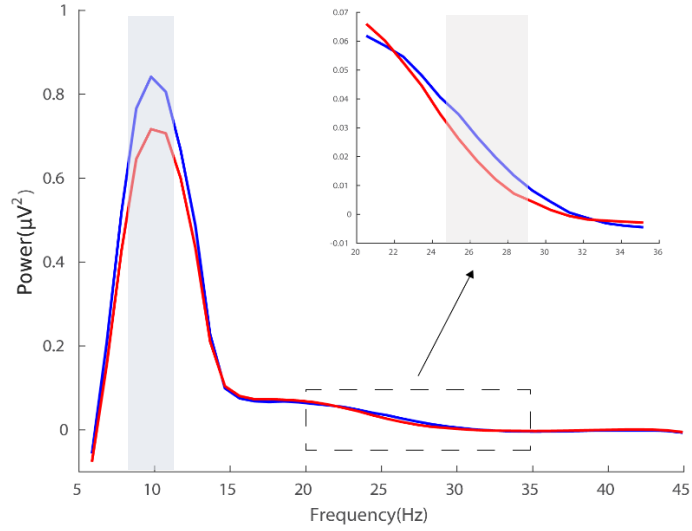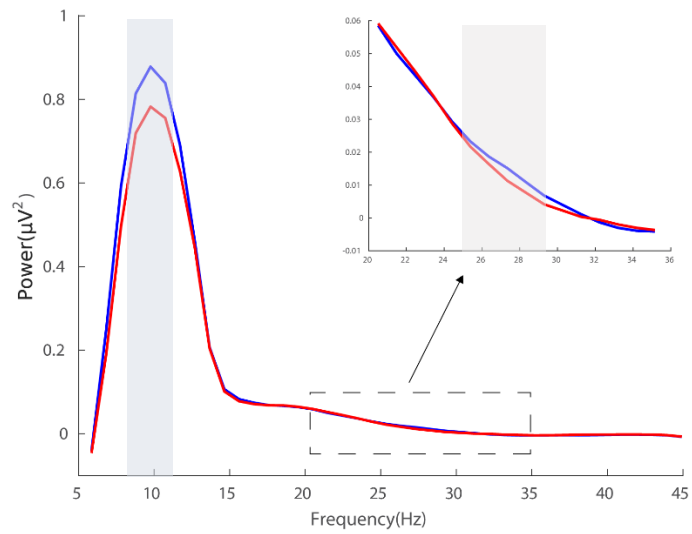
(c) Condition III

Figure 3.4. Power spectral density. The mean global power spectra plots while performing tasks in (a) Condition I, (b) Condition II and (c) Condition III are shown, representing the 1/f noise removed periodic power spectra of without saliency (WT) and saliency trials (ST). The insets are the zoomed-in portions at frequencies ~ 20 to 35 Hz. The gray shaded regions represent the frequencies with significant differences in power between WT and ST.

3.3.3. Distribution of power modulations in the sensor space

The sensor-wise distribution of the decrease (ST-WT) in alpha (8-10 Hz) and late beta (25-29 Hz) powers for conditions I, II and III are represented using topoplots in **Figure 3.5**. In condition I, the maximum decrease in alpha power was observed in sensors P7, P5, P3, P1, Pz, P6, P8, PO8, PO4, POz, PO3 and PO7; in sensors P7, PO7, PO3, O1, POz, Oz, PO4, O2, PO8, P6 and P8 for condition II; and in sensors P7, P5, P3, P1, Pz, P4, P6, P8, PO8, PO4, O2, POz, PO3, PO and O1 for condition III.   The maximum decrease in the late beta power was seen in sensors F7, F5, AF7, Fp1, AF3, Fp2, AF4, AF8, F4, F6, F8, FC6, FT8, T8 and PO8 for condition I; in sensors F7, F5, AF7, Fp1, AF3, AFz, AF4, F4, FC4, FC6, F8 and PO8 for condition II; and in sensors FT7, F7, F5, AF7, Fp1, Fp2, AF4, AF8, F2, F4, F6, F8, FC4, FC6, FT8, T8 and PO8 for condition III.

Alpha power modulation to process auditory salient distractors

Late beta power modulation to process auditory salient distractors

(a) Condition I   **(b) Condition II**   **(c) Condition III**
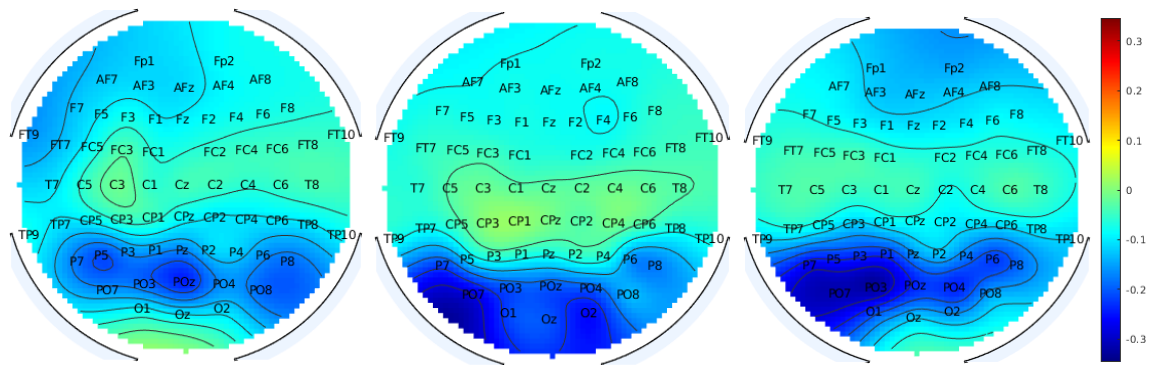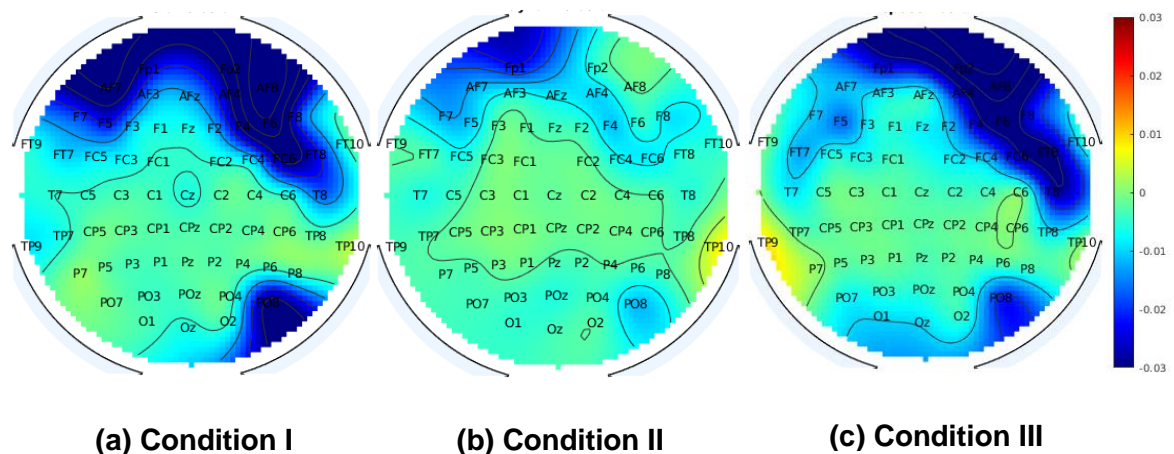
Figure 3.5. Power distribution in sensor space. The top panel shows the sensor-wise distribution of significantly decreased alpha power (WT-ST) between 8-10 Hz in the presence of salient distractors for (a) Condition I, (b) Condition II and (c) Condition III. The bottom panel depicts the sensor-wise distribution of significantly decreased late beta power (WT-ST) between 25-29 Hz for (a) Condition I, (b) Condition II and (c) Condition III. The plots show differences of 1/f corrected power of ST and WT at the two frequency bands.

3.4. Discussion

We investigated the neural correlates of processing salient distractors while actively attending to three auditory tasks with sound stimuli having different spectro-temporal properties. Our results reveal a condition-independent effect in auditory distractor processing as both the behavioral and spectral changes associated with distractor processing remain conserved across the three task conditions. We observed a drop in the accuracies of ST in conditions I, II and III, more so for condition III as speech stimuli was the most complex condition out of the three and separating speech from auditory distractors during task performance was evidently, more difficult. The reaction times of the three stimulus conditions also followed the same pattern where the RTs of NT>ST>WT. All the between trial-category differences were significant within a condition. Since these behavioral responses can be thought of as a manifestation of the neural processes, higher reaction times of ST as compared to WT can be owed to the presence of distractors in ST which perhaps caused a brief reorientation from the main task, adding on to the reaction time. The design of NT was such that both the sounds in a trial were presented for exactly the same duration but since the participants were unaware of it, they were made to think that the two audio durations were very close to each other, adding to the difficulty level and thus, producing highest reaction times in all the three task conditions. We next looked at the spectral changes associated with salient distractor processing and found that there were modulations in the alpha and beta frequency bands invariably in all three conditions. There were significant reductions in the alpha (8-10 Hz) and the late beta (25-29 Hz) powers in ST as compared to WT. There were no such observable differences between the powers of NT and WT validating that the power changes in ST are actually due to salient distractor processing and is not just a byproduct of added difficulty to the task. According to literature, an increase in

alpha power represents an inhibited/suppressed state (Pfurtscheller and Lopes Da Silva, 1999) and therefore, a reduction in alpha power should represent cortical facilitation (Klimesch, 1996). The sensor space distribution of the alpha power revealed that it was mostly the parieto-occipital and occipital regions contributing to the reduced alpha power in ST in all three conditions. Concordant with these observations, a recent study (Keefe et al., 2021) showed that exogenous spatial orienting of attention to audio cues resulted in visual-cortical facilitation in the hemisphere contralateral to the attended location, without any suppression in the opposite hemisphere in the occipital cortex. Since the auditory stimuli delivered during our experiment were essentially binaural, it is not surprising to see bilateral visual-cortical facilitation in the occipital region (marked by the alpha power reduction) in the presence of auditory salient distractors(ST). However in condition III, the alpha modulation is stronger on the left parieto-occipital region as compared to the right side suggesting some speech specific effects from the task context (Zatorre et al., 1992). Moreover, alpha desynchronization during involuntary attention in response to salient sounds in the complete absence of visual stimuli has also been previously reported (Störmer et al., 2016). Based on our results and previous studies (Feng et al., 2017), one may conclude that salient unexpected sounds promote alpha power decrease in occipital regions to improve visual perception, suggesting that novelty detection in one sensory modality may enhance the processing of potentially relevant information in another one in anticipation of danger/reward.

The pattern of beta power reduction in ST is also similar for all three stimulus conditions. The sensors contributing majorly to the beta power modulation are mostly around the cortical regions of the right temporo-parietal junction, right insula and the left and right pre-frontal cortices. These areas primarily make up the ventral attention network (VAN) in the brain

(Corbetta et al., 2008; Corbetta & Shulman, 2002) and the same areas were seen to be underlying the processing of visual salient distractors in the alpha frequency band (Ghosh et al., 2021). This suggests that reorientation of attention to salient distractors in the auditory modality is mediated by beta oscillations in the brain marked by a reduced late beta power (25-29 Hz). These results however, need to be validated in the source space for further claims involving the VAN. In this direction, we have collected MRIs from all the participants to perform accurate source localization techniques using individual subject head co-registration and obtain the Brodmann areas underlying the spectral changes. Nonetheless, the present results of our study clearly indicate that the appearance of naturalistic auditory salient distractors while performing goal-driven auditory tasks are processed by the brain in a context-independent manner.

Chapter 4

Spatiotemporal mapping of neural markers of prediction error processing across unisensory and multisensory modalities

4.1. Introduction

The brain attends to complex stimuli by minimizing its response to frequent events that do not require extensive processing thus, freeing up the cognitive resources to process unexpected events (Fontolan et al., 2014; Friston, 2005). To subserve this goal, a neural representation (internal model) is constructed based on prior information from previous sensory inputs and any mismatch between the model and the subsequent sensory input gives rise to a "prediction error" (Kok et al., Winkler and Czigler, 2012). The prediction errors, at the cortical level, are known to generate two ERPs in the brain – the MMN (Mismatch Negativity) and the P300 (Banellis et al., 2020; Calcus et al., 2015; Chennu et al., 2013; Stefanics et al., 2014). The study of these two prediction error signals under multisensory contexts can aid in our understanding of how the brain scans the environment for regularity and change, making top-down predictions to facilitate the processing of novel bottom-up stimuli by trying to maximize the prediction accuracy. Prediction error propagation is organized hierarchically, such that the prediction error arising from a given area in turn serves as the input to the next area (Friston, 2005), consequently updating the internal models

at the hierarchical stages (Wacongne et al., 2011). To study these stages, we use an oddball paradigm, the most widely used paradigm because of its simplicity, reproducibility, and applicability across sensory modalities, where repetitive 'standard' stimuli are interspersed with rare 'deviant' stimuli.

A brief history of MMN and P300

The foundation of MMN and P300 research was laid more than half a century ago when the two ERPs were recognized as the markers of "uncertainty" (Sutton et al., 1965). Since then, both these markers have been extensively studied under various stimulus conditions and clinical scenarios. MMN appears as a negative deflection in the difference waveform between deviant and standard EEG signals around 100-250 ms post onset of a deviant stimulus with frontal/central/temporal generators in the brain (Garrido et al., 2009; Näätänen et al., 2007, 1978; Näätänen and Michie, 1979; Sams et al., 1985). It is known to index any deviance from a recognized pattern in sensory stimuli, with its amplitude indicating the degree of salience of the prediction error (Picton et al., 2000; Winkler, 2008). P300, on the other hand, is a positive deflection in voltage with a latency between 250 to 500 ms distributed across the fronto-central scalp locations indexing the possible attention switch and conscious perception of stimulus change (Giard et al., 1990; Polich, 2007a; Sutton et al., 1967). Its amplitude is sensitive to oddball probability and the amount of deviance from the standard stimulus, and its latency reflects oddball evaluation time (Johnson and Donchin, 1980). The MMN or N2a, N2b, and N2c are subtypes of the N200 ERP (Patel and Azzam 2005; Folstein and Van Petten, 2008). Both attended and unattended stimuli are capable of eliciting N2a, whereas the N2b and N2c only occur when attention is directed to target stimuli (Folstein and Van Petten, 2008; Muller-Gass et al., 2005). The P300 wave too, is

further separable into the slightly earlier (250-300ms), fronto-central P3a and the later (300-350ms), centro-parietal P3b, thought to be evoked by unpredictable/ task-irrelevant distractors and rare-target/ task-relevant stimuli, respectively (Courchesne et al., 1975; Kok, 2001; Polich and Criado, 2006; Squires et al., 1975). Our study, however, includes the temporal and spatial properties of only P3b as we use a two stimuli oddball paradigm where the oddball is the target. P300 being a late component, is associated with updating the working memory in oddball counting tasks (Donchin, 1981; Donchin and Coles, 1988) and has been linked to decision-making processes as well (Rohrbaugh et al., 1974). P3b is particularly thought to be involved in the deployment of selective attention to task-relevant stimuli under conscious awareness (Kok, 2001; Polich and Criado, 2006). On the contrary, MMN can be elicited pre-attentively, during non-attentive states such as sleep (Molholm et al., 2005), behavioral unconsciousness (Atienza et al., 2001; Koelsch et al., 2006), or even in coma (Morlet and Fischer, 2014). It has provided researchers access to pre-conscious processing of temporal structure in mostly auditory information beyond the basic sensory stage before it enters conscious perception or stages of attention (Chennu and Bekinschtein, 2012; Wijnen et al., 2007). It however, can also be modulated by attention (Alain and Woods, 1997; Woldorff et al., 1998), the reason why there is a sustained empirical interest in MMN to date. Earlier, MMN was thought to reflect auditory mechanisms only (Nyman et al., 1990) but substantial pieces of evidence now suggest it has a visual counterpart too, popularly known as vMMN (Pazo-Alvarez et al., 2003; Stefanics et al., 2014).

Importance of research on multisensory prediction errors

Most prediction mismatches in our surroundings are perceived through not one but multiple sensory modalities (Luca et al., 2009), e.g. noticing the brake lights of a car in front while

engaged in listening to the radio. From a predictive coding perspective, the internal mental model of sight, sound, smell, taste and touch are integrated with our existing cognitive schemata (Talsma, 2015). Processing of novel bottom-up stimuli in one modality can subsequently modify the neural representation and hence top-down prediction, of a stimulus in another sensory modality. If multisensory integration involves such complex interactions between top-down and bottom-up processes, then it should take place at multiple stages of processing, based on the complexity of the stimuli involved (Molholm et al., 2002). The first distinct stage of multisensory integration was identified at about 100 ms of speech stimulus onset where the audio-visual N1 component peaked earlier than that of the auditory speech stimulus alone (Stekelenburg and Vroomen, 2007; Van Wassenhove et al., 2005). Interestingly, a few studies using oddball stimuli have also shown that multimodal stimulation (visual-audio-tactile and visual-audio) induces a significant early onset of latency (Marucci et al., 2021; Stefanics et al., 2005), and a significant increase in the amplitude of the P300 potentials (Fleming et al., 2020; Marucci et al., 2021) as compared to the corresponding unimodal stimulations. Feng et al.(2008), however, did not observe such multisensory benefits for P300 latencies along with Giard and Peronnet (1999) who reported that multimodal P300 may not necessarily be a linear sum of unimodal P300 components. In a recent study using the oddball paradigm (Shiramatsu et al., 2021), the latency of audio-visual MMN resembled closely to the latency of audio MMN than that of visual MMN, indicating the advantage of audio MMN over visual MMN. On the contrary, a previous study (Sittiprapaporn, 2012) using a different oddball paradigm showed visual and audio-visual MMN had shorter latencies than auditory MMN. Thus, the properties of both MMN and P300 based on latency and amplitude vary with the paradigm and experimental parameters like length of the stimulus, stimulus probability, target to target interval and discrimination difficulty (Gonsalvez et al., 2007; Gonsalvez & Polich, 2002; Magliero et al., 1984; Patel &

Azzam, 2005; Polich, 2007) as well as physiological variables such as age, attention and neurophysiological disorders (Blackwood, 2000; Dinteren et al., 2014; Erickson et al., 2016; Polich et al., 1990). A critical question that still remains is if the modality of the prediction error changes, whether a common set of neural areas generate these ERPs, or are they an outcome of information processing within the modality-specific sensory regions?

On what is yet to be known

Despite a huge body of research on MMN and P300, a single comprehensive study comparing the spatiotemporal properties of these two prediction error markers for unisensory and multisensory modalities is not available. From this perspective, we hypothesize that (i) the speeded responses to multisensory stimuli are also seen in the middle/late processing stages of prediction errors, i.e., for MMN/P300, and (ii) there exists a sensory-cognitive dissociation in the source distribution of MMN and P300. To validate our hypotheses, we investigate the properties of prediction error markers - MMN and P300, from very simplistic active viewing and listening tasks using a multimodal oddball paradigm. Furthermore, we perform rigorous source analysis using co-registration with individual subjects' MRI data to reveal the overlapping cortical networks and specialized brain regions specific to unimodal/ multimodal MMN and P300. Traditional oddball paradigms consist of a mismatch between frequent and deviant stimuli belonging to the "same modality". However, a "cross-modality", where the modality of the frequent and the deviant stimuli are different, may recruit different brain regions for oddball processing as the non-target standard modality can be completely ignored, unlike the usual multisensory interactions. The goal of the current article is to replicate previous findings of MMN and P300 research in the light of prediction

error processing with conceptual advancement in the organization of the cortical sources along the predictive coding hierarchy in the brain.

4.2. Methods

4.2.1. Participants

22 healthy volunteers (9 males and 13 females) in the age group of 22 to 43 (mean=25.7, SD=±4.19) years participated in the study. They had normal or corrected-to-normal vision and were right-handed. All participants had University degrees or higher and reported no history of neurological or audiological problems. They were requested to avoid the intake of any medication/stimulant (e.g., sedative, coffee, etc.) before the experiment. They provided informed written consent at the beginning of the experiment and were remunerated for their participation. The study was carried out following the ethical guidelines and prior approval of the Institutional Human Ethics Committee of the National Brain Research Centre, India.

4.2.2. Stimuli

The experiment consisted of five different conditions and each condition consisted of two categories of stimuli, i.e., repetitive/frequent/standard and non-repetitive/oddball/deviant. Two of the five conditions presented were ***unimodal,*** i.e., audio only and visual only; the third was ***bimodal,*** i.e., audio-visual; and the remaining two were ***cross-modal*** in nature. In the first three conditions, the standard and the oddball stimuli were of the same sensory modality which means that the *audio-only condition* comprised of an audio standard and an audio oddball stimuli; the *visual only condition* comprised of a visual standard and a visual oddball stimuli, and; the *audio-visual (AV) condition* comprised of an audio-visual standard

and an audio-visual oddball stimuli. The remaining 2 conditions, namely, the *cross-audio* consisted of an audio deviant and a visual standard and the *cross-visual* consisted of a visual oddball and an audio repetitive stimuli. The contents of each condition are tabulated in **Table 4.1**. Each condition consisted of 400 trials, out of which oddballs constituted 14 percent of the total trials. Each condition was presented in the form of a block of 100 stimuli, where the standard and oddball stimuli of a particular condition were presented in random order and the number of oddball stimuli varied across each block. There were 20 such blocks (5 conditions x 4 blocks) that were randomized and presented to the participants. The participants were prompted about the modality of the upcoming block before every run and to engage their attention throughout the entire block, they were asked to count the number of oddballs presented in each block and report at the end of the block.

Condition	Standard / Frequent / Repetitive	Deviant / Oddball / Infrequent / Non-repetitive
Unimodal (Audio only)	261.6 Hz	523.3 Hz
Unimodal (Visual only)	Blue Square	Red Triangle
Bimodal (Audio-Visual)	261.6 Hz and Blue Square	523.3 Hz and Red Triangle
Cross-modal (Audio deviant)	Blue Square	523.3 Hz
Cross-modal (Visual deviant)	261.6 Hz	Red Triangle

Table 4.1. The table lists the standard and the deviant stimuli used in our oddball paradigm for all the five sensory modality conditions.

The stimuli of the visual only condition consisted of a standard blue square and a deviant red triangle. The auditory stimuli were inspired from musical notes, the standard as the C4 note and the deviant as the C5 note (higher octave), according to the tuning of the A440 pitch standard. All stimuli were presented on a white background on a 21″ LED screen (1280 × 1024 pixels). The participants were asked to keep their eyes open and fixate on a central cross on the screen during the presentation of all auditory stimuli. The inter-stimulus interval also consisted of the same cross-fixation. The length of each oddball and standard stimulus was 350 ms and the inter-trial interval ranged between 800-1200 ms (mean=1000 ms). AV and cross-modal conditions were constructed from combinations of the audio only and the visual only stimuli (listed in **Table 4.1**).

4.2.3. Data Acquisition

EEG was recorded with 64 Ag/AgCl electrodes, using a Neuroscan system (Compumedics NeuroScan, SynAmps2). The electrodes were attached to an elastic cap in a 10−20 International system montage. The data were acquired at a sampling rate of 1000 Hz with the default reference near Cz, grounded to electrode AFz. During the experiment, the participants were seated comfortably at a distance of 60-70cm from the monitor in a sound attenuated and dimly lit room. The participants were requested to make minimal body movements and blink normally during the experiment. The impedance of all electrodes was initially set below 5kΩ and was also monitored in between blocks. Additionally, head digitization was performed using Polhemus Fastrak (Polhemus Inc.) to mark the position of the electrodes and the fiducials based on the placement of the cap on individual participants at the end of the entire EEG session. Individual T1-weighted structural images (MPRAGE)

were also obtained using a 3.0 T Philips Achieva MRI scanner (TR = 8.4 ms, FOV = 250 × 230 × 170, flip angle = 8°).

4.2.4. Preprocessing

EEG was acquired from 22 participants out of which data from 1 participant was discarded due to noisy recordings. The raw data of the remaining 21 participants were imported and each block was epoched. A high pass filter of 0.1 Hz was applied to the data to remove slow drifts in the signal. The data were visually inspected further and 1 channel (F4 in 3 subjects) was interpolated to neighboring electrodes. To identify and remove blink artifacts from the data, independent component analysis (ICA) was employed for each block. Only the blink component obtained as independent component (IC) from eye regions was visually identified and subsequently that IC was rejected. Each block was further epoched to trials of [-500 550] ms where 0 ms marked the onset of the stimulus. The trials were further divided into standard and oddball categories. Subsequently, all trials were subjected to a low pass filter of <45 Hz, baseline correction was applied and the data was re-referenced to linked mastoids. Trials with signal amplitude greater than 100µV and lesser than -100µV were removed and at most 6% of all oddball trials were discarded per subject. To equate the number of standard and oddball trials from each participant, we chose the minimum number of trials that survived artifact rejection in any condition and those many trials were randomly sampled from each condition for each participant. For all conditions, 885 trials each for deviant and standard categories were used. All analyses were done using the MATLAB based FieldTrip toolbox developed at Donders Institute for Brain, Cognition and Behaviour, in Nijmegen, Netherlands (Oostenveld et al., 2011) and custom-written scripts in MATLAB (www.mathworks.com).

4.2.5. Extracting MMN and P300 peaks

Based on previous literature (Garrido et al., 2009; Näätänen et al., 2007, 1978), we defined an MMN response as the largest negative deflection in the difference waveform (deviant-standard) between 120ms to 250ms (instead of 100-250ms to avoid picking up N100 peaks) from the onset of the stimulus and P300 response as the largest positive peak (oddball-standard) occurring between 250ms to 500ms in all modalities. To identify these peaks in our data, the group averaged activity of the standard trials was subtracted from the deviant trials of each channel for the audio, visual and audio-visual (AV) conditions. The MMN and P300 peaks were visually identified from the ERP plots and condition-wise topographies were subsequently plotted at the corresponding peak latencies of each modality (**Figure 4.1**).
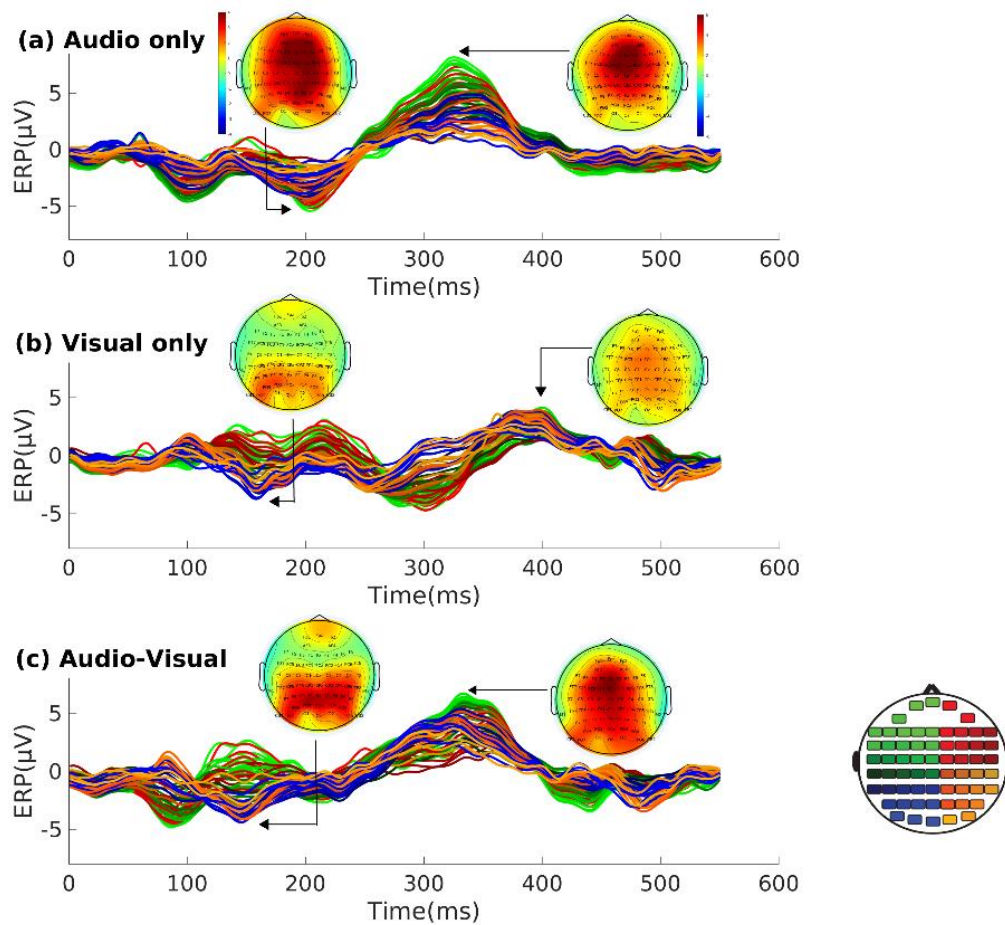
Figure 4.1. Grand averaged ERPs plotted across 21 subjects showing the differences between deviant and standard trials (deviant-standard) for (a) Audio, (b) Visual and (c) AV conditions. The corresponding topoplots indicate the distribution of ERPs across the brain at the identified MMN and P300 peaks. The topoplot on the bottom right displays the color code assigned to respective scalp channel locations used for plotting the ERPs in (a), (b) and (c).

Next, we sought to determine the top 5 sensors contributing individually to the MMN and P300 peaks in each condition by identifying the sensors showing maximum difference (deviant-standard) in their voltage activities. The top 5 sensors showing maximum MMN activity were F1/z/2, FCz/2 in the *audio only* condition; P1/3, PO3/5/7 in the *visual only* condition; P1/z/2/4, PO3 in the *AV* condition; POz/3/4/5, Oz in the *cross-audio* condition and CP1/3/5, P1/3 in the *cross-visual* condition. Similarly, electrodes F1/z/2, FC1/z showed maximum P300 activity in the *audio only* condition; electrodes FC1/z, Cz, Cpz, Pz showed maximum activity in the *visual only* condition; electrodes Fz, FC1/z, Cz, Pz in the *AV* condition; electrodes F1/z/2, FC1/z in the *cross-audio* condition and electrodes F1/z, FC1/z/2 showed maximum P300 activity in the *cross-visual* condition. Since different sensors were under consideration for different modalities, we reduced the dimensionality across the sensor space by applying principal component analysis (PCA) on the trial-level data (time-points X trials X sensors), separately for standard and deviant categories. The PCA function in MATLAB computes the eigenvectors of the covariance matrix ("principal axes") and sorts them by their eigenvalues (amount of explained variance). The first 3 principal components of the standard and deviant categories thus obtained, along with their explained variance have been reported for the *audio only*, *visual only* and *AV* conditions (**Figure 4.2**). Based on the eigenvalues of the covariance matrices, more than 80% of the data were explained by the first Principal Components (PCs) itself in all the conditions.

Therefore, to capture maximum variance from the top 5 sensors in each condition, the transpose of the first eigenvector was multiplied with PCA score projected along with the first principal component. Finally, the mean across time points was added to this product to reconstruct the original variables from the principal component subspace.

Note:- For a detailed amplitude and latency characterization, we mainly considered the audio only, visual only and AV conditions here due to the unavailability of 'equivalent standard categories' to subtract from the other two cross-modal deviant conditions. However, the two cross-modal conditions have been incorporated later in the study to investigate the robustness of the source distribution results.

Figure 4.2. The figure represents the first 3 (out of 5) principal components of deviant (in maroon) and standard (in gray) categories and their explained variances in the *audio only* (4.2(a), 4.2(d)), *visual only* (4.2(b), 4.2(e)) and *AV* (4.2(c), 4.2(f)) conditions when considering the top 5 sensors showing maximum MMN and P300 responses independently.

(Next page)

Principal components of MMN

Principal components of P300

(a)

audio deviant

Variance explained
1st PC- 94.54%
2nd PC- 3.01%
3rd PC- 1.52%

audio standard

1st PC- 93.82%
2nd PC- 3.40%
3rd PC- 1.75%

(d)

audio deviant

1st PC- 94.82%
2nd PC- 2.42%
3rd PC- 1.79%

audio standard

1st PC- 94.19%
2nd PC- 2.78%
3rd PC- 1.94%

(b)

visual deviant

1st PC- 90.24%
2nd PC- 6.68%
3rd PC- 1.91%

visual standard

1st PC- 89.60%
2nd PC- 7.14%
3rd PC- 2.06%

(e)

visual deviant

1st PC- 87.16%
2nd PC- 10.15%
3rd PC- 1.52%

visual standard

1st PC- 85.19%
2nd PC- 11.88%
3rd PC- 1.64%

(c)

AV deviant

1st PC- 86.93%
2nd PC- 8.03%
3rd PC- 3.55%

AV standard

1st PC- 84.10%
2nd PC- 10.10%
3rd PC- 4.13%

(f)

AV deviant

1st PC- 86.33%
2nd PC- 10.73%
3rd PC- 1.49%

AV standard

1st PC- 81.86%
2nd PC- 14.79%
3rd PC- 1.67%

86

4.2.6. Source Localization

Source localization was performed to obtain the MMN and P300 generators in the brain across various modalities. The EEG data were re-referenced with an average reference before source-localization. 19 participants' structural MRI data were re-sliced and segmented to identify the brain, skull and scalp tissues. 2 subjects' MRI scans could not be obtained because of their incompatibility with the fMRI scanner. The origin (0,0,0) of all the T1 images was set to the anterior commissure. Participant-specific headmodel was computed using the OpenMEEG toolbox (Gramfort et al., 2010), using realistic conductivity values. The Polhemus data was imported to place the sensor locations on the head model of each participant. To obtain high accuracy of electrode positions, individual co-registration was employed by firstly visually marking the fiducials (nasion, left preauricular and right preauricular) in the MRI volume and finally matching the marked points with the fiducial locations as per the Polhemus data. Next, the sources were placed in the segmented part of the headmodel at a distance of 5 mm from each other and the leadfield matrix was computed, i.e., a transfer function between each source point and each electrode. Source localization of each individual was performed using their respective headmodel, leadfield and electrode positions. eLORETA, belonging to a class of current density measures to calculate the distribution of neuronal sources, was used to solve the inverse problem (Pascual-Marqui, 2007a). eLORETA also generates the least amount of false positives hence beneficial for exploratory source analysis, e g., where prior hypotheses regarding approximate locations may not be available (Halder et al., 2019b). Lambda of 0.1 was used as the regularization parameter for localization of P300 and MMN ERPs. After localization, each individual's source intensities were interpolated to their respective MRI volume. Further, to calculate the grand average of the source values, the interpolated images were normalized to a common structural template. Finally, we subtracted the voxel intensities of oddball and standard

categories and the voxels having intensities more than 95 percent of the maximum value were thresholded. This was done separately for each hemisphere.

4.2.7. Data availability and codes

Codes used to analyze the data and reproduce the figures can be obtained from the bitbucket repository using the link: https://bitbucket.org/cbdl/pe_erpandsourceanalysis/src/master/. EEG data would be made available by the authors for public access upon acceptance of the manuscript. Copyright of the data and codes are held by the National Brain Research Centre, an autonomous institution of the Government of India.

4.3. Results

4.3.1. Middle and late stages of prediction error processing are conserved across unisensory and multisensory contexts

The difference in voltages between the deviant and standard categories (deviant-standard) of the dimensionality reduced data (refer to section 4.2.5) were calculated for each participant for the *audio only, visual only* and *audio-visual* conditions (heat maps in **Figure 4.3**). The MMN and P300 peaks were then subject-wise visualized within the pre-defined windows of interest (120-250ms for MMN and 250-500ms for P300). Furthermore, we narrowed down these windows in a modality-defined manner by centering the window around the group-averaged peak (±50ms) of each modality to obtain an equal window length of 100 ms for MMN and P300. Since the basis of defining the trials of prediction error processing constituting the oddballs (deviant trials) was their heightened responses at MMN and P300 latencies, we statistically verified whether the standard and deviant trials significantly

differed from each other within the defined latencies at both the ERPs of interest in all conditions. A Student's t-test was employed on the 100 ms windows described above which revealed that the amplitude of MMN in the oddball trials was significantly lower than that of the standard trials in *audio only* (t(20)=5.85, SD=2.16, p<0.0001), *visual only* (t(20)=6.02, SD=1.33, p<0.0001) and *audio-visual* (t(20)=6.65, SD=1.82, p<0.0001) conditions (**Figure 4.3(a)-(c), lower panels**). Similarly, the P300 amplitudes were significantly higher for oddball trials in *audio only* (t(20)=9.91, SD=2.49, p<0.0001), *visual only* (t(20)=6.18, SD=1.93, p<0.0001) and *audio-visual* (t(20)=6.26, SD=3.54, p<0.0001) conditions (**Figure 4.3(d)-(f), lower panels**).

Figure 4.3. The heatmaps (top-panels) depict the time-course of participant-wise subtraction waveforms from deviant-standard projections of the first principal components, followed by their respective grand-averaged plots (bottom-panels) for (a) audio only MMN, (b) visual only MMN, (c) audio-visual MMN, (d) audio only P300, (e) visual only P300, and (f) audio-visual P300. The white dotted boundaries in all top-panels are the condition-invariant pre-defined windows of interest for subject-wise MMN (120-250ms) and P300 (250-500ms) visualization. Participants are stacked along the y-axis in ascending order of their latencies. The shaded orange regions in the bottom panels (100 ms windows) represent a regime of significant difference (revealed by t-test on the ERPs of interest, i.e, MMN and P300) between standard and deviant categories. The shadings with each of the deviant and standard trials reflect the standard error of the mean across 21 participants.

(Next page)
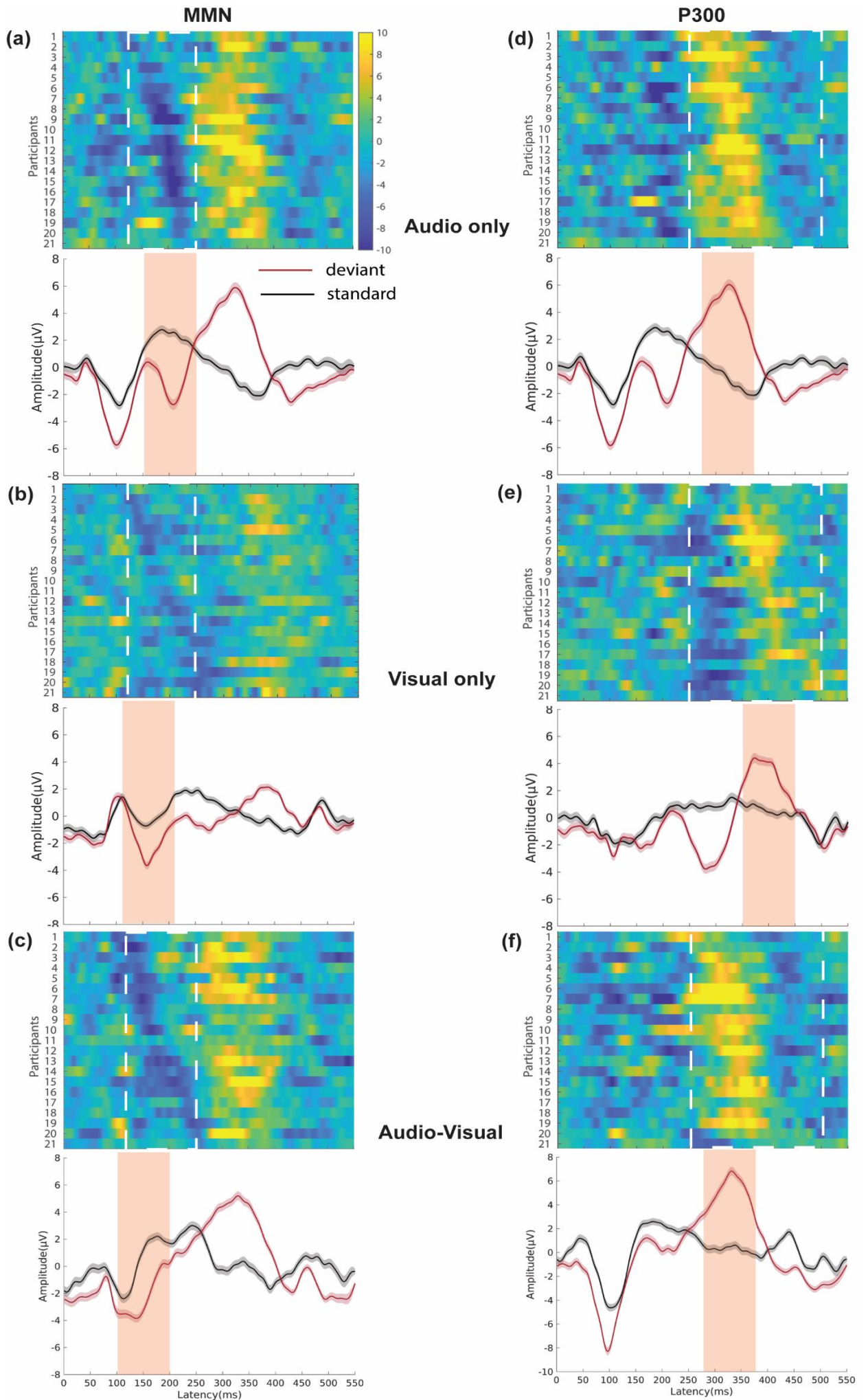
4.3.2. Multisensory context speeds the processing of prediction errors

For latency and amplitude characterization of prediction error markers across *audio only*, *visual only* and *AV* conditions, the peak values (maximum negative amplitudes of subtraction waveform for MMN and maximum positive amplitude values from oddball conditions for P300) and their corresponding latencies were extracted from the 100 ms windows for each trial and subsequently, the means and standard deviations of latencies and amplitudes were obtained for all conditions as listed in **Table 4.2** for P300 and in **Table 4.3** for MMN.

Table 4.2. Table shows the mean±SD of the peak P300 amplitudes and their corresponding latencies across all the trials for audio only, visual only and audio-visual conditions.

Condition (P300)	Amplitude(μV)	Latency(ms)
Audio	16.49±10.42	327.41±30.99
Visual	14.57±8.18	399.93±32.04
AV	16.14±9.40	332.00±30.04

Table 4.3. The table shows the mean±SD of the peak MMN amplitudes and their corresponding latencies across all the trials for audio only, visual only and audio-visual conditions.

Condition (MMN)	Amplitude(μV)	Latency(ms)
Audio	20.87±11.97	206.51±30.81
Visual	15.53±8.75	160.11±30.66
AV	18.73±10.41	150.13±30.69

To decipher the effect of modality on the latencies/amplitudes of MMN and P300, a repeated-measures analysis of variances (rmANOVAs) was conducted on the subject-level data which revealed a significant effect of modality on the amplitudes of both MMN ($F_{(2,40)}=25.09$, $p<0.0001$, $\eta^2=0.56$) and P300 ($F_{(2,40)}=3.65$, $p=0.03$, $\eta^2=0.15$). In case of MMN latency, Mauchly's test revealed a low p-value ($p = 0.04$) which indicated that the assumption of sphericity was violated. Hence, a Greenhouse-Geisser correction was applied ($\varepsilon =0.78$) and subsequently, a significant effect of modality was detected by rmANOVA on MMN latencies also ($F_{(1.57,31.43)}=383.51$, $p<0.0001$, $\eta^2=0.78$). The assumption of sphericity was not violated ($p>0.05$) for P300 latencies even though the p-value obtained through Mauchly's test was low($p=0.06$). rmANOVA showed a significant effect of modality on the P300 latencies ($F_{(2,40)}=786.51$, $p<0.0001$, $\eta^2=0.97$) as well.

Post-hoc comparisons with Bonferroni-adjusted p-values indicated significant differences in the P300 and MMN latencies and amplitudes across modalities (as shown in **Figure 4.4**) reflecting a significant effect of conditions on the amplitudes and latencies of both the ERPs. While comparing the peak latencies of MMN, we observed that AV condition had the shortest MMN latency (AV < audio only/visual only at $p<0.0001$), followed by visual only condition (visual only < audio only at $p<0.0001$) while the slowest MMN latency was seen for the audio only condition. On the contrary, P300 latency was fastest for the audio only condition (audio only < visual only at $p<0.0001$; audio only < AV at $p=0.01$), followed by the AV condition (AV < visual only at $p<0.0001$). While comparing the MMN amplitudes, the MMN peak of the audio only condition showed the largest negative amplitude (audio only > visual only at $p<0.0001$; audio only > AV at $p=0.03$), followed by the AV condition (AV > visual only at $p=0.0002$). On the other hand, P300 amplitudes of visual only, audio only and AV conditions were not significantly different from each other.
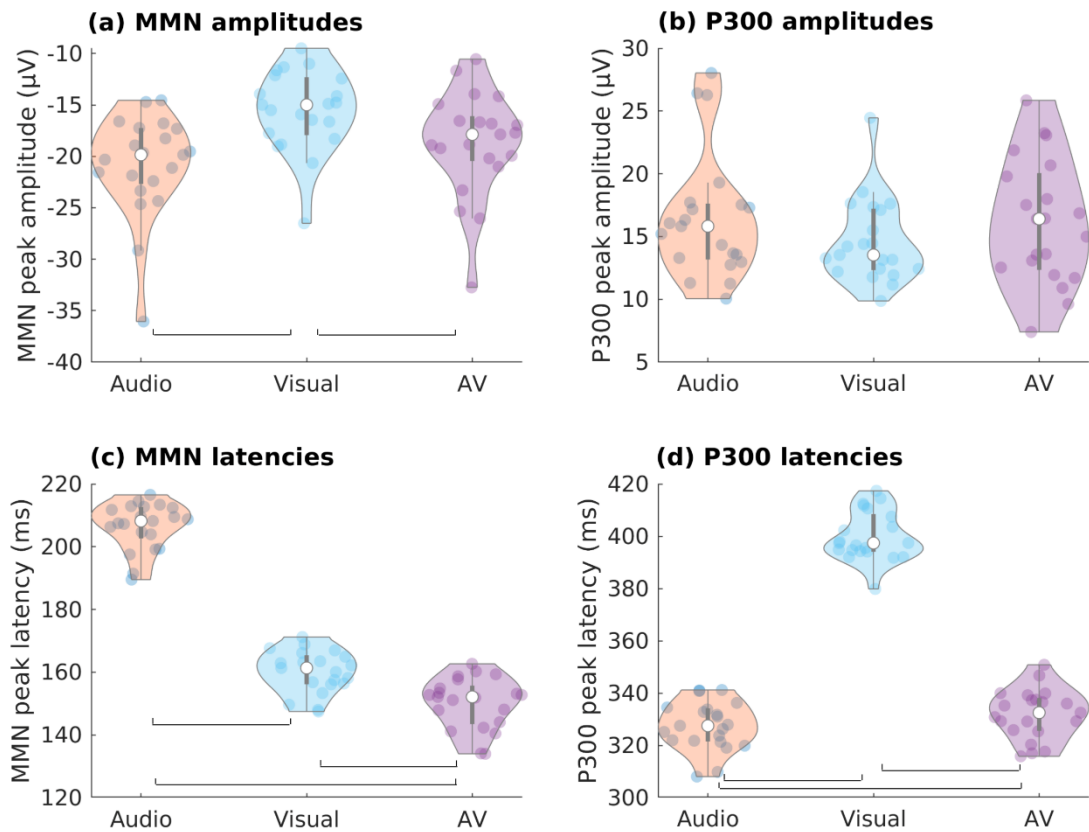
Figure 4.4. The violin plots represent the MMN (a) peak amplitudes (maximum magnitude on the negative y axis of the subtraction waveform of deviant – standard trials of each participant) and their corresponding (c) latencies. Similarly, the P300 (b) peak amplitudes and their corresponding (d) latencies are plotted for each participant. The colored dots represent each participant's peak amplitude and peak latency values in µV and ms, respectively. The white dot at the center of the gray box represents the median of the data and the gray box itself represents the inter-quartile range. The horizontal open square bracket represents a significant difference (p<0.05) between the two conditions.

4.3.3. Spatial representations of unisensory and multisensory contexts in source space

The 100 ms windows of each modality were used to obtain the covariance matrices, separately for standard and oddball trials of MMN. The clusters of P300 sources obtained using 100 ms windows, however, were noisy (did not fall into any Brodmann area), because of which we recomputed the P300 sources using a longer time window to obtain a better estimate of variance in the data. Thus, the P300 peaks were identified between 250-500 ms post-stimulus onset where maximum peak values of every trial were extracted along with their corresponding latencies. Based on these latencies, we calculated the mean and standard deviation for each modality and defined the windows as [mean-SD : mean+SD]. The covariance matrices were now obtained from these windows and the same steps were repeated to obtain the P300 sources. Using co-registration of individual participant MR data with their EEG sensor locations, we generated the source maps underlying MMN and P300 activity using eLORETA (details in Methods). Parcels from the Brainnetome atlas were interpolated to the same common structural template as used for normalization of the individual sources. Only those parcels were chosen which included the sources or a part of them. As revealed in **Figure 4.5 (a)**, the MMN sources were distributed throughout the brain and were different for different modalities (locations in **Table 4.4**). The dorsolateral areas of the left and right superior frontal gyri were found to underlie the MMN response in the *audio only* condition; the caudal cuneus gyrus in medio-ventral occipital cortex on the left, the middle occipital gyrus in the right lateral occipital cortex, the rostro-dorsal area of the right inferior parietal lobule and the dorso-lateral area of the right middle temporal gyrus elicited MMN in the *visual only* condition; and the *audio-visual* condition yielded sources that were located in the rostral areas of left superior parietal lobule and the caudal areas of multisensory regions STG (superior-temporal gyrus) and MTG (medial-temporal gyrus) on

the right. Interestingly, source analysis of P300 revealed many overlapping fronto-central areas for all the three sensory modality conditions (as illustrated in **Figure 4.5 (b)**). P300 was elicited at the dorso-lateral areas of left superior frontal gyri for *audio only, visual only* and *audio-visual* conditions; at right superior frontal gyri for the *audio only* and *audio-visual* conditions; at the trunk and caudal dorso-lateral areas in left precentral gyri for the *audio only* and *visual only* conditions, respectively; and additionally, at the ventro-lateral area of right middle frontal gyrus for the *visual only* condition (details in **Table 4.4**).
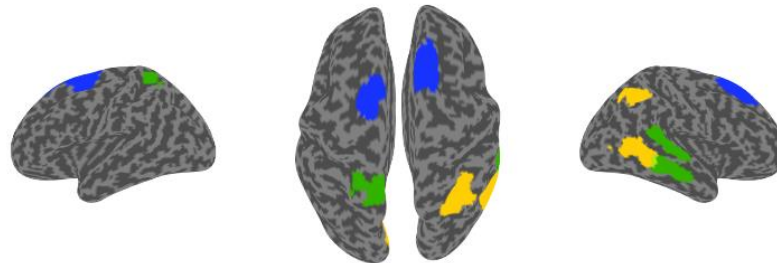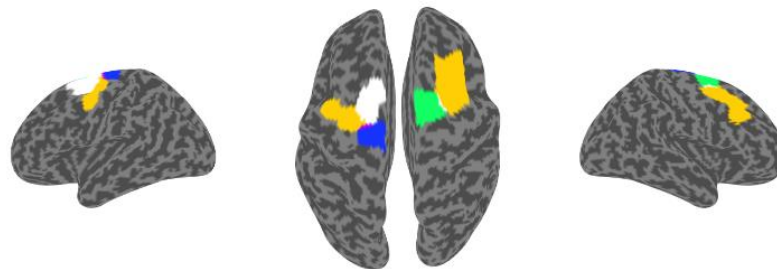
Figure 4.5. eLORETA source localization results using time locked analysis (at threshold level 95%) representing the underlying (a) MMN and (b) P300 sources for Audio, Visual and Audio-Visual modalities.

Condition	MMN	P300
Audio	SFG, Left Superior Frontal Gyrus A6dl, dorsolateral area 6 SFG, Right Superior Frontal Gyrus A8dl, dorsolateral area 8	SFG, Left Superior Frontal Gyrus A6dl, dorsolateral area 6PrG Left Precentral Gyrus A4t, area 4 (trunk region) SFG, Right Superior Frontal Gyrus A6dl, dorsolateral area 6
Visual	MVOcC, Left Medio-Ventral Occipital Cortex cCunG, caudal cuneus gyrus LOcC, Right lateral Occipital Cortex mOccG, middle occipital gyrus IPL, Right Inferior Parietal Lobule A39rd, rostro-dorsal area 39 (Hip3) MTG, Right Middle Temporal Gyrus A37dl, dorsolateral area37	SFG, Left Superior Frontal Gyrus A6dl, dorsolateral area 6 PrG, Left Precentral Gyrus A6cdl, caudal dorsolateral area 6 MFG, Right Middle Frontal Gyrus A8vl, ventrolateral area 8 MFG, Right Middle Frontal Gyrus A6vl, ventrolateral area 6
AV	STG, Right Superior Temporal Gyrus A22c, caudal area 22 MTG, Right Middle Temporal Gyrus A21c, caudal area 21 SPL, Left Superior Parietal Lobule A7r, rostral area 7	SFG, Left Superior Frontal Gyrus A6dl, dorsolateral area 6 SFG, Right Superior Frontal Gyrus A6dl, dorsolateral area 6

Table 4.4. The table lists the brain areas underlying the peak MMN and P300 activations across the audio only, visual only and audio-visual conditions.

4.4. Discussion

We employed two-stimuli oddball tasks using *Audio alone*, *Visual alone* and *synchronous Audio-Visual* conditions to evoke MMN and P300 responses in the brain. It is already known that visual modality speeds up auditory processing for both speech and non-speech stimuli (Begau et al., 2021; Diaconescu et al., 2011; Leone and Mccourt, 2015; van Wassenhove et al., 2005) previously demonstrated mostly using speeded N100 latencies in multisensory (audio+visual) contexts. Our study is an advancement to these previous findings and our first result elucidates how the simultaneous occurrence of audio and visual oddballs, shorten the latencies of both MMN and P300 ERPs, indicating that the processing of prediction errors gets facilitated under multisensory contexts at "any stage" of information processing in the brain (early N100, middle MMN or late P300). This information is crucial and can serve as a powerful tool to generalize all predictive coding models trying to understand prediction error processing at different stages/hierarchies in the brain (Wacongne et al., 2012). No single study before ours has demonstrated this so explicitly involving both the prediction error markers using a common oddball paradigm in healthy humans. The second major outcome of our study in the context of prediction error processing is the modality-specific and modality-agnostic nature of the MMN and the P300 sources, respectively. This is the first study as per our knowledge to use accurate source localization techniques to report all the underlying areas of MMN and P300 in audio, visual and AV modalities. We found a reorganization of brain regions along the temporal hierarchy of prediction error processing (MMN followed by P300) as the mismatch information flows up the spatial hierarchy of the brain (sensory to higher order regions). This was revealed by an initial "modality-sensitive" stage indexed by MMN where different modalities had different cortical generators, which transitioned to a "modality-independent" stage indexed by P300 where the different

modalities had common cortical sources (**Figure 4.5, 4.6**). Though such a transition may appear unsurprising in terms of sensory-cognitive processing, it is extremely important to document that modality specificity during prediction error processing is lost at the P300 level itself and is not something that is attained at further later stages of prediction error processing like during the reorienting negativity (RON) component. The RON in the brain appears as a negative deflection at 400-600ms in response to the reorientation of attention to the predictive/standard stimuli after it has been switched (indexed by P300) towards the preceding deviant stimuli (Correa-Jaraba et al., 2016; Ungan et al., 2019). Even though in our analysis we could not cover this ERP, since it did not come out as a prominent peak in the subtraction waveforms (**Figure 4.1**), we argue that RON too would, being an even later component, have common brain generators across modalities, probably more frontal, as also seen in recent studies (Correa-Jaraba et al., 2016; Justo-Guillén et al., 2019; Ungan et al., 2019). One may also note here that in our study, we have specifically focussed on only the two ERPs of interest- MMN and P300, as they have been widely reported as the markers of prediction error across various modalities in extant literature (Banellis et al., 2020; Calcus et al., 2015; Chennu et al., 2013; Stefanics et al., 2014). Other prominent peaks in response to auditory stimuli such as N100 (as seen in **Figure 4.1(a), (c)**), are out of the scope and interest of this study.

We analyzed the MMN and P300 latency differences for processing prediction errors presented in *audio only*, *visual only* and *audio-visual* conditions. The MMN latencies in our oddball paradigm followed the order: *Audio-visual<Visual only<Audio only* (**Table 4.3**). According to our results, the auditory MMN appears much later than the visual MMN as also reported earlier in a few studies (Berti and Schröger, 2001; Sittiprapaporn, 2012). The appearance of a delayed auditory MMN might be because of the time taken for the sensory

mismatch information to pass from one hierarchal cortical stage to the next, up to the frontal gyri. Visual MMN sources were in the occipital cortex whereas auditory MMN was elicited at a comparatively higher hierarchy in the superior frontal gyrus (as also reported previously by Näätänen et al., 2007; Winkler et al., 1998 in the sensor space). Because of the same cortical generators of audio MMN and P300, bottom-up information flow time for further auditory prediction error processing post MMN elicitation was reduced. Consequently, the audio only condition produced the slowest MMN but the fastest P300 peaks (**Figure 4.4 (c), (d)**). The P300 latencies followed the order: *Audio only<Audio-visual<Visual only* (**Table 4.2, Figure 4.4(d)**). Superior-frontal auditory MMN might be indicative of a stronger call for attention towards change in a single stimulus feature i.e., frequency change in tone, that perhaps would require an active comparison of the mismatch with the standard to be identified as a deviant, as opposed to changes in basic visual features like color/shape in the visual oddball condition. This is supported by evidence from literature that suggests object-based irregularities are automatically detected by the visual system (Stefanics et al., 2014). MMN latency speeds up with increasing deviation from the standard (Näätänen et al., 2005) as the mismatch between the deviant and the memory representation of the standard can be detected faster. In our paradigm, the deviation in the visual oddball (change in shape and color) was high (or rather obvious), resulting in a faster processing speed of visual MMN, and was resolved at the level of the secondary sensory cortex itself. However, visual mismatch information had to travel from the occipital cortex higher up to the superior-frontal gyrus for the next level of mismatch processing at P300 latency, resulting in slowest P300. We found this result quite intriguing because the MMN and P300 latencies in the temporal hierarchy organized themselves based on the arrangement of brain areas along the spatial hierarchy of the predictive brain supporting previous studies stating that MMN may be

influenced by recurrent feedback activation from higher order areas (Garrido et al., 2007, 2009). More importantly, fastest elicitation of audio-visual MMN (**Figure 4.4(c)**) suggests that the faster visual component in the AV oddball temporally facilitated its slower auditory component which speeded up the process of change detection in the audio-visual condition. Evidently, this facilitation for audio-visual deviants was propagated further up the deviant processing ladder which resulted in a faster audio-visual P300 at the superior-frontal gyrus. The latency of AV oddball processing is however, second to the audio only condition at the level of P300 but is significantly faster than the slowest visual P300, indicating that the audio-visual ERPs are always temporally facilitated by the fastest unisensory component (by visual at MMN and auditory at P300) at "all stages" of prediction error processing. The faster audio-visual P300 can perhaps be attributed to an early association between the constituent unisensory audio and unisensory visual deviant stimuli during the audio-visual MMN latency at the superior-temporal gyrus and middle temporal gyrus (regions placed higher in spatial hierarchy as compared to the visual MMN areas) which have been implicated as the areas of multisensory integration (Beauchamp, 2005; Callan et al., 2004). Although, unlike speech stimuli, in our paradigm the audio and visual stimuli together did not form any meaningful stimuli as such, the simultaneous presentation of the audio and visual stimuli was sufficient to induce a multisensory context. Taken together, our results clearly reveal that the presence of a multisensory context, shifts the oddball processing speed towards the faster unisensory modality indicating a multisensory benefit always for processing prediction errors. It may also be noted that the two auditory stimuli presented, were pure tones with musical relation in terms of pitch (deviance was one octave higher, **Table 4.1**). This may indicate that the MMN and the P300 obtained for *audio only* condition represent the neural signatures of auditory pitch mismatch processing.

Source localization results for MMN show scattered activations throughout the brain which are different for different sensory modalities (as shown in **Figure 4.6(a)**). For the *visual only* modality, we saw activations in the left medio-ventral occipital cortex, the right lateral occipital cortex, the right inferior parietal lobule and the right middle temporal gyrus; for *audio only* condition, there were activations in the left and right superior frontal gyri; for the *audio-visual* modality, activations were seen in the left superior parietal lobule and the right superior-temporal and medial-temporal gyri; for the *cross-visual* modality, we found activations in the left and the right superior parietal lobules; and that for *cross-audio* modality, in the left and the right lateral occipital cortex (**Figure 4.6(a)**). From these results, we concur that mostly the secondary sensory areas along with other cortical areas distributed throughout the brain are employed during the process of early prediction mismatch, based on the modality. An interesting point to be noted here is that even though the deviant stimuli were exactly the same in the *Audio only* and *Cross-Audio* conditions (and similarly in the *Visual only* and *Cross-Visual* conditions), their cortical generators were different only because their corresponding standard stimuli were different suggesting that the MMN sources are not only sensitive to the modality of the deviant stimuli but also to the modality of the standards. In traditional literature, MMN is widely considered as a "perceptual" prediction error signal carrying important novel information which initiates a call for further processing of prediction mismatches (Escera et al., 2000; Mäntysalo and Näätänen, 1987; Schröger, 1997). Such novel information should necessarily feed into the higher cognitive processing areas for further evaluation, as is reflected by the occurrence of the late event-related potential, P300 (Bledowski et al., 2004b; David and Linden, 2005). Our source results revealed overlapping source activations for P300 in all the five modality conditions, localized around the fronto-central regions for *audio only, visual only* and *audio-visual*

conditions (as shown in **Table 4.4**) and also at the right superior frontal gyrus, the left and the right precentral gyri for *cross-audio* condition and, at the left and the right superior frontal gyri for *cross-visual* condition (as shown in **Figure 4.6(b)**). Common brain generators for P300 across modalities suggest that this neural marker might particularly be responsible for domain-general higher evaluative processes like keeping a count of the number of oddballs as in our paradigm, after a change detection signal has been relayed by MMN generators of corresponding modalities in the brain.
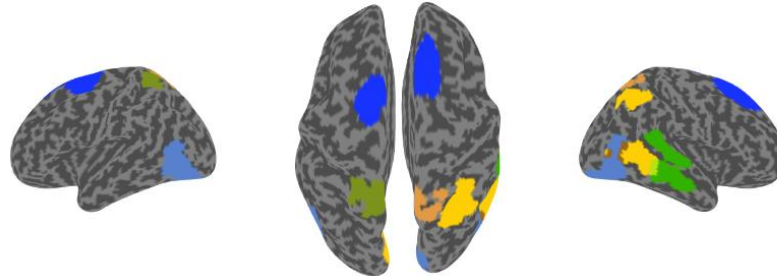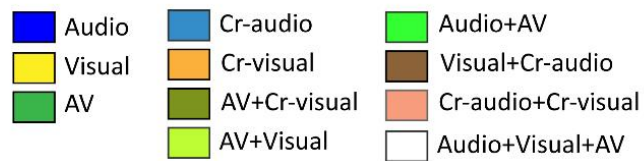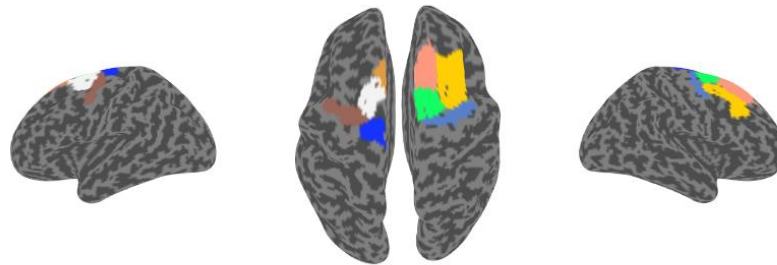
Figure 4.6. eLORETA source localization results using time locked analysis (at threshold level 95%) representing the underlying (a) MMN and (b) P300 sources for Audio, Visual and Audio-Visual, Cross-visual and Cross-audio modalities.

Many recent and past studies have argued that the brain is not a passive input-output device but acts as a predictive system capable of anticipating the future by making predictions about sensory inputs and minimizing prediction errors (Bubic et al., 2010; Clark, 2013; Ficco et al., 2021; Friston, 2010). Thus, there arises a need to further understand the neural mechanisms by which the brain processes prediction errors in complex scenarios and multiple modality combinations. A detailed neuronal model of the auditory, visual and audio-visual cortices, based on the underlying processes of predictive mismatch that account for the critical features of MMN, P300 and RON could better explain the process of temporal facilitation and supra-additivity in the audio-visual modality (Pattamadilok and Sato, 2022; Molholm et al., 2002). Our empirical investigations in the context of hierarchical processing of prediction errors would have implications beyond the theoretical domain as well. Based on the models of MMN and P300 responses from patients with disorders of consciousness like in vegetative and minimally conscious states (Boly et al., 2011; Daltrozzo et al., 2007), attention (Polich, 2007b; Szuromi et al., 2011), and schizophrenia (Blackwood, 2000; Erickson et al., 2016), researchers can isolate the deficits in predictive information flow that might underlie these states of profound cognitive and neurological dysfunction. Such foundational advances can be of extreme value to clinical neuroscience researchers. From a neural networks' perspective, two well-known attentional networks, the dorsal attention network (DAN) and the ventral attention network (VAN) have been largely reported in oddball studies (Bledowski et al., 2004a; Clark et al., 2000; Stevens et al., 2000). The VAN in particular has been exclusively involved in the detection of deviant stimuli (Kim, 2014b; Palaniyappan and Liddle, 2012) and is activated at both MMN and P300 stages (Justen and Herbert, 2018). Further connectivity analysis between the regions underlying the VAN during MMN and P300 latencies across various modalities can further our understanding of

the function of this important attentional network beyond recent evidence in the frequency domain (Ghosh et al., 2021). Although a few studies have also attempted to draw a relationship between pre-stimulus brain states and P300 (Karch et al., 2016; Reinhart et al., 2011), a detailed source connectivity analysis will be informative about the mechanisms of P300 and MMN generation, thus providing an important direction to future research.

Chapter 5

Conclusion

"Truth is found neither in the thesis nor the antithesis,

but in an emergent synthesis which reconciles the two."

— *Hegel*

Behavior and cognition are manifestations of highly coordinated spatiotemporal activity in the neural networks of the brain. Even though there is amassed knowledge about neural oscillations associated with the various forms of attention, understanding the brain rhythms associated with the reorientation of attention across various sensory modalities is of profound interest. Most of the previous empirical studies examining reorientation of attention have used the visual modality where the exogenous and endogenous trials were structured separately, which does not necessarily mirror the neural mechanisms underlying reorientation to complex distractors in real-life situations. We are surrounded by multisensory information around us, yet it is actually the auditory modality that is majorly capable of detecting events that happen from any direction within our surroundings. Do the neural correlates for processing visual and auditory violation of expectations remain same or do they differ across modalities? Even though the Ventral Attention Network seems to be controlling the process of change detection in both modalities (Corbetta et al., 2008), which frequency oscillations are responsible for this process? Which are the driver and effector

nodes in the Ventral Attention Network? Do multisensory violations receive a processing

advantage over their unisensory counterparts?

Using three novel behavioral paradigms and experimental EEG on healthy humans, we try

to find answers to these questions in chapters 2, 3 and 4. The major conclusions of the thesis

are as follows:

1. In the visual modality, the regions of the Ventral Attention Network (VAN), i.e., the
    right temporo-parietal junction, the right insula and the right lateral prefrontal cortex,
    show bidirectional causal interactions with each other to process salient distractors
    during reorientation from the goal-driven tasks. These directed interactions are
    mediated by significantly enhanced alpha frequency oscillations (8-9 Hz) and exist
    only in the presence of salient distractors. The neural mechanisms for processing
    static and moving visual salient distractors, while performing visual attention tasks
    that vary across the temporal scale, do not change.

2. In the auditory modality, the reorientation from goal-driven auditory attention tasks
    towards naturalistic salient sounds is associated with a significant decrease in the
    power of the alpha (8-12 Hz) and late beta (25-29 Hz) frequency oscillations in the
    brain. The underlying sources of beta power correspond to the regions of the VAN
    and thus, unlike the visual modality, the VAN in the auditory modality operates via
    beta oscillations. The neural mechanisms governing the violations of expectations
    during both speech and non-speech auditory tasks remain invariable. Hence, the
    neural mechanisms underlying VAN activity are dependent on the sensory modality
    but within a modality are context-independent.

3. The event-related potentials (ERPs) elicited in the brain in response to violation of expectations, i.e., the mismatch negativity (MMN) and the P300, show a temporal facilitation in the audio-visual modality over the unisensory modalities, marked by an early onset in its latency. Such multisensory benefits have been reported previously for N100 (Van Wassenhove et al., 2005) but never for MMN and P300 in a common oddball paradigm. Source localization of these ERPs revealed that the sources of MMN were modality dependent (with modality-specific sensory activations) but as the mismatch signal propagated up the hierarchical brain, the modality dependence was lost at the P300 level (with common fronto-central generators for all modalities).

References

Alain, C., Woods, D.L., 1997. Attention modulates auditory pattern memory as indexed by event-related brain potentials. Psychophysiology 34, 534–546. https://doi.org/10.1111/J.1469-8986.1997.TB01740.X

Allan, P.G., Briggs, R.G., Conner, A.K., O'Neal, C.M., Bonney, P.A., Maxwell, B.D., Baker, C.M., Burks, J.D., Sali, G., Glenn, C.A., Sughrue, M.E., 2020. Parcellation-based tractographic modeling of the ventral attention network. J. Neurol. Sci. 408, 116548. https://doi.org/10.1016/j.jns.2019.116548

Anzolin, A., Presti, P., Van De Steen, F., Astolfi, L., Haufe, S., Marinazzo, D., 2019. Quantifying the Effect of Demixing Approaches on Directed Connectivity Estimated Between Reconstructed EEG Sources. Brain Topogr. 32, 655–674. https://doi.org/10.1007/S10548-019-00705-Z/FIGURES/9

Atienza, M., Cantero, J.L., Escera, C., 2001. Auditory information processing during human sleep as revealed by event-related brain potentials. Clin. Neurophysiol. 112, 2031–2045. https://doi.org/10.1016/S1388-2457(01)00650-2

Aulanko, R., Hari, R., Lounasmaa, O. V., Näätänen, R., Sams, M., 1993. Phonetic invariance in the human auditory cortex. Neuroreport 4, 1356–1358. https://doi.org/10.1097/00001756-199309150-00018

Banellis, L., Sokoliuk, R., Wild, C.J., Bowman, H., Cruse, D., 2020. Event-related potentials reflect prediction errors and pop-out during comprehension of degraded speech. Neurosci. Conscious. 2020. https://doi.org/10.1093/NC/NIAA022

Banerjee, S., Snyder, A.C., Molholm, S., Foxe, J.J., 2011. Oscillatory alpha-band mechanisms and the deployment of spatial attention to anticipated auditory and visual targetlocations: Supramodal or sensory-specific control mechanisms? J. Neurosci. 31, 9923–9932. https://doi.org/10.1523/JNEUROSCI.4660-10.2011

Barnett, L., Barrett, A.B., Seth, A.K., 2018a. Misunderstandings regarding the application of Granger causality in neuroscience. Proc. Natl. Acad. Sci. U. S. A. https://doi.org/10.1073/pnas.1714497115

Barnett, L., Barrett, A.B., Seth, A.K., 2018b. Solved problems for Granger causality in neuroscience: A response to Stokes and Purdon. Neuroimage. https://doi.org/10.1016/j.neuroimage.2018.05.067

Barnett, L., Seth, A.K., 2014. The MVGC multivariate Granger causality toolbox: A new approach to Granger-causal inference. J. Neurosci. Methods 223, 50–68. https://doi.org/10.1016/j.jneumeth.2013.10.018

Battelli, L., Cavanagh, P., Intriligator, J., Tramo, M.J., Hénaff, M.-A., Michèl, F., Barton, J.J.S., 2001. Unilateral Right Parietal Damage Leads to Bilateral Deficit for High-Level Motion. Neuron 32, 985–995. https://doi.org/10.1016/S0896-6273(01)00536-0

Battelli, L., Pascual-Leone, A., Cavanagh, P., 2007. The 'when' pathway of the right parietal lobe. Trends Cogn. Sci. 11, 204–210. https://doi.org/10.1016/j.tics.2007.03.001

Beauchamp, M.S., 2005. See me, hear me, touch me: multisensory integration in lateral occipital-temporal cortex. Curr. Opin. Neurobiol. 15, 145–153. https://doi.org/10.1016/J.CONB.2005.03.011

Begau, A., Klatt, L.I., Wascher, E., Schneider, D., Getzmann, S., 2021. Do congruent lip

movements facilitate speech processing in a dynamic audiovisual multi-talker scenario? An ERP study with older and younger adults. Behav. Brain Res. 412, 113436. https://doi.org/10.1016/J.BBR.2021.113436

Bersagliere, A., Pascual-Marqui, R.D., Tarokh, L., Achermann, P., 2018. Mapping Slow Waves by EEG Topography and Source Localization: Effects of Sleep Deprivation. Brain Topogr. 31, 257–269. https://doi.org/10.1007/s10548-017-0595-6

Berti, S., 2012. Automatic processing of rare versus novel auditory stimuli reveal different mechanisms of auditory change detection. Neuroreport 23, 441–446. https://doi.org/10.1097/WNR.0B013E32835308B5

Berti, S., 2008. Cognitive control after distraction: Event-related brain potentials (ERPs) dissociate between different processes of attentional allocation. Psychophysiology 45, 608–620. https://doi.org/10.1111/J.1469-8986.2008.00660.X

Berti, S., Roeber, U., Schröger, E., 2004. Bottom-up influences on working memory: Behavioral and electrophysiological distraction varies with distractor strength. Exp. Psychol. 51, 249–257. https://doi.org/10.1027/1618-3169.51.4.249

Berti, S., Schröger, E., 2001. A comparison of auditory and visual distraction effects: Behavioral and event-related indices. Cogn. Brain Res. 10, 265–273. https://doi.org/10.1016/S0926-6410(00)00044-6

Blackwood, D., 2000. P300, a state and a trait marker in schizophrenia. Lancet 355, 771–772. https://doi.org/10.1016/S0140-6736(99)00261-5

Bledowski, C., Prvulovic, D., Goebel, R., Zanella, F.E., Linden, D.E.J., 2004a. Attentional systems in target and distractor processing: a combined ERP and fMRI study.

Neuroimage 22, 530–540. https://doi.org/10.1016/J.NEUROIMAGE.2003.12.034

Bledowski, C., Prvulovic, D., Hoechstetter, K., Scherg, M., Wibral, M., Goebel, R., Linden, D.E.J., 2004b. Localizing P300 Generators in Visual Target and Distractor Processing: A Combined Event-Related Potential and Functional Magnetic Resonance Imaging Study. J. Neurosci. 24, 9353. https://doi.org/10.1523/JNEUROSCI.1897-04.2004

Bokil, H., Andrews, P., Kulkarni, J.E., Mehta, S., Mitra, P.P., 2010. Chronux: A platform for analyzing neural signals. J. Neurosci. Methods 192, 146–151. https://doi.org/10.1016/j.jneumeth.2010.06.020

Boly, M., Garrido, M.I., Gosseries, O., Bruno, M.A., Boveroux, P., Schnakers, C., Massimini, M., Litvak, V., Laureys, S., Friston, K., 2011. Preserved feedforward but impaired top-down processes in the vegetative state. Science (80-.). 332, 858–862. https://doi.org/10.1126/SCIENCE.1202043/SUPPL_FILE/1202043.BOLY.SOM.PDF

Brain stem reticular formation and activation of the EEG, 1949. . Electroencephalogr. Clin. Neurophysiol. 1, 455–473. https://doi.org/10.1016/0013-4694(49)90219-9

Bressler, S.L., Tang, W., Sylvester, C.M., Shulman, G.L., Corbetta, M., 2008. Top-down control of human visual cortex by frontal and parietal cortex in anticipatory visual spatial attention. J. Neurosci. 28, 10056–10061. https://doi.org/10.1523/JNEUROSCI.1776-08.2008

Bubic, A., Von Yves Cramon, D., Jacobsen, T., Schröger, E., Schubotz, R.I., 2009. Violation of Expectation: Neural Correlates Reflect Bases of Prediction. J. Cogn. Neurosci. 21, 155–168. https://doi.org/10.1162/JOCN.2009.21013

Bubic, A., Yves von Cramon, D., Schubotz, R.I., 2010. Prediction, cognition and the brain.

Front. Hum. Neurosci. 4, 25. https://doi.org/10.3389/FNHUM.2010.00025/BIBTEX

Calcus, A., Deltenre, P., Hoonhorst, I., Collet, G., Markessis, E., Colin, C., 2015. MMN and P300 are both modulated by the featured/featureless nature of deviant stimuli. Clin. Neurophysiol. 126, 1727–1734. https://doi.org/10.1016/J.CLINPH.2014.11.020

Callan, D.E., Jones, J.A., Munhall, K., Kroos, C., Callan, A.M., Vatikiotis-Bateson, E., 2004. Multisensory integration sites identified by perception of spatial wavelet filtered visual speech gesture information. J. Cogn. Neurosci. 16, 805–816. https://doi.org/10.1162/089892904970771

Capilla, A., Schoffelen, J.-M., Paterson, G., Thut, G., Gross, J., 2014. Dissociated α-Band Modulations in the Dorsal and Ventral Visual Pathways in Visuospatial Attention and Perception. Cereb. Cortex 24, 550–561. https://doi.org/10.1093/cercor/bhs343

Capotosto, P., Babiloni, C., Romani, G.L., Corbetta, M., 2009. Frontoparietal cortex controls spatial attention through modulation of anticipatory alpha rhythms. J. Neurosci. 29, 5863–5872. https://doi.org/10.1523/JNEUROSCI.0539-09.2009

Carretié, L., Kessel, D., García-Rubio, M.J., Giménez-Fernández, T., Hoyos, S., Hernández-Lorca, M., 2017. Magnocellular Bias in Exogenous Attention to Biologically Salient Stimuli as Revealed by Manipulating Their Luminosity and Color. J. Cogn. Neurosci. 29, 1699–1711. https://doi.org/10.1162/jocn_a_01148

Carter, A.R., Shulman, G.L., Corbetta, M., 2012. Why use a connectivity-based approach to study stroke and recovery of function? Neuroimage 62, 2271–2280. https://doi.org/10.1016/J.NEUROIMAGE.2012.02.070

Carter, R.M., Huettel, S.A., 2013. A nexus model of the temporal-parietal junction. Trends

Cogn. Sci. 17, 328–36. https://doi.org/10.1016/j.tics.2013.05.007

Cavanagh, P., Alvarez, G., 2005. Tracking multiple targets with multifocal attention. Trends Cogn. Sci. 9, 349–354. https://doi.org/10.1016/j.tics.2005.05.009

Cavanagh, P., Battelli, L., Holcombe, A.O., 2014. Dynamic attention Introduction: Tracking Events as They Unfold in Time.

Chen, Y., Bressler, S.L., Ding, M., 2006. Frequency decomposition of conditional Granger causality and application to multivariate neural field potential data. J. Neurosci. Methods 150, 228–237. https://doi.org/10.1016/j.jneumeth.2005.06.011

Chennu, S., Bekinschtein, T.A., 2012. Arousal modulates auditory attention and awareness: Insights from sleep, sedation, and disorders of consciousness. Front. Psychol. 3, 65. https://doi.org/10.3389/FPSYG.2012.00065/BIBTEX

Chennu, S., Noreika, V., Gueorguiev, D., Blenkmann, A., Kochen, S., Ibáñez, A., Owen, A.M., Bekinschtein, T.A., 2013. Expectation and Attention in Hierarchical Auditory Prediction. J. Neurosci. 33, 11194–11205. https://doi.org/10.1523/JNEUROSCI.0114-13.2013

Clark, A., 2013. Whatever next? Predictive brains, situated agents, and the future of cognitive science. Behav. Brain Sci. 36, 181–204. https://doi.org/10.1017/S0140525X12000477

Clark, V.P., Fannon, S., Lai, S., Benson, R., Bauer, L., 2000. Responses to rare visual target and distractor stimuli using event- related fMRI. J. Neurophysiol. 83, 3133–3139. https://doi.org/10.1152/JN.2000.83.5.3133/ASSET/IMAGES/LARGE/9K0500943001.JPEG

Cohen, M.X., Van Gaal, S., 2013. Dynamic interactions between large-scale brain networks predict behavioral adaptation after perceptual errors. Cereb. Cortex 23, 1061–1072. https://doi.org/10.1093/cercor/bhs069

Corbetta, M., Kincade, J.M., Ollinger, J.M., McAvoy, M.P., Shulman, G.L., 2000. Voluntary orienting is dissociated from target detection in human posterior parietal cortex. Nat. Neurosci. 2000 33 3, 292–297. https://doi.org/10.1038/73009

Corbetta, M., Kincade, M.J., Lewis, C., Snyder, A.Z., Sapir, A., 2005. Neural basis and recovery of spatial attention deficits in spatial neglect. Nat. Neurosci. 8, 1603–1610. https://doi.org/10.1038/nn1574

Corbetta, M., Miezin, F.M., Shulman, G.L., Petersen, S.E., 1993. A PET study of visuospatial attention. J. Neurosci. 13, 1202–1226. https://doi.org/10.1523/JNEUROSCI.13-03-01202.1993

Corbetta, M., Patel, G., Shulman, G.L., 2008. The Reorienting System of the Human Brain: From Environment to Theory of Mind. Neuron 58, 306–324. https://doi.org/10.1016/j.neuron.2008.04.017

Corbetta, M., Shulman, G.L., 2002. Control of goal-directed and stimulus-driven attention in the brain. Nat. Rev. Neurosci. 2002 33 3, 201–215. https://doi.org/10.1038/nrn755

Correa-Jaraba, K.S., Cid-Fernández, S., Lindín, M., Díaz, F., 2016. Involuntary Capture and Voluntary Reorienting of Attention Decline in Middle-Aged and Old Participants. Front. Hum. Neurosci. 10, 1–13. https://doi.org/10.3389/FNHUM.2016.00129

Coull, J.T., Nobre, A.C., 1998. Where and When to Pay Attention: The Neural Systems for Directing Attention to Spatial Locations and to Time Intervals as Revealed by Both

PET and fMRI. J. Neurosci. 18, 7426–7435. https://doi.org/10.1523/JNEUROSCI.18-18-07426.1998

Courchesne, E., Hillyard, S.A., Galambos, R., 1975. Stimulus novelty, task relevance and the visual evoked potential in man. Electroencephalogr. Clin. Neurophysiol. 39, 131–143. https://doi.org/10.1016/0013-4694(75)90003-6

Dale, A.M., Liu, A.K., Fischl, B.R., Buckner, R.L., Belliveau, J.W., Lewine, J.D., Halgren, E., 2000. Dynamic Statistical Parametric Mapping: Combining fMRI and MEG for High-Resolution Imaging of Cortical Activity. Neuron 26, 55–67. https://doi.org/10.1016/S0896-6273(00)81138-1

Daltrozzo, J., Wioland, N., Mutschler, V., Kotchoubey, B., 2007. Predicting coma and other low responsive patients outcome using event-related brain potentials: A meta-analysis. Clin. Neurophysiol. 118, 606–614. https://doi.org/10.1016/J.CLINPH.2006.11.019

Das, M., Singh, V., Uddin, L.Q., Banerjee, A., Roy, D., 2020. OUP accepted manuscript. Cereb. Cortex. https://doi.org/10.1093/cercor/bhaa334

Dattola, S., Morabito, F.C., Mammone, N., La Foresta, F., 2020. Findings about LORETA Applied to High-Density EEG—A Review. Electronics 9, 660. https://doi.org/10.3390/electronics9040660

David, N., Linden, E.J., 2005. The P300: Where in the Brain Is It Produced and What Does It Tell Us? https://doi.org/10.1177/1073858405280524

De Fockert, J., Rees, G., Frith, C., Lavie, N., 2004. Neural Correlates of Attentional Capture in Visual Search. J. Cogn. Neurosci. 16, 751–759. https://doi.org/10.1162/089892904970762

Decety, J., Lamm, C., 2007. The Role of the Right Temporoparietal Junction in Social Interaction: How Low-Level Computational Processes Contribute to Meta-Cognition. Neurosci. 13, 580–593. https://doi.org/10.1177/1073858407304654

Delorme, A., Makeig, S., 2004. EEGLAB: An open source toolbox for analysis of single-trial EEG dynamics including independent component analysis. J. Neurosci. Methods 134, 9–21. https://doi.org/10.1016/j.jneumeth.2003.10.009

Dhamala, M., Rangarajan, G., Ding, M., 2008. Analyzing information flow in brain networks with nonparametric Granger causality. Neuroimage 41, 354–362. https://doi.org/10.1016/j.neuroimage.2008.02.020

Diaconescu, Andreea Oliviana, Alain, C., Mcintosh, A.R., Diaconescu, A O, 2011. The co-occurrence of multisensory facilitation and cross-modal conflict in the human brain. J Neurophysiol 106, 2896–2909. https://doi.org/10.1152/jn.00303.2011.-Perceptual

Ding, M., Chen, Y., Bressler, S.L., 2006. Granger Causality: Basic Theory and Application to Neuroscience, in: Handbook of Time Series Analysis: Recent Theoretical Developments and Applications. Wiley-VCH Verlag GmbH & Co. KGaA, pp. 437–460. https://doi.org/10.1002/9783527609970.ch17

Dinteren, R., Arns, M., Jongsma, M.L.A., Kessels, R.P.C., 2014. P300 Development across the Lifespan: A Systematic Review and Meta-Analysis. PLoS One 9. https://doi.org/10.1371/JOURNAL.PONE.0087347

DiQuattro, N.E., Sawaki, R., Geng, J.J., 2014. Effective Connectivity During Feature-Based Attentional Capture: Evidence Against the Attentional Reorienting Hypothesis of TPJ. Cereb. Cortex 24, 3131–3141. https://doi.org/10.1093/cercor/bht172

Donchin, E., 1981. Surprise!… Surprise? Psychophysiology 18, 493–513. https://doi.org/10.1111/J.1469-8986.1981.TB01815.X

Donchin, E., Coles, M.G.H., 1988. Is the P300 component a manifestation of context updating? Behav. Brain Sci. 11, 357–374. https://doi.org/10.1017/S0140525X00058027

Downar, J., Crawley, A.P., Mikulis, D.J., Davis, K.D., 2001. The effect of task relevance on the cortical response to changes in visual and auditory stimuli: An event-related fMRI study. Neuroimage 14, 1256–1267. https://doi.org/10.1006/nimg.2001.0946

Downar, J., Crawley, A.P., Mikulis, D.J., Davis, K.D., 2000. A multimodal cortical network for the detection of changes in the sensory environment. Nat. Neurosci. 2000 33 3, 277–283. https://doi.org/10.1038/72991

Dugué, L., Merriam, E.P., Heeger, D.J., Carrasco, M., 2018. Specific visual subregions of TPJ mediate reorienting of spatial attention. Cereb. Cortex 28, 2375–2390. https://doi.org/10.1093/cercor/bhx140

Eddy, C.M., 2016. The junction between self and other? Temporo-parietal dysfunction in neuropsychiatry. Neuropsychologia 89, 465–477. https://doi.org/10.1016/J.NEUROPSYCHOLOGIA.2016.07.030

Erickson, M.A., Ruffle, A., Gold, J.M., 2016. A meta-analysis of mismatch negativity in schizophrenia: from clinical risk to disease specificity and progression. Biol. Psychiatry 79, 980. https://doi.org/10.1016/J.BIOPSYCH.2015.08.025

Escera, C., Alho, K., Schröger, E., Winkler, I., 2000. Involuntary Attention and Distractibility as Evaluated with Event-Related Brain Potentials. Audiol. Neurotol. 5,

151–166. https://doi.org/10.1159/000013877

Escera, C., Alho, K., Winkler, I., Näätänen, R., 1998. Neural Mechanisms of Involuntary Attention to Acoustic Novelty and Change. J. Cogn. Neurosci. 10, 590–604. https://doi.org/10.1162/089892998562997

Escera, C., Corral, M.J., 2007. Role of mismatch negativity and novelty-P3 in involuntary auditory attention. J. Psychophysiol. 21, 251–264. https://doi.org/10.1027/0269-8803.21.34.251

Escera, C., Yago, E., Alho, K., 2001. Electrical responses reveal the temporal dynamics of brain events during involuntary attention switching. Eur. J. Neurosci. 14, 877–883. https://doi.org/10.1046/J.0953-816X.2001.01707.X

Eulitz, C., Diesch, E., Pantev, C., Hampson, S., Elbert, T., 1995. Magnetic and electric brain activity evoked by the processing of tone and vowel stimuli. J. Neurosci. 15, 2748. https://doi.org/10.1523/JNEUROSCI.15-04-02748.1995

Faes, L., Krohova, J., Pernice, R., Busacca, A., Javorka, M., 2019. A new Frequency Domain Measure of Causality based on Partial Spectral Decomposition of Autoregressive Processes and its Application to Cardiovascular Interactions. Proc. Annu. Int. Conf. IEEE Eng. Med. Biol. Soc. EMBS 4258–4261. https://doi.org/10.1109/EMBC.2019.8857312

Farrant, K., Uddin, L.Q., 2015. Asymmetric development of dorsal and ventral attention networks in the human brain. Dev. Cogn. Neurosci. 12, 165–174. https://doi.org/10.1016/j.dcn.2015.02.001

Feng, T., Qiu, Y., Zhu, Y., Tong, S., 2008. Attention rivalry under irrelevant audiovisual

stimulation. Neurosci. Lett. 438, 6–9. https://doi.org/10.1016/J.NEULET.2008.04.049

Feng, W., Störmer, V.S., Martinez, A., McDonald, J.J., Hillyard, S.A., 2017a. Involuntary orienting of attention to a sound desynchronizes the occipital alpha rhythm and improves visual perception. Neuroimage 150, 318–328. https://doi.org/10.1016/j.neuroimage.2017.02.033

Feng, W., Störmer, V.S., Martinez, A., McDonald, J.J., Hillyard, S.A., 2017b. Involuntary orienting of attention to a sound desynchronizes the occipital alpha rhythm and improves visual perception. Neuroimage 150, 318–328. https://doi.org/10.1016/J.NEUROIMAGE.2017.02.033

Ficco, L., Mancuso, L., Manuello, J., Teneggi, A., Liloia, D., Duca, S., Costa, T., Kovacs, G.Z., Cauda, F., 2021. Disentangling predictive processing in the brain: a meta-analytic study in favour of a predictive network. Sci. Reports 2021 111 11, 1–14. https://doi.org/10.1038/s41598-021-95603-5

Fleming, J.T., Noyce, A.L., Shinn-Cunningham, B.G., 2020. Audio-visual spatial alignment improves integration in the presence of a competing audio-visual stimulus. Neuropsychologia 146, 107530. https://doi.org/10.1016/J.NEUROPSYCHOLOGIA.2020.107530

Folstein, J.R., Van Petten, C., 2008. Influence of cognitive control and mismatch on the N2 component of the ERP: A review. Psychophysiology 45, 152–170. https://doi.org/10.1111/J.1469-8986.2007.00602.X

Fontolan, L., Morillon, B., Liegeois-Chauvel, C., Giraud, A.L., 2014. The contribution of frequency-specific activity to hierarchical information processing in the human auditory cortex. Nat. Commun. 2014 51 5, 1–10. https://doi.org/10.1038/ncomms5694

Fox, M.D., Corbetta, M., Snyder, A.Z., Vincent, J.L., Raichle, M.E., 2006. Spontaneous neuronal activity distinguishes human dorsal and ventral attention systems. Proc. Natl. Acad. Sci. U. S. A. 103, 10046–10051. https://doi.org/10.1073/PNAS.0604187103/SUPPL_FILE/04187FIG9.JPG

Foxe, J.J., Simpson, G. V., Ahlfors, S.P., 1998. Parieto-occipital ~10 Hz activity reflects anticipatory state of visual attention mechanisms. Neuroreport 9, 3929–3933. https://doi.org/10.1097/00001756-199812010-00030

Foxe, J.J., Simpson, G. V., Ahlfors, S.P., Saron, C.D., 2005. Biasing the brain's attentional set: I. Cue driven deployments of intersensory selective attention. Exp. Brain Res. 166, 370–392. https://doi.org/10.1007/S00221-005-2378-7/FIGURES/9

Foxe, J.J., Snyder, A.C., 2011. The role of alpha-band brain oscillations as a sensory suppression mechanism during selective attention. Front. Psychol. 2, 154. https://doi.org/10.3389/FPSYG.2011.00154/BIBTEX

Frey, J.N., Mainy, N., Lachaux, J.-P., Müller, N., Bertrand, O., Weisz, N., 2014. Selective Modulation of Auditory Cortical Alpha Activity in an Audiovisual Spatial Attention Task. https://doi.org/10.1523/JNEUROSCI.4813-13.2014

Friedman, D., Cycowicz, Y.M., Gaeta, H., 2001. The novelty P3: an event-related brain potential (ERP) sign of the brain's evaluation of novelty. Neurosci. Biobehav. Rev. 25, 355–373. https://doi.org/10.1016/S0149-7634(01)00019-7

Fries, P., Reynolds, J.H., Rorie, A.E., Desimone, R., 2001. Modulation of oscillatory neuronal synchronization by selective visual attention. Science (80-.). 291, 1560–1563. https://doi.org/10.1126/science.1055465

Friston, K., 2010. The free-energy principle: a unified brain theory? Nat. Rev. Neurosci. 2010 112 11, 127–138. https://doi.org/10.1038/nrn2787

Friston, K., 2005. A theory of cortical responses. Philos. Trans. R. Soc. B Biol. Sci. 360, 815–836. https://doi.org/10.1098/RSTB.2005.1622

Fritz, J.B., Elhilali, M., David, S. V., Shamma, S.A., 2007. Auditory attention — focusing the searchlight on sound. Curr. Opin. Neurobiol. 17, 437–455. https://doi.org/10.1016/J.CONB.2007.07.011

Fu, K.M.G., Foxe, J.J., Murray, M.M., Higgins, B.A., Javitt, D.C., Schroeder, C.E., 2001. Attention-dependent suppression of distracter visual input can be cross-modally cued as indexed by anticipatory parieto-occipital alpha-band oscillations. Cogn. Brain Res. 12, 145–152. https://doi.org/10.1016/S0926-6410(01)00034-9

Garrido, M.I., Kilner, J.M., Stephan, K.E., Friston, K.J., 2009. The mismatch negativity: A review of underlying mechanisms. Clin. Neurophysiol. 120, 453. https://doi.org/10.1016/J.CLINPH.2008.11.029

Geweke, J., 1982. Measurement of linear dependence and feedback between multiple time series. J. Am. Stat. Assoc. 77, 304–313. https://doi.org/10.1080/01621459.1982.10477803

Ghosh, P., Roy, D., Banerjee, A., 2021. Organization of directed functional connectivity among nodes of ventral attention network reveals the common network mechanisms underlying saliency processing across distinct spatial and spatio-temporal scales. Neuroimage 117869. https://doi.org/10.1016/j.neuroimage.2021.117869

Giard, M. -H, Perrin, F., Pernier, J., Bouchet, P., 1990. Brain Generators Implicated in the

Processing of Auditory Stimulus Deviance: A Topographic Event-Related Potential Study. Psychophysiology 27, 627–640. https://doi.org/10.1111/J.1469-8986.1990.TB03184.X

Gillebert, C.R., Mantini, D., Peeters, R., Dupont, P., Vandenberghe, R., 2013. Cytoarchitectonic mapping of attentional selection and reorienting in parietal cortex. Neuroimage 67, 257–272. https://doi.org/10.1016/j.neuroimage.2012.11.026

Gonsalvez, C.J., Barry, R.J., Rushby, J.A., Polich, J., 2007. Target-to-target interval, intensity, and P300 from an auditory single-stimulus task. Psychophysiology 44, 245–250. https://doi.org/10.1111/J.1469-8986.2007.00495.X

Gonsalvez, C.J., Polich, J., 2002. P300 amplitude is determined by target-to-target interval. Psychophysiology 39, 388–396. https://doi.org/10.1017/S0048577201393137

Gootjes, L., Raij, T., Salmelin, R., Hari, R., 1999. Left-hemisphere dominance for processing of vowels: a whole-scalp neuromagnetic study. Neuroreport 10, 2987–2991. https://doi.org/10.1097/00001756-199909290-00021

Gramfort, A., Papadopoulo, T., Olivi, E., Clerc, M., 2010. OpenMEEG: Opensource software for quasistatic bioelectromagnetics. Biomed. Eng. Online 9, 1–20. https://doi.org/10.1186/1475-925X-9-45/TABLES/2

Granger, C.W.J., 1969. Investigating Causal Relations by Econometric Models and Cross-spectral Methods. Econometrica 37, 424. https://doi.org/10.2307/1912791

Haegens, S., Cousijn, H., Wallis, G., Harrison, P.J., Nobre, A.C., 2014. Inter- and intra-individual variability in alpha peak frequency. Neuroimage 92, 46–55. https://doi.org/10.1016/j.neuroimage.2014.01.049

Halder, T., Talwar, S., Jaiswal, A.K., Banerjee, A., 2019. Quantitative Evaluation in Estimating Sources Underlying Brain Oscillations Using Current Source Density Methods and Beamformer Approaches. eneuro 6, ENEURO.0170-19.2019. https://doi.org/10.1523/eneuro.0170-19.2019

Hale, T.S., Smalley, S.L., Hanada, G., Macion, J., McCracken, J.T., McGough, J.J., Loo, S.K., 2009. Atypical alpha asymmetry in adults with ADHD. Neuropsychologia 47, 2082–2088. https://doi.org/10.1016/j.neuropsychologia.2009.03.021

Han, S.W., Marois, R., 2014. Functional fractionation of the stimulus-driven attention network. J. Neurosci. 34, 6958–6969. https://doi.org/10.1523/JNEUROSCI.4975-13.2014

Haufe, S., Nikulin, V. V., Müller, K.R., Nolte, G., 2013. A critical assessment of connectivity measures for EEG data: A simulation study. Neuroimage 64, 120–133. https://doi.org/10.1016/j.neuroimage.2012.09.036

Haufe, S., Nikulin, V. V., Nolte, G., 2012. Alleviating the influence of weak data asymmetries on Granger-causal analyses, in: Lecture Notes in Computer Science (Including Subseries Lecture Notes in Artificial Intelligence and Lecture Notes in Bioinformatics). Springer, Berlin, Heidelberg, pp. 25–33. https://doi.org/10.1007/978-3-642-28551-6_4

Helmholtz, H. von, 1867. Handbuch der physiologischen Optik: mit 213 in den Text eingedruckten ... - Hermann von Helmholtz - Google Books [WWW Document]. URL https://books.google.co.in/books?hl=en&lr=&id=4u7lRLnD11IC&oi=fnd&pg=PA1&dq=Helmholtz,+H.+von+(1867).+Handbuch+der+physiologischen+Optik.+Leipzig:+L.+Voss.&ots=XRgD_e29ws&sig=YCLriwghhzD52rkD0pBlnp9itXs&redir_esc=y#v

=onepage&q=Helmholtz%2C H. von (1867). (accessed 7.29.22).

Helmholtz, H. von, 1866. Treatise on Physiological Optics, Book.

Herrmann, C.S., Munk, M.H.J., Engel, A.K., 2004. Cognitive functions of gamma-band activity: memory match and utilization. Trends Cogn. Sci. 8, 347–355. https://doi.org/10.1016/J.TICS.2004.06.006

Hoffman, R.M., Embury, C.M., Lew, B.J., Heinrichs-Graham, E., Wilson, T.W., Kurz, M.J., 2021. Cortical oscillations that underlie visual selective attention are abnormal in adolescents with cerebral palsy. Sci. Reports 2021 111 11, 1–8. https://doi.org/10.1038/s41598-021-83898-3

Hölig, C., Berti, S., 2010. To switch or not to switch: Brain potential indices of attentional control after task-relevant and task-irrelevant changes of stimulus features. Brain Res. 1345, 164–175. https://doi.org/10.1016/J.BRAINRES.2010.05.047

Hommel, B., Chapman, C.S., Cisek, P., Neyedli, H.F., Song, J.H., Welsh, T.N., 2019. No one knows what attention is. Attention, Perception, Psychophys. 81, 2288–2303. https://doi.org/10.3758/S13414-019-01846-W/FIGURES/3

Horváth, J., Winkler, I., Bendixen, A., 2008. Do N1/MMN, P3a, and RON form a strongly coupled chain reflecting the three stages of auditory distraction? Biol. Psychol. 79, 139–147. https://doi.org/10.1016/J.BIOPSYCHO.2008.04.001

Ikkai, A., Dandekar, S., Curtis, C.E., 2016. Lateralization in Alpha-Band Oscillations Predicts the Locus and Spatial Distribution of Attention. https://doi.org/10.1371/journal.pone.0154796

Jakobs, O., Langner, R., Caspers, S., Roski, C., Cieslik, E.C., Zilles, K., Laird, A.R., Fox,

P.T., Eickhoff, S.B., 2012. Across-study and within-subject functional connectivity of a right temporo-parietal junction subregion involved in stimulus-context integration. Neuroimage 60, 2389–2398. https://doi.org/10.1016/j.neuroimage.2012.02.037

James', W., 1890. An Analysis of William James's The Principles of Psychology. Princ. Psychol. https://doi.org/10.4324/9781912282494

Jensen, O., Bonnefond, M., VanRullen, R., 2012. An oscillatory mechanism for prioritizing salient unattended stimuli. Trends Cogn. Sci. 16, 200–206. https://doi.org/10.1016/J.TICS.2012.03.002

Jensen, O., Mazaheri, A., 2010. Shaping functional architecture by oscillatory alpha activity: Gating by inhibition. Front. Hum. Neurosci. 4. https://doi.org/10.3389/fnhum.2010.00186

Jimenez, A.M., Lee, J., Wynn, J.K., Cohen, M.S., Engel, S.A., Glahn, D.C., Nuechterlein, K.H., Reavis, E.A., Green, M.F., 2016. Abnormal ventral and dorsal attention network activity during single and dual target detection in schizophrenia. Front. Psychol. 7, 323. https://doi.org/10.3389/FPSYG.2016.00323/BIBTEX

Johnson, R., Donchin, E., 1980. P300 and Stimulus Categorization: Two Plus One is not so Different from One Plus One. Psychophysiology 17, 167–178. https://doi.org/10.1111/J.1469-8986.1980.TB00131.X

Justen, C., Herbert, C., 2018. The spatio-temporal dynamics of deviance and target detection in the passive and active auditory oddball paradigm: a sLORETA study. BMC Neurosci. 19, 25. https://doi.org/10.1186/S12868-018-0422-3

Justo-Guillén, E., Ricardo-Garcell, J., Rodríguez-Camacho, M., Rodríguez-Agudelo, Y.,

Lelo de Larrea-Mancera, E.S., Solís-Vivanco, R., 2019. Auditory mismatch detection, distraction, and attentional reorientation (MMN-P3a-RON) in neurological and psychiatric disorders: A review. Int. J. Psychophysiol. 146, 85–100. https://doi.org/10.1016/J.IJPSYCHO.2019.09.010

Kahana, M.J., 2006. The Cognitive Correlates of Human Brain Oscillations. J. Neurosci. 26, 1669–1672. https://doi.org/10.1523/JNEUROSCI.3737-05C.2006

Kapur, S., 2003. Psychosis as a state of aberrant salience: A framework linking biology, phenomenology, and pharmacology in schizophrenia. Am. J. Psychiatry 160, 13–23. https://doi.org/10.1176/APPI.AJP.160.1.13

Karch, S., Loy, F., Krause, D., Schwarz, S., Kiesewetter, J., Segmiller, F., Chrobok, A.I., Keeser, D., Pogarell, O., 2016. Increased event-related potentials and alpha-, beta-, and gamma-activity associated with intentional actions. Front. Psychol. 7, 7. https://doi.org/10.3389/FPSYG.2016.00007/BIBTEX

Kastner, S., Pinsk, M.A., De Weerd, P., Desimone, R., Ungerleider, L.G., 1999. Increased Activity in Human Visual Cortex during Directed Attention in the Absence of Visual Stimulation. Neuron 22, 751–761. https://doi.org/10.1016/S0896-6273(00)80734-5

Keefe, J.M., Pokta, E., Störmer, V.S., 2021. Cross-modal orienting of exogenous attention results in visual-cortical facilitation, not suppression. Sci. Reports 2021 111 11, 1–11. https://doi.org/10.1038/s41598-021-89654-x

Kelly, S.P., Lalor, E.C., Reilly, R.B., Foxe, J.J., 2006. Increases in alpha oscillatory power reflect an active retinotopic mechanism for distracter suppression during sustained visuospatial attention. J. Neurophysiol. 95, 3844–3851. https://doi.org/10.1152/jn.01234.2005

KIEHL, K.A., LAURENS, K.R., DUTY, T.L., FORSTER, B.B., LIDDLE, P.F., 2001. Neural sources involved in auditory target detection and novelty processing: An event-related fMRI study. Psychophysiology 38, 133–142. https://doi.org/10.1111/1469-8986.3810133

Kim, H., 2014. Involvement of the dorsal and ventral attention networks in oddball stimulus processing: A meta-analysis. Hum. Brain Mapp. 35, 2265–2284. https://doi.org/10.1002/HBM.22326

Kincade, J.M., Abrams, R.A., Astafiev, S. V., Shulman, G.L., Corbetta, M., 2005. An Event-Related Functional Magnetic Resonance Imaging Study of Voluntary and Stimulus-Driven Orienting of Attention. J. Neurosci. 25, 4593–4604. https://doi.org/10.1523/JNEUROSCI.0236-05.2005

Kiss, M., Grubert, A., Petersen, A., Eimer, M., 2012. Attentional capture by salient distractors during visual search is determined by temporal task demands. J. Cogn. Neurosci. 24, 749–759. https://doi.org/10.1162/jocn_a_00127

Klimesch, W., 2012. Alpha-band oscillations, attention, and controlled access to stored information. Trends Cogn. Sci. 16, 606–617. https://doi.org/10.1016/J.TICS.2012.10.007

Klimesch, W., 1996. Memory processes, brain oscillations and EEG synchronization. Int. J. Psychophysiol. 24, 61–100. https://doi.org/10.1016/S0167-8760(96)00057-8

Klimesch, W., Sauseng, P., Hanslmayr, S., 2007. EEG alpha oscillations: The inhibition-timing hypothesis. Brain Res. Rev. https://doi.org/10.1016/j.brainresrev.2006.06.003

Koelsch, S., Heinke, W., Sammler, D., Olthoff, D., 2006. Auditory processing during deep

propofol sedation and recovery from unconsciousness. Clin. Neurophysiol. 117, 1746–1759. https://doi.org/10.1016/J.CLINPH.2006.05.009

Kok, A., 2001. On the utility of P3 amplitude as a measure of processing capacity. Psychophysiology 38, 557–577. https://doi.org/10.1017/S0048577201990559

Kok, P., Rahnev, D., Jehee, J.F.M., Lau, H.C., De Lange, F.P., 2012. Attention reverses the effect of prediction in silencing sensory signals. Cereb. Cortex 22, 2197–2206. https://doi.org/10.1093/CERCOR/BHR310

Krall, S.C., Rottschy, C., Oberwelland, E., Bzdok, D., Fox, P.T., Eickhoff, S.B., Fink, G.R., Konrad, K., 2015. The role of the right temporoparietal junction in attention and social interaction as revealed by ALE meta-analysis. Brain Struct. Funct. 220, 587–604. https://doi.org/10.1007/s00429-014-0803-z

Kulikowski, J.J., Tolhurst, D.J., 1973. Psychophysical evidence for sustained and transient detectors in human vision. J. Physiol. 232, 149–162. https://doi.org/10.1113/jphysiol.1973.sp010261

Lenartowicz, A., Mazaheri, A., Jensen, O., Loo, S.K., 2018. Aberrant Modulation of Brain Oscillatory Activity and Attentional Impairment in Attention-Deficit/Hyperactivity Disorder. Biol. Psychiatry Cogn. Neurosci. Neuroimaging. https://doi.org/10.1016/j.bpsc.2017.09.009

Leone, L.M., Mccourt, M.E., 2015. Dissociation of perception and action in audiovisual multisensory integration. Eur. J. Neurosci. 42, 2915. https://doi.org/10.1111/EJN.13087

Li, D.-B., Liu, R.-S., Wang, X., Xiong, P.-A., Ren, H.-W., Wei, Y.-F., Zhang, L.-M., Gao,

Y.-J., 2021. Abnormal ventral attention network homogeneity in patients with right temporal lobe epilepsy.

Lins, O.G., Picton, T.W., Berg, P., Scherg, M., 1993. Ocular artifacts in EEG and event-related potentials I: Scalp topography. Brain Topogr. 1993 61 6, 51–63. https://doi.org/10.1007/BF01234127

Liu, J., Xu, P., Zhang, J., Jiang, N., Li, X., Luo, Y., 2019. Ventral attention-network effective connectivity predicts individual differences in adolescent depression. J. Affect. Disord. 252, 55–59. https://doi.org/10.1016/j.jad.2019.04.033

Liu, Y., Bengson, J., Huang, H., Mangun, G.R., Ding, M., 2014. Top-down Modulation of Neural Activity in Anticipatory Visual Attention: Control Mechanisms Revealed by Simultaneous EEG-fMRI. Cereb. Cortex bhu204. https://doi.org/10.1093/cercor/bhu204

Luca, M. Di, Machulla, T.-K., Ernst, M.O., 2009. Recalibration of multisensory simultaneity: Cross-modal transfer coincides with a change in perceptual latency. J. Vis. 9, 7–7. https://doi.org/10.1167/9.12.7

Luo, H., Husain, F.T., Horwitz, B., Poeppel, D., 2005. Discrimination and categorization of speech and non-speech sounds in an MEG delayed-match-to-sample study. Neuroimage 28, 59–71. https://doi.org/10.1016/J.NEUROIMAGE.2005.05.040

Macaluso, E., Doricchi, F., 2013. Attention and predictions: control of spatial attention beyond the endogenous-exogenous dichotomy. Front. Hum. Neurosci. 7. https://doi.org/10.3389/FNHUM.2013.00685

Magliero, A., Bashore, T.R., Coles, M.G.H., Donchin, E., 1984. On the Dependence of P300

Latency on Stimulus Evaluation Processes. Psychophysiology 21, 171–186. https://doi.org/10.1111/J.1469-8986.1984.TB00201.X

Mäntysalo, S., Näätänen, R., 1987. The duration of a neuronal trace of an auditory stimulus as indicated by event-related potentials. Biol. Psychol. 24, 183–195. https://doi.org/10.1016/0301-0511(87)90001-9

Marucci, M., Di Flumeri, G., Borghini, G., Sciaraffa, N., Scandola, M., Pavone, E.F., Babiloni, F., Betti, V., Aricò, P., 2021. The impact of multisensory integration and perceptual load in virtual reality settings on performance, workload and presence. Sci. Rep. 11. https://doi.org/10.1038/S41598-021-84196-8

Mayer, A.R., Harrington, D., Adair, J.C., Lee, R., 2006. The neural networks underlying endogenous auditory covert orienting and reorienting. Neuroimage 30, 938–949. https://doi.org/10.1016/J.NEUROIMAGE.2005.10.050

Mazaheri, A., Fassbender, C., Coffey-Corina, S., Hartanto, T.A., Schweitzer, J.B., Mangun, G.R., 2014. Differential oscillatory electroencephalogram between attention-deficit/ hyperactivity disorder subtypes and typically developing adolescents. Biol. Psychiatry 76, 422–429. https://doi.org/10.1016/j.biopsych.2013.08.023

McCarthy, H., Skokauskas, N., Mulligan, A., Donohoe, G., Mullins, D., Kelly, J., Johnson, K., Fagan, A., Gill, M., Meaney, J., Frodl, T., 2013. Attention Network Hypoconnectivity With Default and Affective Network Hyperconnectivity in Adults Diagnosed With Attention-Deficit/Hyperactivity Disorder in Childhood. JAMA Psychiatry 70, 1329–1337. https://doi.org/10.1001/JAMAPSYCHIATRY.2013.2174

McDermott, T.J., Wiesman, A.I., Mills, M.S., Spooner, R.K., Coolidge, N.M., Proskovec, A.L., Heinrichs-Graham, E., Wilson, T.W., 2019. tDCS modulates behavioral

performance and the neural oscillatory dynamics serving visual selective attention. Hum. Brain Mapp. 40, 729–740. https://doi.org/10.1002/HBM.24405

McDermott, T.J., Wiesman, A.I., Proskovec, A.L., Heinrichs-Graham, E., Wilson, T.W., 2017. Spatiotemporal oscillatory dynamics of visual selective attention during a flanker task. Neuroimage 156, 277–285. https://doi.org/10.1016/J.NEUROIMAGE.2017.05.014

Menon, V., Uddin, L.Q., 2010. Saliency, switching, attention and control: a network model of insula function. Brain Struct. Funct. https://doi.org/10.1007/s00429-010-0262-0

Molholm, S., Martinez, A., Ritter, W., Javitt, D.C., Foxe, J.J., 2005. The neural circuitry of pre-attentive auditory change-detection: an fMRI study of pitch and duration mismatch negativity generators. Cereb. Cortex 15, 545–551. https://doi.org/10.1093/CERCOR/BHH155

Molholm, S., Ritter, W., Murray, M.M., Javitt, D.C., Schroeder, C.E., Foxe, J.J., 2002. Multisensory auditory-visual interactions during early sensory processing in humans: a high-density electrical mapping study. Brain Res. Cogn. Brain Res. 14, 115–128. https://doi.org/10.1016/S0926-6410(02)00066-6

Monsa, R., Peer, M., Arzy, S., 2020. Processing of different temporal scales in the human brain. J. Cogn. Neurosci. 32, 2087–2102. https://doi.org/10.1162/jocn_a_01615

Morlet, D., Fischer, C., 2014. MMN and Novelty P3 in Coma and Other Altered States of Consciousness: A Review. Brain Topogr. 27, 467. https://doi.org/10.1007/S10548-013-0335-5

Mountcastle, V.B., 1978. Brain mechanisms for directed attention. J. R. Soc. Med. 71, 14–

28. https://doi.org/10.1177/014107687807100105

Muller-Gass, A., Stelmack, R.M., Campbell, K.B., 2005. "…and were instructed to read a self-selected book while ignoring the auditory stimuli": The effects of task demands on the mismatch negativity. Clin. Neurophysiol. 116, 2142–2152. https://doi.org/10.1016/J.CLINPH.2005.05.012

Näätänen, R., 1990. The role of attention in auditory information processing as revealed by event-related potentials and other brain measures of cognitive function. Behav. Brain Sci. 13, 201–233. https://doi.org/10.1017/S0140525X00078407

Näätänen, R., Gaillard, A.W.K., Mäntysalo, S., 1978. Early selective-attention effect on evoked potential reinterpreted. Acta Psychol. (Amst). 42, 313–329. https://doi.org/10.1016/0001-6918(78)90006-9

Näätänen, R., Jacobsen, T., Winkler, I., 2005. Memory-based or afferent processes in mismatch negativity (MMN): A review of the evidence. Psychophysiology 42, 25–32. https://doi.org/10.1111/J.1469-8986.2005.00256.X

Näätänen, R., Michie, P.T., 1979. Early selective-attention effects on the evoked potential: A critical review and reinterpretation. Biol. Psychol. 8, 81–136. https://doi.org/10.1016/0301-0511(79)90053-X

Näätänen, R., Paavilainen, P., Rinne, T., Alho, K., 2007. The mismatch negativity (MMN) in basic research of central auditory processing: A review. Clin. Neurophysiol. 118, 2544–2590. https://doi.org/10.1016/J.CLINPH.2007.04.026

Neto, E., Allen, E.A., Aurlien, H., Nordby, H., Eichele, T., 2015. EEG spectral features discriminate between Alzheimer's and vascular dementia. Front. Neurol. 6, 25.

https://doi.org/10.3389/fneur.2015.00025

Nikulin, V. V., Brismar, T., 2006. Phase synchronization between alpha and beta oscillations in the human electroencephalogram. Neuroscience 137, 647–657. https://doi.org/10.1016/j.neuroscience.2005.10.031

Nimmrich, V., Draguhn, A., Axmacher, N., 2015. Neuronal Network Oscillations in Neurodegenerative Diseases. NeuroMolecular Med. 17, 270–284. https://doi.org/10.1007/S12017-015-8355-9/TABLES/1

Nobre, A.C., Coull, J.T., 2012. Attention and Time, Attention and Time. Oxford University Press. https://doi.org/10.1093/acprof:oso/9780199563456.001.0001

Nobre, A.C., Coull, J.T., Frith, C.D., Mesulam, M.M., 1999. Orbitofrontal cortex is activated during breaches of expectation in tasks of visual attention. Nat. Neurosci. 1999 21 2, 11–12. https://doi.org/10.1038/4513

Noonan, M.A.P., Adamian, N., Pike, A., Printzlau, F., Crittenden, B.M., Stokes, M.G., 2016. Distinct mechanisms for distractor suppression and target facilitation. J. Neurosci. 36, 1797–1807. https://doi.org/10.1523/JNEUROSCI.2133-15.2016

Nyman, G., Alho, K., Laurinen, P., Paavilainen, P., Radil, T., Reinikainen, K., Sams, M., Näätänen, R., 1990. Mismatch negativity (MMN) for sequences of auditory and visual stimuli: evidence for a mechanism specific to the auditory modality. Electroencephalogr. Clin. Neurophysiol. Evoked Potentials 77, 436–444. https://doi.org/10.1016/0168-5597(90)90004-W

Oostenveld, R., Fries, P., Maris, E., Schoffelen, J.M., 2011. FieldTrip: Open source software for advanced analysis of MEG, EEG, and invasive electrophysiological data. Comput.

Intell. Neurosci. 2011. https://doi.org/10.1155/2011/156869

Pagnotta, M.F., Dhamala, M., Plomp, G., 2018a. Benchmarking nonparametric Granger causality: Robustness against downsampling and influence of spectral decomposition parameters. Neuroimage 183, 478–494. https://doi.org/10.1016/j.neuroimage.2018.07.046

Pagnotta, M.F., Dhamala, M., Plomp, G., 2018b. Assessing the performance of Granger– Geweke causality: Benchmark dataset and simulation framework. Data Br. 21, 833– 851. https://doi.org/10.1016/j.dib.2018.10.034

Palaniyappan, L., Liddle, P.F., 2012. Does the salience network play a cardinal role in psychosis? An emerging hypothesis of insular dysfunction. J. Psychiatry Neurosci. 37, 17–27. https://doi.org/10.1503/JPN.100176

Palva, S., Palva, J.M., Shtyrov, Y., Kujala, T., Ilmoniemi, R.J., Kaila, K., Näätänen, R., 2002. Distinct gamma-band evoked responses to speech and non-speech sounds in humans. J. Neurosci. 22. https://doi.org/10.1523/JNEUROSCI.22-04-J0003.2002

Papo, D., 2013. Time scales in cognitive neuroscience. Front. Physiol. 4 APR. https://doi.org/10.3389/fphys.2013.00086

Parviainen, T., Helenius, P., Salmelin, R., 2005. Cortical differentiation of speech and nonspeech sounds at 100 ms: implications for dyslexia. Cereb. Cortex 15, 1054–1063. https://doi.org/10.1093/CERCOR/BHH206

Pascual-Marqui, R.D., 2007a. Discrete, 3D distributed, linear imaging methods of electric neuronal activity. Part 1: exact, zero error localization.

Pascual-Marqui, R.D., 2007b. Discrete, 3D distributed, linear imaging methods of electric

neuronal activity. Part 1: exact, zero error localization. Llinas.

Pascucci, D., Hervais-Adelman, A., Plomp, G., 2018. Gating by induced Α–Γ asynchrony in selective attention. Hum. Brain Mapp. 39, 3854–3870. https://doi.org/10.1002/HBM.24216

Patel, S.H., Azzam, P.N., 2005. Characterization of N200 and P300: Selected Studies of the Event-Related Potential. Int. J. Med. Sci. 2, 147. https://doi.org/10.7150/IJMS.2.147

Pattamadilok, C., Sato, M., 2022. How are visemes and graphemes integrated with speech sounds during spoken word recognition? ERP evidence for supra-additive responses during audiovisual compared to auditory speech processing. Brain Lang. 225, 105058. https://doi.org/10.1016/J.BANDL.2021.105058

Pazo-Alvarez, P., Cadaveira, F., Amenedo, E., 2003. MMN in the visual modality: a review. Biol. Psychol. 63, 199–236. https://doi.org/10.1016/S0301-0511(03)00049-8

Pedrazzini, E., Ptak, R., 2019. Damage to the right temporoparietal junction, but not lateral prefrontal or insular cortex, amplifies the role of goal-directed attention. Sci. Rep. 9, 306. https://doi.org/10.1038/s41598-018-36537-3

Peelen, M. V., Heslenfeld, D.J., Theeuwes, J., 2004. Endogenous and exogenous attention shifts are mediated by the same large-scale neural network. Neuroimage 22, 822–830. https://doi.org/10.1016/j.neuroimage.2004.01.044

Pfurtscheller, G., Lopes Da Silva, F.H., 1999. Event-related EEG/MEG synchronization and desynchronization: basic principles. Clin. Neurophysiol. 110, 1842–1857. https://doi.org/10.1016/S1388-2457(99)00141-8

Phillips, C., Pellathy, T., Marantz, A., Yellin, E., Wexler, K., Poeppel, D., McGinnis, M.,

Roberts, T., 2000. Auditory cortex accesses phonological categories: an MEG mismatch study. J. Cogn. Neurosci. 12, 1038–1055. https://doi.org/10.1162/08989290051137567

Picton, T.W., Alain, C., Otten, L., Ritter, W., Achim, A., 2000. Mismatch Negativity: Different Water in the Same River. Audiol. Neurotol. 5, 111–139. https://doi.org/10.1159/000013875

Polich, J., 2007a. Updating P300: an integrative theory of P3a and P3b. Clin. Neurophysiol. 118, 2128–2148. https://doi.org/10.1016/J.CLINPH.2007.04.019

Polich, J., 2007b. Updating P300: An Integrative Theory of P3a and P3b. Clin. Neurophysiol. 118, 2128. https://doi.org/10.1016/J.CLINPH.2007.04.019

Polich, J., Criado, J.R., 2006. Neuropsychology and neuropharmacology of P3a and P3b. Int. J. Psychophysiol. 60, 172–185. https://doi.org/10.1016/J.IJPSYCHO.2005.12.012

Polich, J., Ladish, C., Burns, T., 1990. Normal variation of P300 in children: age, memory span, and head size. Int. J. Psychophysiol. 9, 237–248. https://doi.org/10.1016/0167-8760(90)90056-J

Posner, M.I., 1980. Orienting of Attention*: https://doi.org/10.1080/00335558008248231 32, 3–25. https://doi.org/10.1080/00335558008248231

Posner, M.I., Raichle, M.E., 1998. The neuroimaging of human brain function. Proc. Natl. Acad. Sci. U. S. A. 95, 763–764. https://doi.org/10.1073/PNAS.95.3.763/ASSET/DDA9631B-6A0E-46FA-9ECF-3B549F18B0A7/ASSETS/PNAS.95.3.763.FP.PNG

Posner, M.I., Raichle, M.E., 1994. Images of mind. - PsycNET [WWW Document]. URL

https://psycnet.apa.org/record/1994-97426-000 (accessed 7.29.22).

Posner, M.I., Walker, J.A., Friedrich, F.J., Rafal, R.D., 1984. EFFECTS OF PARIETAL INJURY ON COVERT ORIENTING OF ATTENTION' 4, 1863–1874.

Raghavachari, S., Kahana, M.J., Rizzuto, D.S., Caplan, J.B., Kirschen, M.P., Bourgeois, B., Madsen, J.R., Lisman, J.E., 2001. Gating of Human Theta Oscillations by a Working Memory Task. J. Neurosci. 21, 3175–3183. https://doi.org/10.1523/JNEUROSCI.21-09-03175.2001

Reinhart, R.M.G., Mathalon, D.H., Roach, B.J., Ford, J.M., 2011. Relationships between pre-stimulus gamma power and subsequent P300 and reaction time breakdown in schizophrenia. Int. J. Psychophysiol. 79, 16–24. https://doi.org/10.1016/J.IJPSYCHO.2010.08.009

Rihs, T.A., Michel, C.M., Thut, G., 2007. Mechanisms of selective inhibition in visual spatial attention are indexed by ?-band EEG synchronization. Eur. J. Neurosci. 25, 603–610. https://doi.org/10.1111/j.1460-9568.2007.05278.x

Rogers, J.C., Möttönen, R., Boyles, R., Watkins, K.E., 2014. Discrimination of speech and non-speech sounds following theta-burst stimulation of the motor cortex. Front. Psychol. 5, 754. https://doi.org/10.3389/FPSYG.2014.00754/BIBTEX

Rohrbaugh, J.W., Donchin, E., Eriksen, C.W., 1974. Decision making and the P300 component of the cortical evoked response. Percept. Psychophys. 1974 152 15, 368–374. https://doi.org/10.3758/BF03213960

Said, S.E., Dickey, D.A., 1984. Testing for unit roots in autoregressive-moving average models of unknown order. Biometrika 71, 599–607.

https://doi.org/10.1093/biomet/71.3.599

Salmi, J., Rinne, T., Koistinen, S., Salonen, O., Alho, K., 2009. Brain networks of bottom-up triggered and top-down controlled shifting of auditory attention. Brain Res. 1286, 155–164. https://doi.org/10.1016/J.BRAINRES.2009.06.083

Sams, M., Paavilainen, P., Alho, K., Näätänen, R., 1985. Auditory frequency discrimination and event-related potentials. Electroencephalogr. Clin. Neurophysiol. Potentials Sect. 62, 437–448. https://doi.org/10.1016/0168-5597(85)90054-1

Schneider, D., Göddertz, A., Haase, H., Hickey, C., Wascher, E., 2019. Hemispheric asymmetries in EEG alpha oscillations indicate active inhibition during attentional orienting within working memory. Behav. Brain Res. 359, 38–46. https://doi.org/10.1016/j.bbr.2018.10.020

Schröger, E., 1997. On the detection of auditory deviations: A pre-attentive activation model. Psychophysiology 34, 245–257. https://doi.org/10.1111/J.1469-8986.1997.TB02395.X

Schröger, E., 1996. A Neural Mechanism for Involuntary Attention Shifts to Changes in Auditory Stimulation. J. Cogn. Neurosci. 8, 527–539. https://doi.org/10.1162/JOCN.1996.8.6.527

Schröger, E., Wolff, C., 1998. Behavioral and electrophysiological effects of task-irrelevant sound change: a new distraction paradigm. Cogn. Brain Res. 7, 71–87. https://doi.org/10.1016/S0926-6410(98)00013-5

Schuwerk, T., Schurz, M., Müller, F., Rupprecht, R., Sommer, M., 2017. The rTPJ's overarching cognitive function in networks for attention and theory of mind. Soc. Cogn. Affect. Neurosci. 12, 157–168. https://doi.org/10.1093/scan/nsw163

Seeley, W.W., Menon, V., Schatzberg, A.F., Keller, J., Glover, G.H., Kenna, H., Reiss, A.L., Greicius, M.D., 2007. Dissociable intrinsic connectivity networks for salience processing and executive control. J. Neurosci. 27, 2349–2356. https://doi.org/10.1523/JNEUROSCI.5587-06.2007

Serences, J.T., Yantis, S., 2007. Spatially Selective Representations of Voluntary and Stimulus-Driven Attentional Priority in Human Occipital, Parietal, and Frontal Cortex. Cereb. Cortex 17, 284–293. https://doi.org/10.1093/CERCOR/BHJ146

Seth, A.K., Barrett, A.B., Barnett, L., 2015. Granger causality analysis in neuroscience and neuroimaging. J. Neurosci. 35, 3293–3297. https://doi.org/10.1523/JNEUROSCI.4399-14.2015

Shiramatsu, T.I., Mori, K., Ishizu, K., Takahashi, H., 2021. Auditory, Visual, and Cross-Modal Mismatch Negativities in the Rat Auditory and Visual Cortices. Front. Hum. Neurosci. 15, 536. https://doi.org/10.3389/FNHUM.2021.721476/BIBTEX

Shtyrov, Y., Kujala, T., Palva, S., Ilmoniemi, R.J., Näätänen, R., 2000. Discrimination of speech and of complex nonspeech sounds of different temporal structure in the left and right cerebral hemispheres. Neuroimage 12, 657–663. https://doi.org/10.1006/NIMG.2000.0646

Sittiprapaporn, W., 2012. An effect of attention on mismatch negativity in audiovisual visual modalities. Pakistan J. Biol. Sci. 15, 542–546. https://doi.org/10.3923/pjbs.2012.542.546

Slepian, D., Pollak, H.O., 1961. Prolate Spheroidal Wave Functions, Fourier Analysis and Uncertainty - I. Bell Syst. Tech. J. 40, 43–63. https://doi.org/10.1002/j.1538-7305.1961.tb03976.x

Snyder, A.C., Foxe, J.J., 2010. Anticipatory Attentional Suppression of Visual Features Indexed by Oscillatory Alpha-Band Power Increases:A High-Density Electrical Mapping Study. J. Neurosci. 30, 4024–4032. https://doi.org/10.1523/JNEUROSCI.5684-09.2010

Sokoliuk, R., Mayhew, S.D., Aquino, K.M., Wilson, R., Brookes, M.J., Francis, S.T., Hanslmayr, S., Mullinger, K.J., 2019. Two spatially distinct posterior alpha sources fulfill different functional roles in attention. J. Neurosci. 1993–18. https://doi.org/10.1523/JNEUROSCI.1993-18.2019

Squires, N.K., Squires, K.C., Hillyard, S.A., 1975. Two varieties of long-latency positive waves evoked by unpredictable auditory stimuli in man. Electroencephalogr. Clin. Neurophysiol. 38, 387–401. https://doi.org/10.1016/0013-4694(75)90263-1

Stefanics, G., Stavrinou, M., Sestieri, C., Ciancetta, L., Belardinelli, P., Cianflone, F., Bernáth, L., Hernádi, I., Pizzella, V., Romani, G.L., 2005. Cross-modal visual-auditory-somatosensory integration in a multimodal object recognition task in humans. Int. Congr. Ser. 1278, 163–166. https://doi.org/10.1016/J.ICS.2004.11.074

Stefanics, G., Stefanics, G., Kremláček, J., Czigler, I., 2014. Visual mismatch negativity: A predictive coding view. Front. Hum. Neurosci. 8, 1–19. https://doi.org/10.3389/FNHUM.2014.00666/BIBTEX

Stekelenburg, J.J., Vroomen, J., 2007. Neural Correlates of Multisensory Integration of Ecologically Valid Audiovisual Events. J. Cogn. Neurosci. 19, 1964–1973. https://doi.org/10.1162/JOCN.2007.19.12.1964

Stevens, A.A., Skudlarski, P., Gatenby, J.C., Gore, J.C., 2000. Event-related fMRI of auditory and visual oddball tasks. Magn. Reson. Imaging 18, 495–502.

https://doi.org/10.1016/S0730-725X(00)00128-4

Stigliani, A., Jeska, B., Grill-Spector, K., 2017. Encoding model of temporal processing in human visual cortex. Proc. Natl. Acad. Sci. U. S. A. 114, E11047–E11056. https://doi.org/10.1073/pnas.1704877114

Störmer, V.S., Feng, W., Martinez, A., Mcdonald, J.J., Hillyard, S.A., 2016. Salient, Irrelevant Sounds Reflexively Induce Alpha Rhythm Desynchronization in Parallel with Slow Potential Shifts in Visual Cortex. J. Cogn. Neurosci. 28, 433–445. https://doi.org/10.1162/JOCN_A_00915

Sutton, S., Braren, M., Zubin, J., John, E.R., 1965a. Evoked-potential correlates of stimulus uncertainty. Science 150, 1187–1188. https://doi.org/10.1126/SCIENCE.150.3700.1187

Sutton, S., Braren, M., Zubin, J., John, E.R., 1965b. Evoked-Potential Correlates of Stimulus Uncertainty. Science (80-.). 150, 1187–1188. https://doi.org/10.1126/SCIENCE.150.3700.1187

Sutton, S., Tueting, P., Zubin, J., John, E.R., 1967. Information Delivery and the Sensory Evoked Potential. Science (80-.). 155, 1436–1439. https://doi.org/10.1126/SCIENCE.155.3768.1436

Szuromi, B., Czobor, P., Komlósi, S., Bitter, I., 2011. P300 deficits in adults with attention deficit hyperactivity disorder: a meta-analysis. Psychol. Med. 41, 1529–1538. https://doi.org/10.1017/S0033291710001996

Tait, L., Ozkan, A.A., Szul, M.J., Zhang, J., 2020. Cortical source imaging of resting-state MEG with a high resolution atlas: An evaluation of methods. bioRxiv

2020.01.12.903302. https://doi.org/10.1101/2020.01.12.903302

Talsma, D., 2015. Predictive coding and multisensory integration: an attentional account of the multisensory mind. Front. Integr. Neurosci. 9, 19. https://doi.org/10.3389/FNINT.2015.00019

Teichert, T., Grinband, J., Ferrera, V., 2016. The importance of decision onset. J. Neurophysiol. 115, 643–61. https://doi.org/10.1152/jn.00274.2015

Theeuwes, J., 1996. Perceptual selectivity for color and form: On the nature of the interference effect. Converging Oper. study Vis. Sel. attention. 297–314. https://doi.org/10.1037/10187-010

Thut, G., Nietzel, A., Brandt, S.A., Pascual-Leone, A., 2006. Behavioral/Systems/Cognitive-Band Electroencephalographic Activity over Occipital Cortex Indexes Visuospatial Attention Bias and Predicts Visual Target Detection. https://doi.org/10.1523/JNEUROSCI.0875-06.2006

Tiitinen, H., Sivonen, P., Alku, P., Virtanen, J., Näätänen, R., 1999. Electromagnetic recordings reveal latency differences in speech and tone processing in humans. Brain Res. Cogn. Brain Res. 8, 355–363. https://doi.org/10.1016/S0926-6410(99)00028-2

Ungan, P., Karsilar, H., Yagcioglu, S., 2019. Pre-attentive mismatch response and involuntary attention switching to a deviance in an earlier-than-usual auditory stimulus: An ERP study. Front. Hum. Neurosci. 13, 58. https://doi.org/10.3389/FNHUM.2019.00058/BIBTEX

Van de Steen, F., Faes, L., Karahan, E., Songsiri, J., Valdes-Sosa, P.A., Marinazzo, D., 2019. Critical Comments on EEG Sensor Space Dynamical Connectivity Analysis. Brain

Topogr. 32, 643–654. https://doi.org/10.1007/s10548-016-0538-7

Van Os, J., 2009. 'Salience syndrome' replaces 'schizophrenia' in DSM-V and ICD-11: psychiatry's evidence-based entry into the 21st century? Acta Psychiatr. Scand. 120, 363–372. https://doi.org/10.1111/J.1600-0447.2009.01456.X

Van Voorhis, S., Hillyard, S.A., 1977. Visual evoked potentials and selective attention to points in space. Percept. Psychophys. 1977 221 22, 54–62. https://doi.org/10.3758/BF03206080

van Wassenhove, V., Grant, K.W., Poeppel, D., 2005. Visual speech speeds up the neural processing of auditory speech. PNAS 102, 1181–1186.

Van Wassenhove, V., Grant, K.W., Poeppel, D., 2005. Visual speech speeds up the neural processing of auditory speech. Proc. Natl. Acad. Sci. 102, 1181–1186. https://doi.org/10.1073/PNAS.0408949102

Vihla, M., Lounasmaa, O. V., Salmelin, R., 2000. Cortical processing of change detection: dissociation between natural vowels and two-frequency complex tones. Proc. Natl. Acad. Sci. U. S. A. 97, 10590–10594. https://doi.org/10.1073/PNAS.180317297

Vinck, M., Huurdeman, L., Bosman, C.A., Fries, P., Battaglia, F.P., Pennartz, C.M.A., Tiesinga, P.H., 2015. How to detect the Granger-causal flow direction in the presence of additive noise? Neuroimage 108, 301–318. https://doi.org/10.1016/j.neuroimage.2014.12.017

Vossel, S., Geng, J.J., Fink, G.R., 2014. Dorsal and Ventral Attention Systems. Neurosci. 20, 150–159. https://doi.org/10.1177/1073858413494269

Vossel, S., Weidner, R., Driver, J., Friston, K.J., Fink, G.R., 2012. Deconstructing the

architecture of dorsal and ventral attention systems with dynamic causal modeling. J. Neurosci. 32, 10637–10648. https://doi.org/10.1523/JNEUROSCI.0414-12.2012

Voytek, B., Samaha, J., Rolle, C.E., Greenberg, Z., Gill, N., Porat, S., Kader, T., Rahman, S., Malzyner, R., Gazzaley, A., 2017. Preparatory encoding of the fine scale of human spatial attention. J. Cogn. Neurosci. 29, 1302–1310. https://doi.org/10.1162/jocn_a_01124

Wacongne, C., Changeux, J.P., Dehaene, S., 2012. A Neuronal Model of Predictive Coding Accounting for the Mismatch Negativity. J. Neurosci. 32, 3665–3678. https://doi.org/10.1523/JNEUROSCI.5003-11.2012

Wacongne, C., Labyt, E., Van Wassenhove, V., Bekinschtein, T., Naccache, L., Dehaene, S., 2011. Evidence for a hierarchy of predictions and prediction errors in human cortex. Proc. Natl. Acad. Sci. U. S. A. 108, 20754–20759. https://doi.org/10.1073/PNAS.1117807108/ASSET/DAC9C788-CFB9-4565-B3B3-65AC6F69F37F/ASSETS/GRAPHIC/PNAS.1117807108FIG03.JPEG

Webb, T.W., Igelström, K.M., Schurger, A., Graziano, M.S.A., 2016. Cortical networks involved in visual awareness independent of visual attention. Proc. Natl. Acad. Sci. 113, 13923–13928. https://doi.org/10.1073/PNAS.1611505113

Wen, X., Rangarajan, G., Ding, M., 2013. Multivariate Granger causality: an estimation framework based on factorization of the spectral density matrix. Philos. Trans. R. Soc. A Math. Phys. Eng. Sci. 371, 20110610. https://doi.org/10.1098/rsta.2011.0610

Wen, X., Yao, L., Liu, Y., Ding, M., 2012. Causal interactions in attention networks predict behavioral performance. J. Neurosci. 32, 1284–1292. https://doi.org/10.1523/JNEUROSCI.2817-11.2012

White, T., Gilleen, J.K., Shergill, S.S., 2013. Dysregulated but not decreased salience network activity in schizophrenia. Front. Hum. Neurosci. 0, 65. https://doi.org/10.3389/FNHUM.2013.00065/BIBTEX

Wijnen, V.J.M., van Boxtel, G.J.M., Eilander, H.J., de Gelder, B., 2007. Mismatch negativity predicts recovery from the vegetative state. Clin. Neurophysiol. 118, 597–605. https://doi.org/10.1016/J.CLINPH.2006.11.020

Wilk, H.A., Ezekiel, F., Morton, J.B., 2012. Brain regions associated with moment-to-moment adjustments in control and stable task-set maintenance. Neuroimage 59, 1960–1967. https://doi.org/10.1016/j.neuroimage.2011.09.011

Wilson, G.T., 1978. A convergence theorem for spectral factorization. J. Multivar. Anal. 8, 222–232. https://doi.org/10.1016/0047-259X(78)90073-8

Winkler, I., 2008. Interpreting the Mismatch Negativity. http://dx.doi.org/10.1027/0269-8803.21.34.147 21, 147–163. https://doi.org/10.1027/0269-8803.21.34.147

Winkler, I., Czigler, I., 2012. Evidence from auditory and visual event-related potential (ERP) studies of deviance detection (MMN and vMMN) linking predictive coding theories and perceptual object representations. Int. J. Psychophysiol. 83, 132–143. https://doi.org/10.1016/J.IJPSYCHO.2011.10.001

Winkler, I., Czigler, I., Jaramillo, M., Paavilainen, P., Näätänen, R., 1998. Temporal constraints of auditory event synthesis: Evidence from ERPs. Neuroreport 9, 495–499. https://doi.org/10.1097/00001756-199802160-00025

Winkler, I., Panknin, D., Bartz, D., Muller, K.R., Haufe, S., 2016. Validity of Time Reversal for Testing Granger Causality. IEEE Trans. Signal Process. 64, 2746–2760.

https://doi.org/10.1109/TSP.2016.2531628

Woldorff, M.G., Hillyard, S.A., Gallen, C.C., Hampson, S.R., Bloom, F.E., 1998. Magnetoencephalographic recordings demonstrate attentional modulation of mismatch-related neural activity in human auditory cortex. Psychophysiology 35, 283–292. https://doi.org/10.1017/S0048577298961601

Worden, M.S., Foxe, J.J., Wang, N., Simpson, G. V., 2000. Anticipatory biasing of visuospatial attention indexed by retinotopically specific alpha-band electroencephalography increases over occipital cortex. J. Neurosci. 20. https://doi.org/10.1523/jneurosci.20-06-j0002.2000

WURTZ, R., ME, G., DL, R., 1980. BEHAVIORAL MODULATION OF VUSUAL RESPONSES IN THE MONKEY: STIMULUS SELECTION FOR ATTENTION AND MOVEMENT. Behav. Modul. VUSUAL RESPONSES MONKEY Stimul. Sel. Atten. Mov.

Wynn, J.K., Jimenez, A.M., Roach, B.J., Korb, A., Lee, J., Horan, W.P., Ford, J.M., Green, M.F., 2015. Impaired target detection in schizophrenia and the ventral attentional network: Findings from a joint event-related potential–functional MRI analysis. NeuroImage Clin. 9, 95–102. https://doi.org/10.1016/J.NICL.2015.07.004

Xia, M., Wang, J., He, Y., 2013. BrainNet Viewer: A Network Visualization Tool for Human Brain Connectomics. PLoS One 8. https://doi.org/10.1371/journal.pone.0068910

Yantis, S., 1996. Attentional capture in vision. Converging Oper. study Vis. Sel. attention. 45–76. https://doi.org/10.1037/10187-002

Yantis, S., Jonides, J., 1984. Abrupt visual onsets and selective attention: Evidence from

visual search. J. Exp. Psychol. Hum. Percept. Perform. 10, 601–621. https://doi.org/10.1037/0096-1523.10.5.601

Zatorre, R.J., Evans, A.C., Meyer, E., Gjedde, A., 1992. Lateralization of Phonetic and Pitch Discrimination in Speech Processing. Science (80-.). 256, 846–849. https://doi.org/10.1126/SCIENCE.256.5058.846

Zumer, J.M., Scheeringa, R., Schoffelen, J.-M., Norris, D.G., Jensen, O., 2014. Occipital Alpha Activity during Stimulus Processing Gates the Information Flow to Object-Selective Cortex. PLoS Biol. 12, e1001965. https://doi.org/10.1371/journal.pbio.1001965

Appendix

Granger causality scores

All the spectral GC values computed between 8-9 Hz are shown for node pairs that survived the significance tests (permutation test and time-reversed Granger Causality) as described in *Methods*. GC between all pairs of signals (nodes) are represented; Direction of influence is from the node on the left to the node on the top; n.s. – not significant; '--' means pairing of a node with itself which is not valid because the Granger Causality was measured only between two different time-series (nodes).

Table A1. Dynamic Stimulus: Trials with Saliency (ST)

Region	Left aTPJ	Right pTPJ	Right aTPJ	Left lPFC	Right lPFC	Right VA	Left VA	Left Ins	Right Ins
Left aTPJ	--	0.019	0.050	0.062	n.s.	0.068	0.074	n.s.	0.072
Right pTPJ	0.023	--	0.023	n.s.	n.s.	0.030	0.071	n.s.	n.s.
Right aTPJ	0.077	0.042	--	0.126	0.026	0.081	0.028	0.124	0.052
Left lPFC	n.s.	n.s.	0.035	--	0.023	0.039	0.028	n.s.	0.036
Right lPFC	n.s.	n.s.	0.012	0.187	--	0.061	0.023	0.098	0.040
Right VA	0.034	0.021	0.091	0.083	0.025	--	0.058	0.095	0.033
Left VA	0.035	0.035	0.145	0.023	0.036	n.s.	--	0.049	0.113
Left Ins	n.s.	n.s.	0.028	0.086	0.013	0.054	0.039	--	0.026
Right Ins	0.057	0.017	0.028	0.244	0.021	0.162	n.s.	0.162	--

Table A2. Dynamic Stimulus: Trials Without Saliency (WT)

Region	Left aTPJ	Right pTPJ	Right aTPJ	Left IPFC	Right IPFC	Right VA	Left VA	Left Ins	Right Ins
Left aTPJ	--	0.016	n.s.	n.s.	n.s.	0.050	0.025	n.s.	0.025
Right pTPJ	0.063	--	n.s.	0.022	n.s.	0.125	0.034	0.023	0.017
Right aTPJ	0.105	0.064	--	0.034	n.s.	0.159	0.035	0.042	n.s.
Left IPFC	0.080	0.059	0.030	--	n.s.	0.148	0.031	0.017	0.033
Right IPFC	0.019	n.s.	n.s.	n.s.	--	0.205	0.019	n.s.	n.s.
Right VA	n.s.	0.018	0.025	0.033	0.052	--	n.s.	0.022	0.080
Left VA	n.s.	n.s.	n.s.	n.s.	n.s.	0.056	--	n.s.	n.s.
Left Ins	0.051	0.027	n.s.	0.017	n.s.	0.064	0.078	--	n.s.
Right Ins	0.030	0.025	n.s.	n.s.	n.s.	0.201	n.s.	n.s.	--

Table A3. Static Stimulus: Trials with Saliency (ST)

Region	Right aTPJ	Right IPFC	Right VA	Left Ins	Right Ins
Right aTPJ	--	0.017	n.s.	n.s.	0.025
Right IPFC	0.089	--	0.174	0.017	0.023
Right VA	n.s.	0.027	--	0.011	n.s.
Left Ins	n.s.	n.s.	0.013	--	0.036
Right Ins	0.037	0.031	0.016	0.022	--

Table A4. Static Stimulus: Trials Without Saliency (WT)

Region	Right aTPJ	Right IPFC	Right VAA	Left Ins	Right Ins
Right aTPJ	--	0.0920	n.s.	0.0246	n.s.
Right IPFC	n.s.	--	0.0428	n.s.	n.s.
Right VA	n.s.	0.1049	--	0.0189	0.0483
Left Ins	0.0389	n.s.	n.s.	--	0.1309
Right Ins	n.s.	n.s.	n.s.	n.s.	--

List of Publications

1. **Ghosh, P.**, Roy, D., & Banerjee, A., 2021. Organization of directed functional connectivity among nodes of ventral attention network reveals the common network mechanisms underlying saliency processing across distinct spatial and spatio-temporal scales. NeuroImage, 231, 117869. https://doi.org/10.1016/J.NEUROIMAGE.2021.117869

2. **Ghosh, P**., Roy, D., Banerjee, A., 2021. Psychophysical data to study the brain network mechanisms involved in reorienting attention to salient events during goal-directed visual discrimination and search tasks. Data Br. 36, 107020. https://doi.org/10.1016/J.DIB.2021.107020

3. Talwar, S.*, **Ghosh, P.***, Banerjee, A., 2022. Prediction error processing speeds up in presence of multisensory contexts (Under review). bioRxiv 2022.02.11.480053. https://doi.org/10.1101/2022.02.11.480053

4. Singhal, S., **Ghosh, P.,** Kumar, N., Banerjee, A., 2022. Concurrent separation of phase-locked and non-phase-locked activity (Under revision). bioRxiv 2022.03.14.484222. https://doi.org/10.1101/2022.03.14.484222

*Authors with equal contribution